Fundão Tailings Dam Review Panel

Report on the Immediate Causes of the Failure of the Fundão Dam

Panel:
Norbert R. Morgenstern (Chair)
Steven G. Vick
Cássio B. Viotti
Bryan D. Watts

August 25, 2016

EXECUTIVE SUMMARY

The Fundão Tailings Dam failed on November 5, 2015 in a liquefaction flowslide that initiated at the dam's left abutment. This Investigation was performed to determine its cause.

In structuring its investigation process, the Panel systematically identified and evaluated multiple causation hypotheses. It further imposed hypothesis testing by means of the following three questions that the candidate failure mechanism should be able to explain:

1. Why did a flowslide occur?
2. Why did the flowslide occur where it did?
3. Why did the flowslide occur when it did?

Forensic methods adopted by the Panel integrated multiple lines of evidence: observations from eyewitness accounts; data and imagery in geographic information system (GIS) format; field evidence from subsurface exploration by the Panel and others; advanced laboratory testing; and sophisticated computer modeling. Responding to the above three questions for hypothesis testing demanded a high level of quantification and exhaustive detail in each of these aspects of the Investigation's evidence-based approach.

To understand the failure first requires understanding the materials the dam contained and their properties. There were two types of tailings, both produced in slurry form and delivered in separate pipelines to the Fundão impoundment. *Sand tailings,* or simply *sands,* are a mixture of sand-sized and finer silt particles. The sands are relatively free-draining, but when loose and saturated are susceptible to *liquefaction*, a process whereby the material loses nearly all of its strength and flows as a fluid. The *slimes*, on the other hand, are much finer and clay-like in nature—soft and compressible with low permeability. How these two materials interacted is key to understanding the failure.

Another central aspect is how their deposition was influenced by a series of unplanned occurrences during the dam's construction and operation. Together, these incidents established the conditions that allowed the failure to take place. These included: (1) damage to the original Starter Dam that resulted in increased saturation; (2) deposition of slimes in areas where this was not intended; and (3) structural problems with a concrete conduit that caused the dam to be raised over the slimes.

It was originally planned to deposit sands behind a compacted earthfill Starter Dam, then raise it by the upstream method to increase progressively its capacity. These sands, in turn, would retain slimes deposited behind them such that the two materials would not intermingle. To preserve the free-draining characteristics of the sands, a 200 m beach width was required to prevent water-borne slimes from being deposited near the dam crest where they would impede drainage. A high-capacity drainage system at the base of the Starter Dam would allow water to drain from the sands, reducing saturation.

The first incident occurred in 2009 shortly after the Starter Dam was completed. Due to construction defects in the base drain, the dam was so badly damaged that the original concept could no longer be implemented. Instead, a revised design substituted a new drainage blanket at a higher elevation.

Together with the revised design there was a fundamental change in the design concept whereby more widespread saturation was allowed and accepted. This increase in the extent of saturation introduced the potential for sand liquefaction.

The second incident associated with slimes and water management occurred over an extended period of time in 2011 and 2012 while the new design was being constructed. During operation, the 200 m beach width criterion was often not met, with water encroaching to as little as 60 m from the crest. This allowed slimes to settle out in areas where they were not intended to exist.

Another incident occurred in late 2012 when a large concrete conduit beneath the dam's left abutment, the Secondary Gallery, was found to be structurally deficient and unable to support further loading. This meant that the dam could not be raised over it until it had been abandoned and filled with concrete. In order to maintain operations in the interim, the alignment of the dam at the left abutment was set back from its former position. This placed the embankment directly over the previously-deposited slimes. With this, all of the necessary conditions for liquefaction triggering were in place.

As dam raising continued, surface seepage began to appear on the left abutment setback at various elevations and times during 2013. The saturated mass of tailings sands was growing, and by August, 2014 the replacement blanket drain intended to control this saturation reached its maximum capacity. Meanwhile, the slimes beneath the embankment were responding to the increasing load being placed on them by the rising embankment. The manner in which they did so, and the consequent effect on the sands, is what ultimately caused the sands to liquefy.

As the softer slimes were loaded, they compressed. At the same time, they also deformed laterally, squeezing out like toothpaste from a tube in a process known as *lateral extrusion*. The sands immediately above, forced to conform to this movement, experienced a reduction in the horizontal stress that confined them. This allowed the sands to, in effect, be pulled apart and in the process become looser.

To replicate this process in the laboratory, the Panel applied these stress changes to the Fundão sand. The saturated specimen completely and abruptly collapsed, losing nearly all its strength—a laboratory demonstration of liquefaction. The Panel then undertook a program of numerical modeling to determine whether stress changes similar to those imposed in the laboratory would have also occurred in the field. Using computer simulation of how the slimes deformed during embankment construction, and tracking the corresponding response of the sands, comparable stress conditions that caused the sands to liquefy in the laboratory were reproduced computationally. Simply put, what is known to have occurred during the failure was replicated in the laboratory, and what occurred in the laboratory is shown to have occurred at the left abutment of the dam.

A related aspect of the failure was the series of three small seismic shocks that occurred about 90 minutes earlier. By then the left abutment of the dam had reached a precarious state of stability. Computer modeling showed that the earthquake forces produced an additional increment of horizontal movement in the slimes that correspondingly affected the overlying sands. Although the movements are quite small and the associated uncertainties large, this additional movement is likely to have accelerated the failure process that was already well advanced.

Hence the failure of the Fundão Tailings Dam by liquefaction flowsliding was the consequence of a chain of events and conditions. A change in design brought about an increase in saturation which introduced the potential for liquefaction. As a result of various developments, soft slimes encroached into unintended areas on the left abutment of the dam and the embankment alignment was set back from its originally-planned location. As a result of this setback, slimes existed beneath the embankment and were subjected to the loading its raising imposed. This initiated a mechanism of extrusion of the slimes and pulling apart of the sands as the embankment height increased. With only a small additional increment of loading produced by the earthquakes, the triggering of liquefaction was accelerated and the flowslide initiated.

Immediately following this Executive Summary is an inventory of structures and their locations to help the reader become oriented to the various features associated with the site.

INVENTORY OF STRUCTURES

Term	Figure Reference
Alegria Mine	1
Auxiliary Foundation (Base) Drain	2
Conveyor	1
Dike 1	1
Dike 1A (a.k.a. Old Dike 1A)	2
Dike 2	1
El. 826 m Blanket Drain	2
Fabrica Nova Waste Pile	1
Fundão Dam	1
Germano Buttress	1
Germano Main Dam	1
Grota da Vale	1
Kananets®	2
Left Abutment (LA)	2
Main Gallery	2
Overflow Channel	2
Plateau	2
Principal Foundation (Base) Drain	2
Reinforcement (Equilibrium) Berm	2
Right Abutment (RA)	2
Santarem Dam	1
Secondary Gallery	2

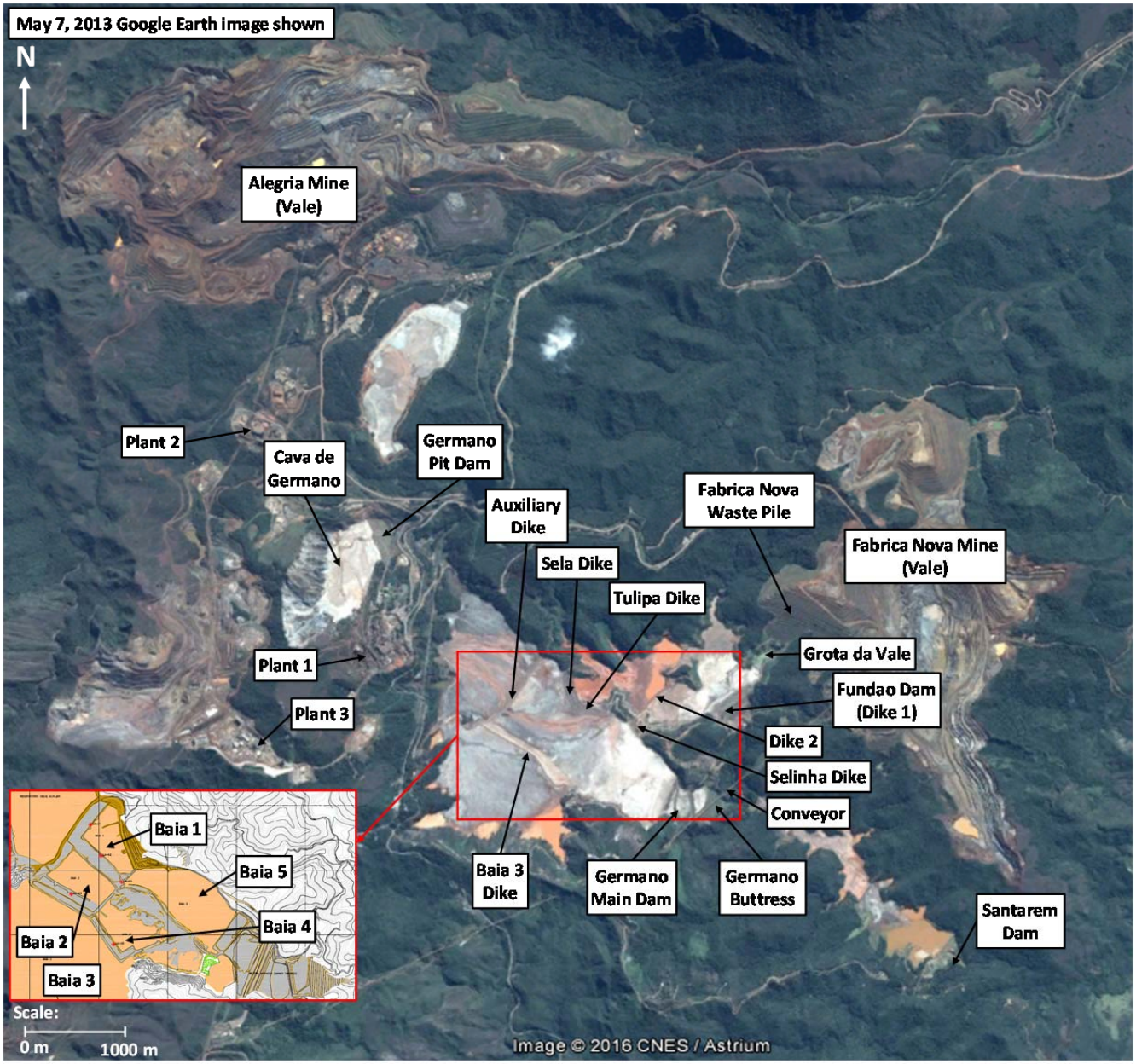

Figure 1 Inventory of structures – Samarco Site

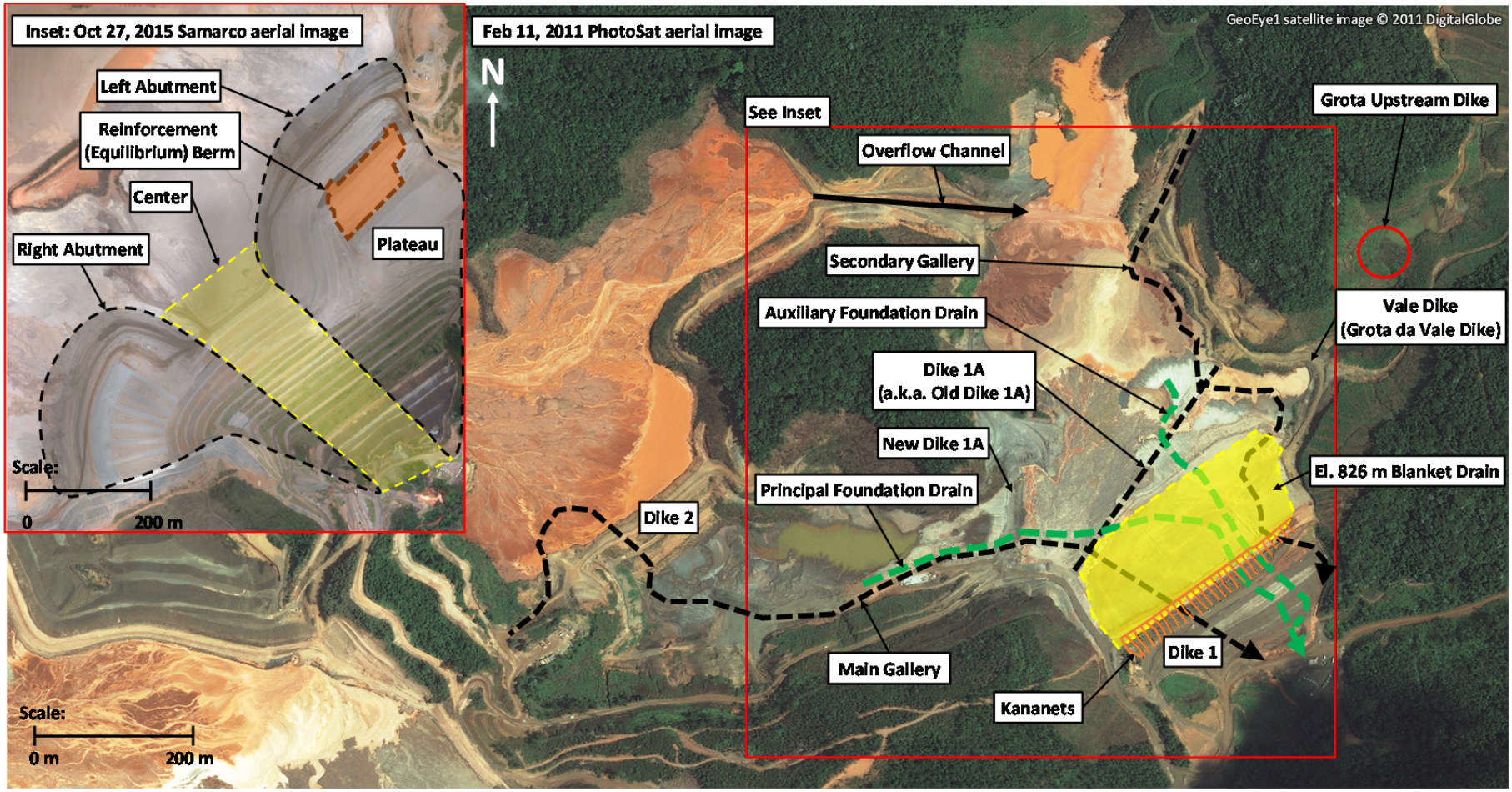

Figure 2 Inventory of structures – Fundão Dam

TABLE OF CONTENTS

TABLE OF CONTENTS
(continued)

List of Tables

List of Figures

TABLE OF CONTENTS

(continued)

TABLE OF CONTENTS

(continued)

List of Appendices

TABLE OF CONTENTS

(continued)

1 INTRODUCTION

1.1 The Failure

On the afternoon of November 5, 2015, the Fundão Tailings Dam in Minas Gerais collapsed. Its crest had reached El. 900 m, making the dam 110 m high. Several dozen people were working on or near the dam at the time. Some were hauling and spreading tailings for raising the dam, others were constructing gravel blanket drains in anticipation of the next stage of construction, and still others were engaged in the daily activities required to operate and maintain the tailings system.

Sometime after about 2:00PM[1] many in the Germano plant complex felt a tremor lasting several seconds. Although windows rattled and objects fell from tables, there did not appear to be any serious damage. Work resumed.

At 3:45PM shouts came over radio that the dam was collapsing. A cloud of dust had formed over the left abutment[2], and those closest to the area designated the "setback" could see cracks forming at the recently-constructed drainage blanket. The slope above them was beginning to undulate "like a wave" as if it were "melting," bringing the dam crest down after it. The tailings that had been solid ground just minutes before transformed into a roiling river, overtopping but not breaching the downstream Santarem Dam, then entering the town of Bento Rodriguez shortly thereafter enroute to its ultimate destination in the sea.

Eyewitness descriptions and videos definitively establish several things. The first is that the Fundão failure initiated at the dam's left abutment, not at the right side or its downstream toe. The second is that the failure occurred due to flow liquefaction of the tailings, a process whereby water pressures in the interstitial voids between the tailings particles increased to such an extent that the mass of material lost strength and flowed like a liquid. And third is that this transformation from solid to liquid was complete and abrupt, leaving a fluid of apparent viscosity and hydraulic behavior little different from water in just seconds.

The question remains as to what triggered liquefaction and what factors promoted its occurrence. That is the focus of this report.

1.2 The Investigation

This Investigation of the Fundão Tailings Dam failure was commissioned by BHP Billiton Brasil Ltda., Vale S.A. and Samarco Mineração S.A. The firm of Cleary Gottlieb Steen & Hamilton LLP (CGSH) was engaged to conduct the Investigation with the assistance of a panel of experts. The Fundão Tailings Dam Review Panel (Panel) includes four members, all specialist geotechnical engineers in water and tailings dams: Norbert R. Morgenstern (Chair), Steven G. Vick, Cássio B. Viotti, and Bryan D. Watts.

[1] All times in this report refer to local Brazilian time.
[2] The conventions *left* and *right* indicate direction, location, or orientation as seen by an observer looking downstream. The left and right *abutments* are where the constructed dam meets the respective valley sides.

The Panel's Terms of Reference defined the scope of its activities. Specifically, the Panel was instructed to provide its independent and unbiased professional judgment and expertise in determining the immediate cause(s) of the incident.

In accomplishing this purpose, the Panel could examine any or all of the following:

- geotechnical designs of the Fundão Tailings Dam and structures associated with the dam, including both intact and breached embankments, and including both the original design and all lifts of the embankment structure;
- interpretation of results of geotechnical investigations and associated laboratory testing of the Fundão Tailings Dam;
- patterns, trends, and relationships in instrumentation behavior of the Fundão Tailings Dam;
- interpretation of instrumentation and performance data in relation to the Fundão Dam's behavior;
- materials, methods, procedures, and quality assurance/quality control practices for the construction and modification of the Fundão Dam;
- water balance and water quality as they relate to the incident;
- seismic activity in the region on the day of the incident;
- operational procedures and planning for tailings deposition and water management at the Fundão Dam;
- inspection and surveillance procedures and implementation, including reports issued by the Independent Tailings Review Board (ITRB) and other outside auditors;
- the Engineer of Record's field reviews;
- issues identified by the National Department of Mineral Production (DNPM) and the Brazilian federal and state environmental agencies in the course of their oversight;
- the design and structure of other similar tailings dams in the vicinity; and
- other matters the Panel deems appropriate to be examined.

Seismologists Gail Atkinson and Ivan Wong provided the Panel with input in their field of expertise. The firm of Klohn Crippen Berger provided analytical, field, and laboratory support, and the firm of TÜV SÜD provided local assistance in Brazil.

The Panel was provided with available information and witnesses necessary to achieving its purpose. The Panel was asked not to assign fault or responsibility to any person or party, or to evaluate environmental or other downstream effects or damages. None of the Panel members had performed previous work for Samarco or was currently engaged in any other assignment for BHP Billiton Brasil or Vale during the conduct of the Investigation.

During the course of the Investigation, the Panel conducted the following activities:

- site inspection and meetings;
- meetings with eyewitnesses and technical personnel;
- compilation and review of project documents;
- assembly of GIS data and imagery;
- reconstruction of tailings stratigraphy;
- compilation and assembly of pre-failure subsurface and laboratory data;
- subsurface investigations at the site and laboratory testing;
- compilation and interpretation of instrumentation data;
- analytical studies:
  - seepage modeling;
  - consolidation modeling;
  - stability analysis;
  - deformation analysis; and
  - dynamic response analysis.
- geologic assessment;
- fault tree analysis; and
- preparation of this report.

2 HISTORY

This section provides a compilation of historical facts and circumstances considered by the Panel to be most relevant to understanding the failure, with particular emphasis on the left abutment where the failure is known to have initiated. The complete history is much more extensive, and no attempt is made here to review it in its entirety.

2.1 The Concept (2004-2007)

Beneficiation of iron ore at Samarco's Germano Complex results in two distinct kinds of tailings produced and transported in slurry form as separate streams. *Sands*, or sand tailings, are actually composed of both sand and silt-sized particles in roughly equal proportion. During deposition, they form a gently-sloping beach through which transport water drains fairly rapidly. *Slimes,* on the other hand, are fine-grained and clayey in nature. The clay-sized particles remain suspended and eventually settle in standing water to produce a softer material of lower permeability.

At Germano, a way was devised to use these two types of tailings and their different characteristics to best advantage. The sands were deposited to form a buttress or "stack" that retained the slimes discharged separately behind it. The sands, in turn, were retained by an earthfill or rockfill *starter dam* at the downstream toe of the stack, as illustrated on Figure 2-1 for Samarco's Germano Buttress structure. Over time, the Germano Starter Dam was raised according to the *upstream method* or *upstream construction*. With this procedure, the dam crest moves progressively upstream over previously-deposited tailings as the dam is raised.

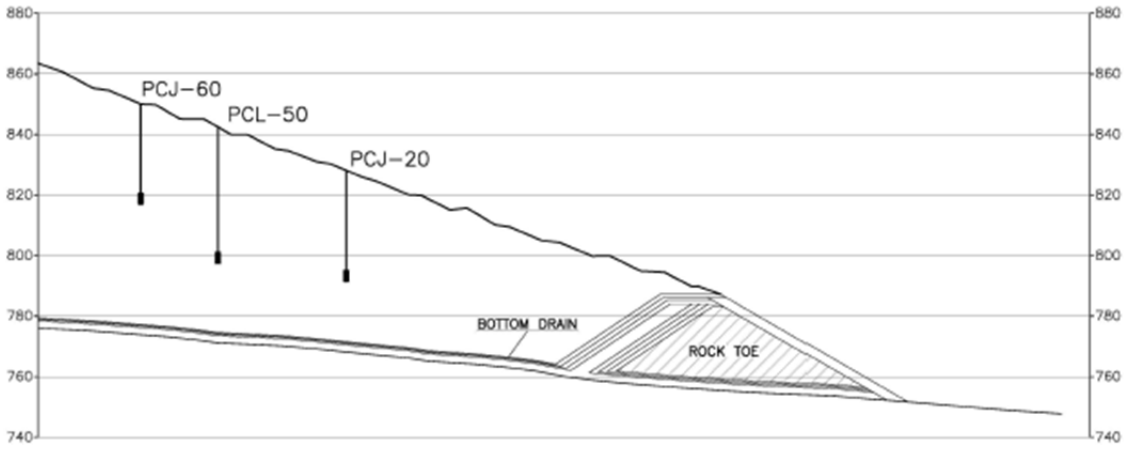

Figure 2-1 Germano Buttress (Pimenta de Ávila 2011)

Adequate drainage of the sands was the key to this concept. Figure 2-1 shows that drainage was promoted by highly-pervious bottom drains underlying the sand and extending beneath the Starter Dam to prevent water from accumulating and saturating the deposit. The absence of any significant water pressure was to be confirmed with the piezometers shown in the figure. Provided that no

slimes were present to impede downward drainage and that the sands remained unsaturated, resistance to liquefaction—a well-known vulnerability of upstream construction—could be assured.

By 2005, the existing tailings facilities at Samarco's Germano operation were nearing capacity, and a new third pellet plant would increase production of both sand and slimes. The adjacent Fundão Valley was chosen as a new tailings site. In the layout that emerged, the sands and slimes would initially be physically separated, with sands deposited behind Dike 1 and slimes behind Dike 2, as represented on Figure 2-2. Retention of the slimes required that the sands deposited between the two dikes always remain at a higher elevation throughout the raising process. This was a matter of reservoir geometry, and the dikes in Figure 2-2 had been strategically positioned for sands and slimes in 70% and 30% proportion of the total received from all plants.

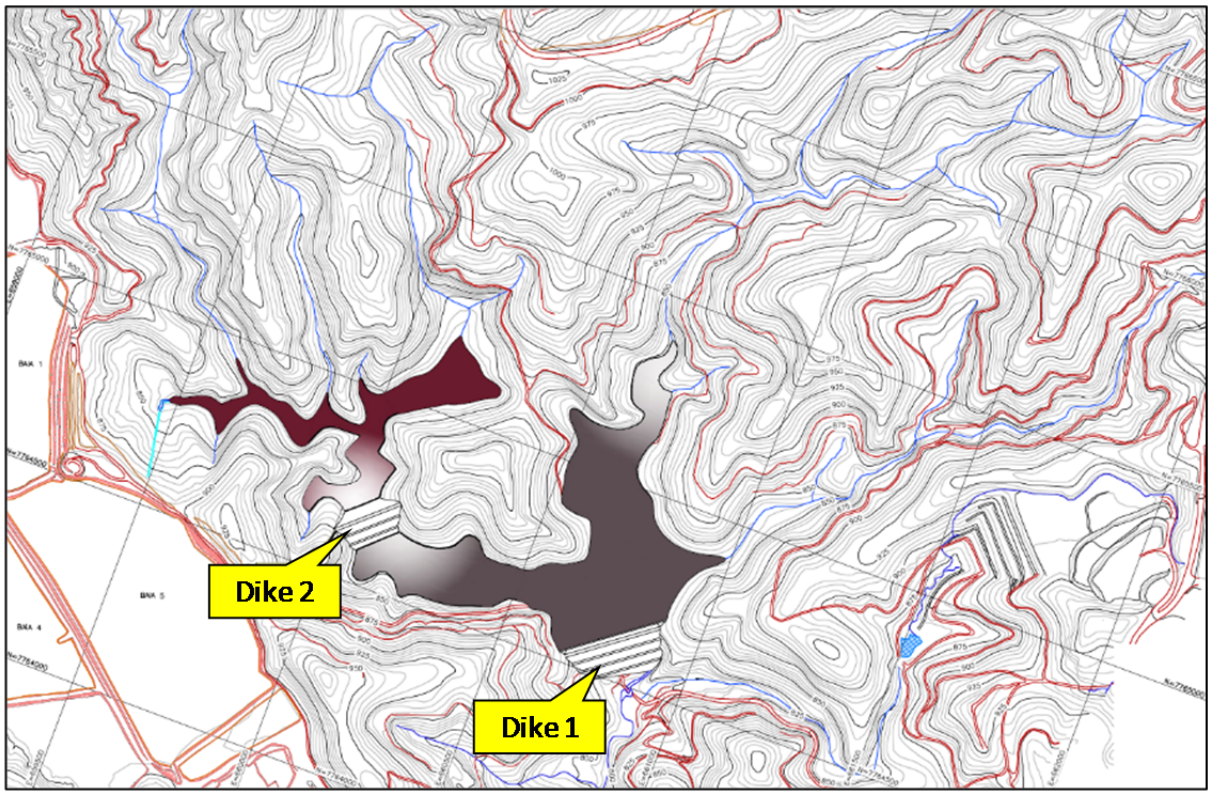

Figure 2-2 Fundão Dikes 1 and 2

Two alternative methods were considered for raising Dike 1 after filling the space between the two dikes with sand. One was *centerline* raising depicted on Figure 2-3 using compacted sand tailings in the downstream slope. This alternative was not selected, with the drained stack concept shown on Figure 2-4 adopted instead. The Dike 1 Starter Dam would be a conventional earthfill structure constructed of compacted saprolite soils to crest El. 830 m, with subsequent upstream raising with sand tailings to El. 920 m.

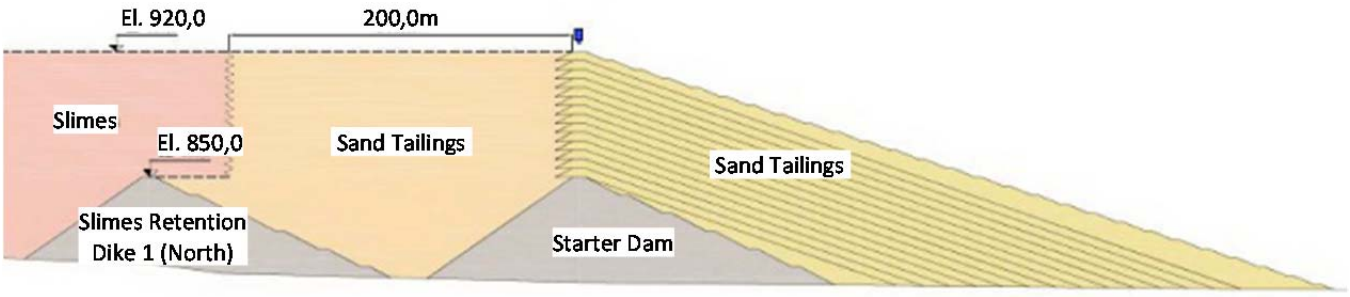

Figure 2-3 Centerline raising of Dike 1 considered but not implemented

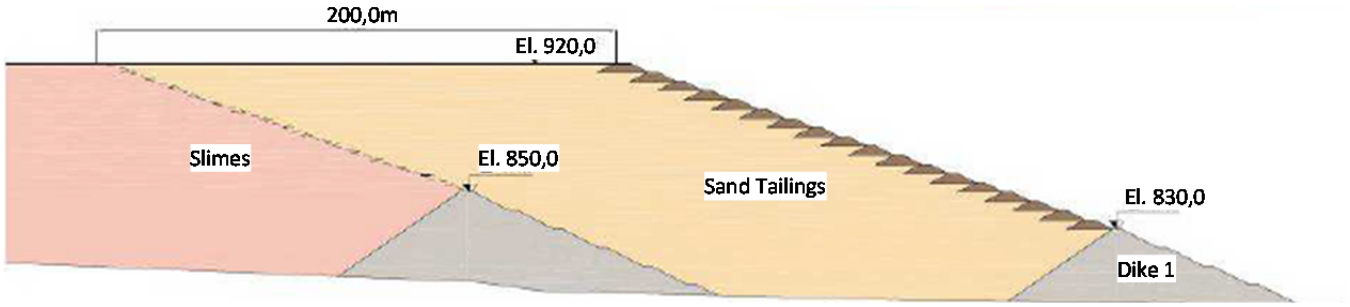

Figure 2-4 Upstream raising of Dike 1 by the "drained stack" concept

Thus, the Germano Buttress structure became the prototype for Fundão. Like its predecessor, the Dike 1 Starter Dam for Fundão would be underlain by a high-capacity base drain of gravel and rock. This would connect to another drain on the Starter Dam's upstream face, along with other complimentary drainage features—all to minimize saturation in the sand deposit behind it.

A remaining design consideration was how to evacuate surface water inflows from ordinary precipitation, floods, and discharged tailings slurry. This would be accomplished by two concrete galleries, 2 m diameter decant conduits of reinforced concrete extending beneath the tailings deposit and Dike 1 itself. The Main Gallery would be beneath the right abutment and the Secondary Gallery beneath the left as indicated on Figure 2-5.

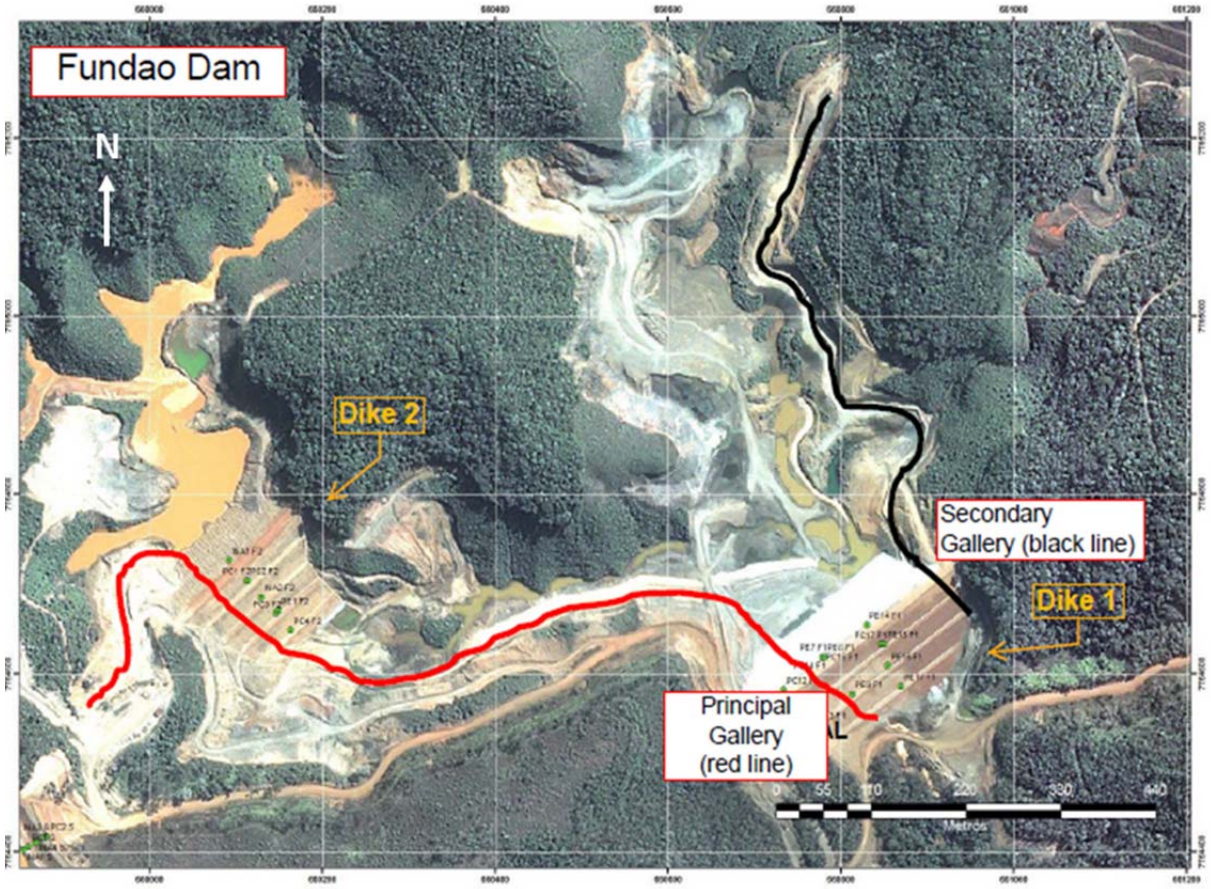

Figure 2-5 Main (Principal) and Secondary Galleries

In the Panel's estimation, this design concept for Fundão offered several advantages. With the dam located in a narrow valley constriction, the site was efficient, requiring a modest amount of dam fill for the storage volume achieved. Once above the valley floor, the reservoir expanded to provide large capacity relative to the area it occupied. But the concept also had certain vulnerabilities. The design was not adaptable to variation in the proportion of sands and slimes received. And most importantly, it depended on achieving adequate drainage of the sands.

2.2 The Piping Incident (2009–2010)

Construction of the Dike 1 Starter Dam, with its requisite drains and galleries, was completed in October, 2008. Shortly after full-scale discharge of sand tailings began on April 13, 2009, large seepage flows carrying fines appeared on the downstream slope above the main underdrain as shown on Figure 2-6, conditions symptomatic of the process of *piping* or *internal erosion*.

Figure 2-6 Internal erosion effects on downstream slope of Dike 1

An Emergency Action Plan in place for the dam at that time was immediately implemented. The reservoir was lowered, a berm was constructed over the affected portion of the dam slope, and provisions were made for holding the reservoir's remaining contents in the downstream Santarem Dam should failure occur. Engineering investigations later revealed serious construction flaws in the base drain and its filters, including a portion of the drain's outlet that had never been completed. This allowed water pressure within it to build until causing the slope to erode and slump.

As these investigations continued, the impending rainy season made it too late to fully restore the drainage features to their original condition, making it impossible to repair the damage. Instead, all of the drains were sealed. With this, the most important element of the original design concept became inoperative.

Additionally, the balance between sands and slimes crucial to the dam raising plan was changed. Filling of Dike 2 had begun earlier than anticipated, making its slimes level higher, not lower, than the projected sands in Dike 1. At the same time, reduction in pellet production reduced the amount of sand available while delivery of slimes continued. This required construction of yet a third dike between Dikes 1 and 2, designated Dike 1A, to provide additional slimes capacity. It was November 2010 before all of the measures made necessary by the piping incident were finally completed.

It remained to devise a new design concept to replace the old one.

2.3 The Recovery (2011–2012)

A revised design for raising Dike 1 to El. 920 m was first described in the 2011 Operations Manual, then updated in the 2012 version when the dam had reached crest El. 845 m. The central feature was the addition of a blanket drain on the surface of the tailings to replace the inoperative base drain below them. As shown on Figure 2-7, the new blanket drain was at El. 826 m just below the Starter Dam crest. Figure 2-8 depicts how the blanket drain would become embedded within the tailings during raising of the dam, intercepting seepage that could otherwise emerge on the slope and reduce its stability. In order to augment capacity for discharging the collected seepage flows, the blanket drain also contained slotted pipes called "Kananets®".

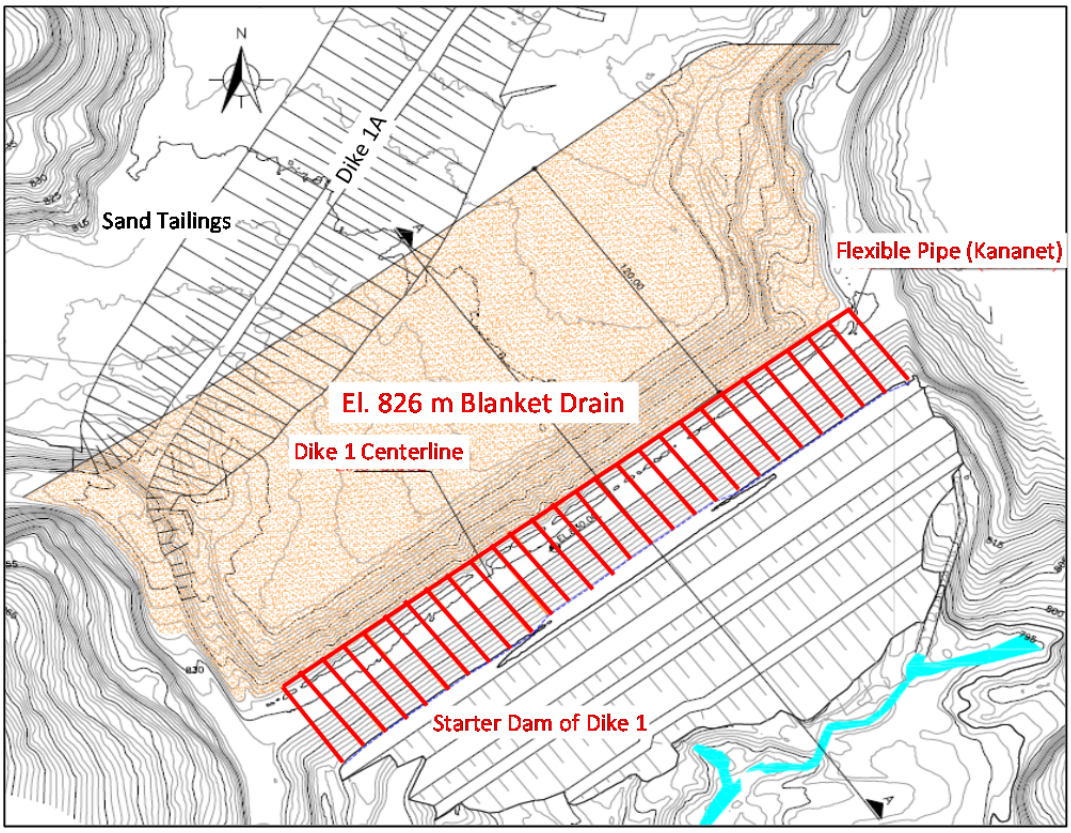

Figure 2-7 Blanket drain (plan view) on tailings surface at El. 826 m

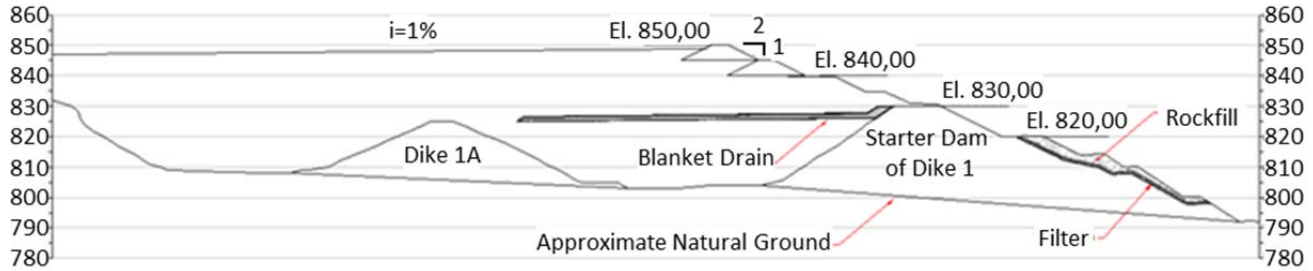

Figure 2-8 El. 826 m blanket drain (section) showing extent behind Dike 1

Comparing Figure 2-8 to Figure 2-1, it can be seen that the new blanket drain represented an attempt to replicate the drained-stack concept by providing drainage for the overlying tailings. But the sands below this drain would remain saturated, as would much of the tailings behind it. Once the base drain became inoperative, the control of saturation embodied in the original design concept could not be restored.

A requirement common to both the original and revised designs was that the sands be free-draining. To ensure that low-permeability slimes would not be deposited where they could impede this drainage, water containing the slimes had to be restricted from the area of sand deposition. To do so, a 200 m minimum beach width had been specified in the original 2007 Operations Manual, a provision retained in the 2011 and 2012 versions.

But as operation proceeded, this beach-width criterion was not consistently achieved. As explained in greater detail in Section 5.1.3, a new Overflow Channel was conveying water and slimes from Dike 2 to the rear of the Dike 1 reservoir, making beach management more difficult. No longer were the sands and slimes physically separated; the interface between them could only be controlled by adjusting the amount of sand spigotted from the dam crest in relation to the amount of slimes-laden water being introduced. As plotted on Figure 2-9 and documented in Appendix B, during much of 2011 and 2012, beach widths violated the 200 m minimum more often than not, at times encroaching to as little as 60 m from the crest.

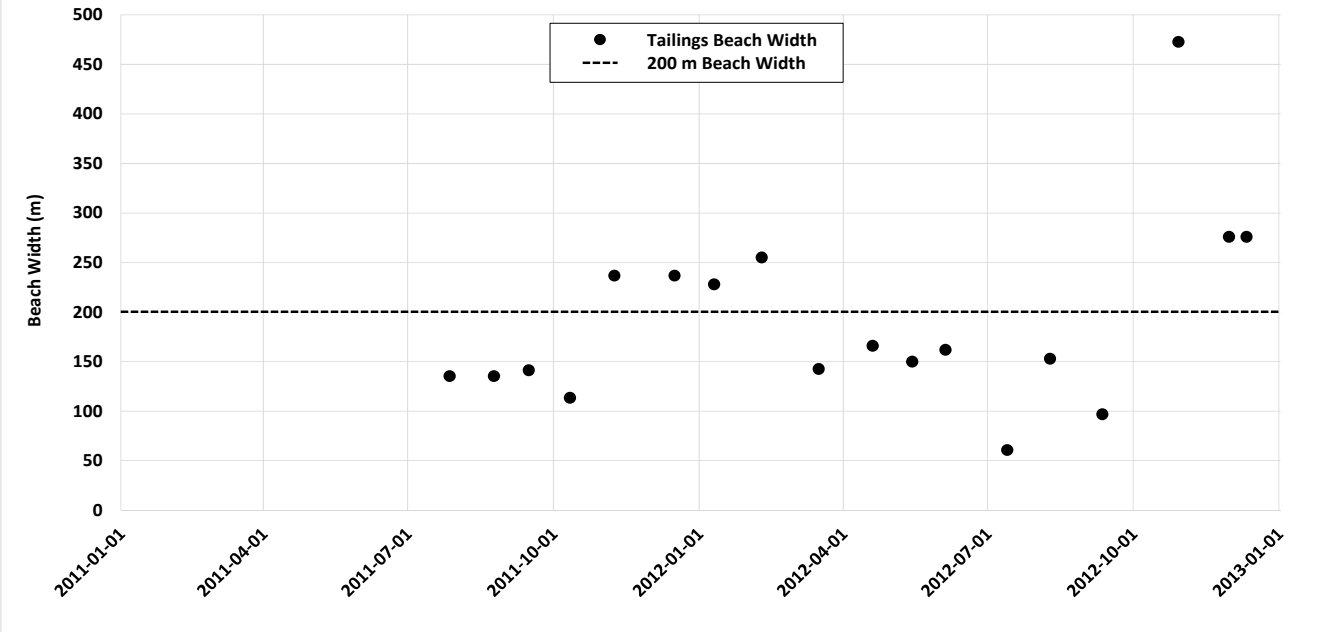

Figure 2-9 Monthly beach width measurements by Samarco, 2011-2012

2.4 The Setback (2012–2014)

Even as recovery from the 2009 Starter Dam piping incident remained underway, new conditions were developing that would directly affect the left abutment. The galleries shown on Figure 2-5 that evacuated water from the Fundão impoundment were found to be structurally deficient. This first

became evident for the Main Gallery at the right abutment when in July, 2010 a vortex appeared in the reservoir above it, showing that tailings and water were entering. Inspections revealed cracking and structural damage from foundation settlement and construction defects. Were either of the galleries to collapse, uncontrolled release of tailings from the reservoir or failure of the dam would be possible. So in January, 2011 a program of jet grouting was initiated to repair the Main Gallery and return it to service.

Similar conditions were discovered for the Secondary Gallery, and jet grouting was undertaken there as well. But by July, 2012, it was apparent that jet grouting had not cured these problems. After a sinkhole appeared in the tailings overlying the Secondary Gallery in November, 2012, repair efforts were abandoned. Instead, plans were made to plug both galleries by filling them with concrete from their outlets to a point beneath the projected crest of the 920 raise in order to prevent their collapse. Moreover, it was discovered from structural analyses that the Secondary Gallery could not support tailings higher than El. 845 m, some 10 m lower than the tailings already were at that time.

Because the height of tailings at the left abutment already exceeded the load capacity of the Secondary Gallery, the dam could not be raised any further over this area until the plugging operation was completed. As a temporary solution, it was decided to realign the dam at the left abutment by moving it back behind the portion of the gallery to be filled with concrete so that embankment raising could continue. This realignment shown on Figure 2-10 became the “setback”.

The setback would move the crest closer to the reservoir water and the slimes it contained, but it was anticipated that the dam would be quickly returned to its original alignment as soon as the plugging operations were done. At the same time, as will be explained more fully in Section 5, moving the crest back from its original alignment would also place it closer to, if not over, areas where beach encroachment and slimes deposition had already occurred.

Filling of the Secondary Gallery was completed on August 22, 2013. Meanwhile, dam raising had continued, with seeps that began to appear at the left abutment as early as June 26, 2012, at El. 845 m. In February, 2013, three-dimensional seepage modeling of the 920 raise showed that additional drains would be needed at the abutments if seepage breakout were to be prevented. This analysis was borne out when seepage, saturation, and cracking began appearing at several locations at the left abutment during 2013. The first such incident occurred in March at El. 855 m, followed by another seep in June at El. 855 m. Both were treated by constructing a drain. A third seep on November 15 appeared at El. 860 m and was accompanied by slumping of the slope shown on Figure 2-11. Another drain was provided to address this condition. On December 26, seepage occurred at El. 860 m and there was cracking on the left abutment crest at El. 875 m.

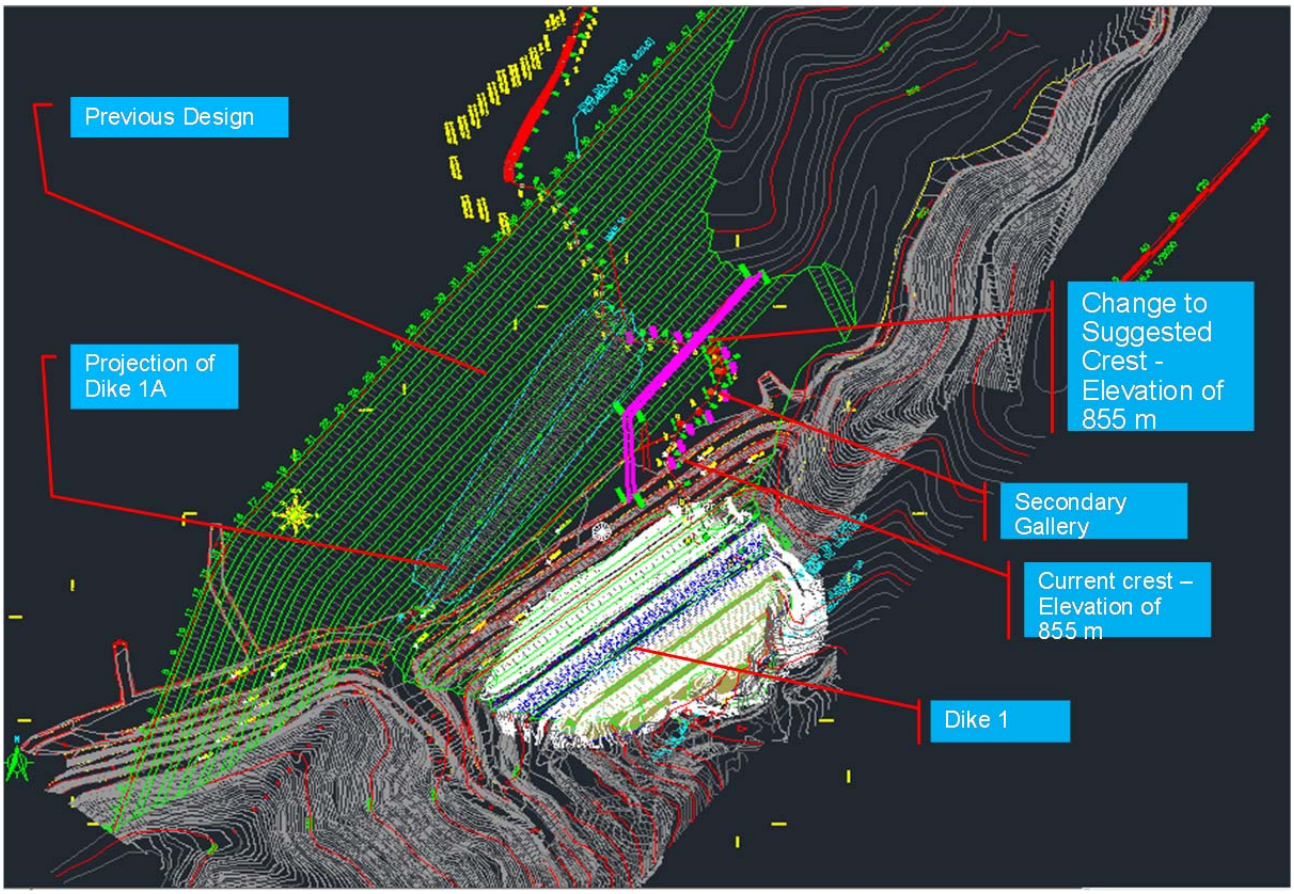

Figure 2-10 Left abutment setback proposed in June, 2012

Figure 2-11 November, 2013 seepage, cracking, and slumping at left abutment El. 860 m

Following these 2013 episodes of seepage and cracking, it had become apparent by January, 2014 that the El. 826 m blanket drain was no longer sufficient and that additional drains would be needed at the left abutment. This coincided with plans for an entirely new project for future raising of the dam by an additional 20 m from its then-planned maximum elevation of 920 m. Not only would this new El. 940 m raise add needed drainage features to the left abutment; it would eventually integrate them with an independent drainage system entering from the adjacent Grota da Vale and Fabrica Nova waste pile. As shown on Figure 2-12, the result would be what the Panel considers to be a complex and elaborate drainage system.

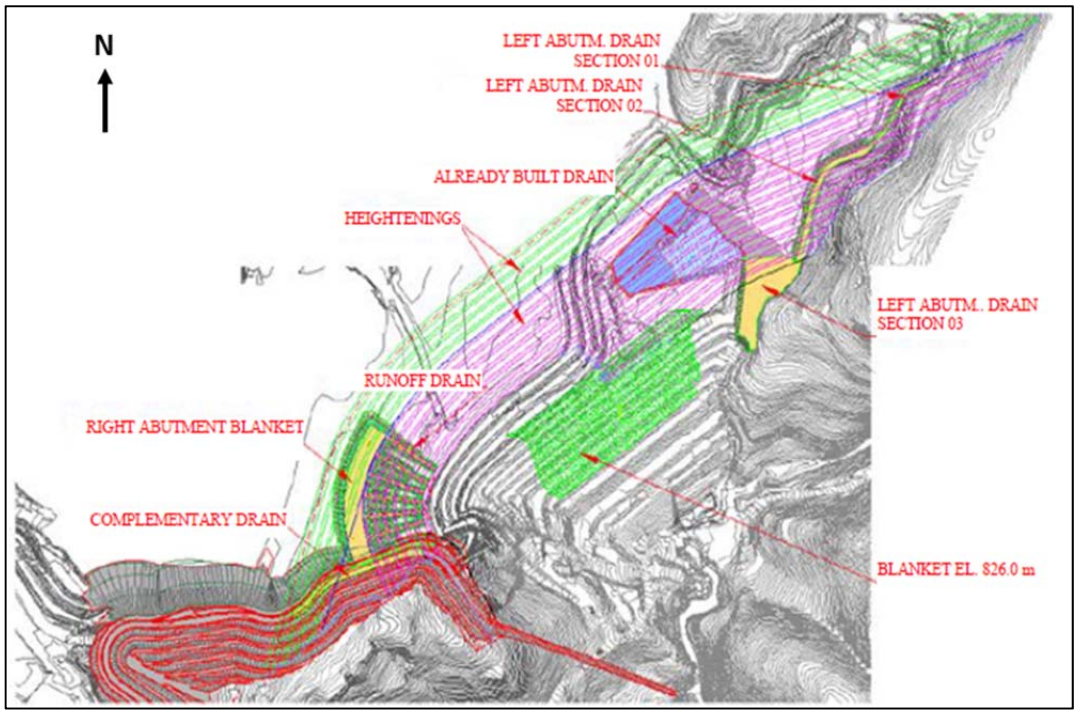

Figure 2-12 Proposed drainage scheme for 940 raise

The more immediate effect was that construction of additional drains in the left abutment area would require the setback to be maintained until they were completed. This entailed further delay in restoring the original alignment. As a result, the setback had risen at an average rate of 18 m/yr during 2013 and 3.0 m in September, a monthly record. In the 18 months since the setback decision had been made, the dam had grown by more than 20 m, and by January 2014 the Fundão Dam looked like Figure 2-13.

Figure 2-13 Fundão Dam in January, 2014 showing left abutment setback and adjacent Grota da Vale

2.5 The Slope Incident (August 2014)

Just after sunrise on August 27, 2014 a series of cracks much more extensive than anything that had occurred the previous year were discovered that extended behind the dam crest, emerged at the toe, and encompassed most of the slope as shown on Figure 2-14. Accompanying the cracking was shallow saturation at the toe, as shown on Figure 2-15.

Figure 2-14 August 27, 2014 cracking at left abutment setback

Figure 2-15 Cracks on dam crest and saturation at toe of slope, August 27, 2014

Stabilizing the slope became paramount, and construction was quickly mobilized to do so. Within two weeks, the reinforcement or "equilibrium" berm shown on Figure 2-16 was completed.

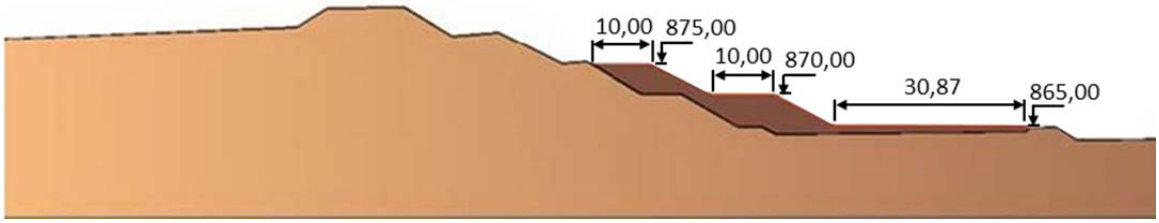

Figure 2-16 Reinforcement berm for left abutment setback, August, 2014

Construction of the left abutment drain was still ongoing, and it was not until a year later, August, 2015, that the drain was completed and fill placement over the area it covered could resume.

October, 2015 was a period of intense activity on the left abutment. The dam crest was being raised to El. 900 m, preparations were being made for cyclone sand placement on the El. 875 m bench, while at the same time the reinforcing berm was being extended by raising the El. 875 m and El. 895 m benches. The net result was that the monthly increase in crest height of 2.9 m—an annualized rate of rise of 35 m/yr—rivaled the record of 3.0 m set in 2013.

2.6 The Earthquakes (November 5, 2015)

Explosions are detonated every day at mines throughout the region, so the small-magnitude seismic events they produce are not unusual. At the same time, while larger earthquakes are rare in Brazil, small earthquakes in Minas Gerais are relatively common. Either way, the tremor on the afternoon of November 5, 2015 was not unprecedented.

According to felt reports at the plant about 2 km from Fundão, shaking was strong enough to cause a computer to fall from a tabletop, but not so strong as to produce structural damage other than minor cracking.

Detailed analysis of instrumentally-recorded events and mine records show that on November 5, 2015, two blasts occurred at a nearby mine within seconds of each other just after 1PM. This was almost three hours before the failure. Later at around 2:15PM a series of three small-magnitude earthquakes occurred over a period of four minutes on the afternoon of November 5, 2015. They preceded the failure by some 90 minutes with the time sequence shown in Table 2-1 below and occurred almost directly beneath the Fundão deposit.

Table 2-1 Pre-failure earthquakes and mine blasts on November 5, 2015 (E.g., Atkinson 2016)

Local time	Moment Magnitude M_w	Distance from Fundão	Identification
1:01:49PM	2.1	2.6 km	mine blast
1:06:06PM	2.3	2.6 km	mine blast
2:12:15PM	2.2	< 2 km	earthquake (foreshock)
2:13:51PM	2.6	< 2 km	earthquake (main shock)
2:16:03PM	1.8	< 2 km	earthquake (aftershock)
3:45PM			*Dam failure*

The implications of the earthquakes will be discussed in Section 6.

2.7 The Collapse (November 5, 2015)

On the afternoon of November 5, 2015, most activity was on or near the right abutment where drains were being constructed, placing several workers in a position to see along the length of the dam crest. On the left abutment, fill was being placed on the El. 875 m bench of the setback in preparation for start-up of cyclone sand placement. Figure 2-17 shows the locations of eyewitnesses engaged in these and other activities at the time of failure.

Figure 2-17 Eyewitness locations on the afternoon of November 5, 2015

The first thing noticed by many workers on the dam, including those at locations 4 and 6, was a cloud of dust drifting up from the left side heralding the failure. A worker at 4 watched as waves developed in the central portion of the reservoir, accompanied by cracks forming on the left side and blocks of sand moving up and down on the left abutment setback. Another worker at 5 saw a crack open up along the crest of the left abutment setback then propagate in both directions, beginning closer to the left abutment, reaching it, then progressing to the right. And at location 9 at the toe of the dam, witnesses experienced an avalanche of mud-like tailings cascading down from the left abutment, but no movement of the starter dike itself.

These observations establish that failure originated at the left abutment setback and that the Starter Dam did not participate in the failure mechanism. However, these workers on the dam crest had been unable to see precisely how and where the failure began, and by the time they made these observations the first stages of failure were already well advanced.

Other observers at the left abutment had a closer view of the developing failure sequence. Workers at locations 1 and 2 were the first to see the failure initiate near the left abutment drain where they were standing, placing the time at 3:45PM. Here, a sudden jet of dirty water “exploded” out of the drain. The first movement and cracking was also reported at the exposed drain and along the adjacent edge of the plateau, placing the exit of the rupture surface at or around El. 857 m. A worker at 1, who was standing on the plateau, felt it begin to move beneath him and crack around him, detaching from the setback slope and moving downstream.

Next to move was the lower slope of the setback. Eyewitnesses at 2, 3, and 5 describe slope movement having propagated “from the bottom up” on the lower benches, not from the crest down, placing the seat of movement at lower elevations. A worker at 3 observed a small bulldozer on the El. 875 m bench moving or being pushed outward, placing the head of the incipient failure at or above this elevation. At first, the lower slope progressed slowly forward “like a snake.” Remaining intact and moving as a unit, it then bulged, becoming grossly distorted as movement accelerated, coming down “like a wave,” or as if it were “melting”. Subsequently, a witness at 3 characterized the violent turbulence of the fluidized mass as “going in somersaults” downstream.

Taken together, these eyewitness observations can be synthesized into the sequence of events at failure initiation portrayed on Figure 2-18.

Figure 2-18 Failure initiation sequence

By the time the events on Figure 2-18 had occurred, the growing failure would have become apparent to the observers on the crest at locations 4, 5, and 6 as it progressed back behind the crest and into the reservoir. Only then did the central and right sides of the dam begin to disintegrate.

A conveyor crossing the Fundão stream channel about 1300 m downstream from the offset crest stopped functioning at 3:49PM, four minutes after failure is reported to have begun at 3:45PM. From this, it is ascertained that the flowslide was moving at about 11 m/s by the time it reached the conveyor. It is calculated that 32 million m^3 of tailings was lost, representing 61% of the impoundment contents—an unusually high proportion in relation to tailings dam failure statistics. In a matter of hours, the Fundão Dam was gone, and what once had been Figure 2-19(a) became Figure 2-19(b).

Figure 2-19 Fundão damsite and reservoir (a) before, (b) after failure

3 WHAT DID THE PANEL DO?

3.1 Diagnostic Strategy

The methodologies adopted and activities conducted during the Panel's Investigation were important to its outcome. The instruction to the Panel in its Terms of Reference was to determine the immediate cause or causes of the breach of the Fundão Tailings Dam on November 5, 2015. This is fundamentally a diagnostic exercise as reflected in the overall framework adopted by the Panel. The Panel's diagnostic strategy consisted of three parts:

1. *Hypothesis formulation.* Candidate failure modes were identified based on known causes of tailings dam failures as they pertain to specific conditions of the Fundão Dam.
2. *Hypothesis screening.* The candidate failure modes were screened using a process of elimination to arrive at one or more that were most consistent with the evidence.
3. *Hypothesis testing.* The surviving failure modes were tested for their ability to predict conditions that occurred at times and locations other than those on November 5, 2015 at the left abutment.

With regard to the third item of hypothesis testing, the Panel developed criteria that its causation conclusion should meet. These took the form of three questions:

1. **Why did a flowslide occur?** That the failure occurred by flowsliding is self-evident but not by itself informative. Any explanation of the failure must go beyond this to determining the events, conditions, and mechanisms that allowed flowsliding to occur.
2. **Why did the flowslide occur where it did?** In principle, there were many places on the Fundão Dam where failure might have occurred. The failure hypothesis must explain what was different about the left abutment that caused the failure to occur there and not at some other location.
3. **Why did the flowslide occur when it did?** Failure occurred when the embankment at the left abutment reached El. 898 m following a series of small earthquakes. The failure explanation must establish why failure did not occur at some previous time at lower elevation and the relationship, if any, between the failure and the earthquakes. The hypothesis must also explain why flowsliding did not occur in association with the cracking incident of August, 2014.

As the tests of the Panel's hypothesis, these three questions constitute the central topics of the remainder of this report and the framework around which it is built.

3.2 Investigation Methodology

The Panel also followed a systematic structure in its investigative efforts. The elements of the Investigation and the tasks that comprised them are described below, with reference to the related appendices.

- **Reconstruction of the dam and its properties.** Most if not all of the key physical evidence was destroyed when the dam washed downstream with the failure. A virtual representation of the dam and its internal composition therefore had to be reconstructed through a lengthy and painstaking process consisting of:
  - *Compilation of digital topographic data and imagery in GIS format*. This allowed the progression of dam raising and tailings deposition to be tracked over time. The methodology adopted is described in Appendix A.
  - *Reconstruction of design, construction, and operational history*. This was done through assembly and interpretation of documents, photographs, and aerial imagery, as described in Appendix B.
  - *Subsurface exploration and laboratory testing*. This incorporated both pre-failure data and independent Panel field investigations at surrogate locations. It allowed estimation of pre-failure engineering properties of dam materials, as contained in Appendices C and D.
- **Compilation of instrumentation data.** The dam contained a large number of instruments that measured internal water pressures, flows, and movements. Together, this data provides a record of the dam's engineering behavior, allowing trends and changes to be tracked throughout its life. Instrumentation data is contained in Appendix E.
- **Synthesis of eyewitness interviews.** The Fundão failure was witnessed by a large number of people at different locations on and near the dam. Their accounts are of content and value unusual for dam failure investigations of this kind and provide insight into the processes that were taking place during the hours and minutes leading up to the failure.
- **Analytical studies.** With the reconstructed dam, instrumentation data, and eyewitness accounts in place, the Panel was able to simulate the operation of potential failure mechanisms and related processes through a variety of numerical modeling techniques:
  - *Consolidation modeling.* This was to evaluate the effects of loading rate on pore pressure development and is described in Appendix F.
  - *Seepage modeling.* This provided information on internal flow and pressure conditions at times and locations where measured instrumentation data was not available. Seepage modeling is described in Appendix G.
  - *Stability analysis.* This provided the calculated degree of embankment stability under various conditions at various times and is found in Appendix H.
  - *Deformation analysis.* Closely linked to stability, deformation modeling provides further insight into failure-related processes and mechanisms as contained in Appendix I. The deformation analysis is central to identifying the causative liquefaction trigger mechanism, and the concluding section of this report is devoted to the development of this topic.
  - *Dynamic response analysis.* This numerically simulates earthquake shaking and is found in Appendix J.
- **Seismological studies.** Conducted independently from the Panel's Investigation, seismological studies provided key input that is contained in a separate report.

3.3 Potential Failure Modes and Triggers

The Panel considers that the evolutionary character of its design and operation makes the Fundão Dam extraordinarily complex. This is reflected in the large number of potential failure modes, which in turn makes a structured process for their evaluation mandatory. Appendix K details how the approach to hypothesis formulation and screening of Section 3.1 was implemented. First, the following potential failure modes were considered:

1. overtopping;
2. internal erosion;
3. Starter Dam foundation or embankment sliding; and
4. liquefaction.

All but liquefaction were ruled out as being inconsistent with physical evidence and/or eyewitness accounts.

Amplifying on liquefaction as the cause of flowsliding, the second stage was to evaluate liquefaction triggering mechanisms, again adopting the same hypothesis formulation and screening process. Here, the Panel used fault trees to structure the assessment in real time, modifying them as the Investigation unfolded. Applied as a heuristic aid rather than a reliability application, formal fault tree symbology was not necessary or adopted. The Panel's final fault tree for liquefaction triggering is shown on Figure 3-1.

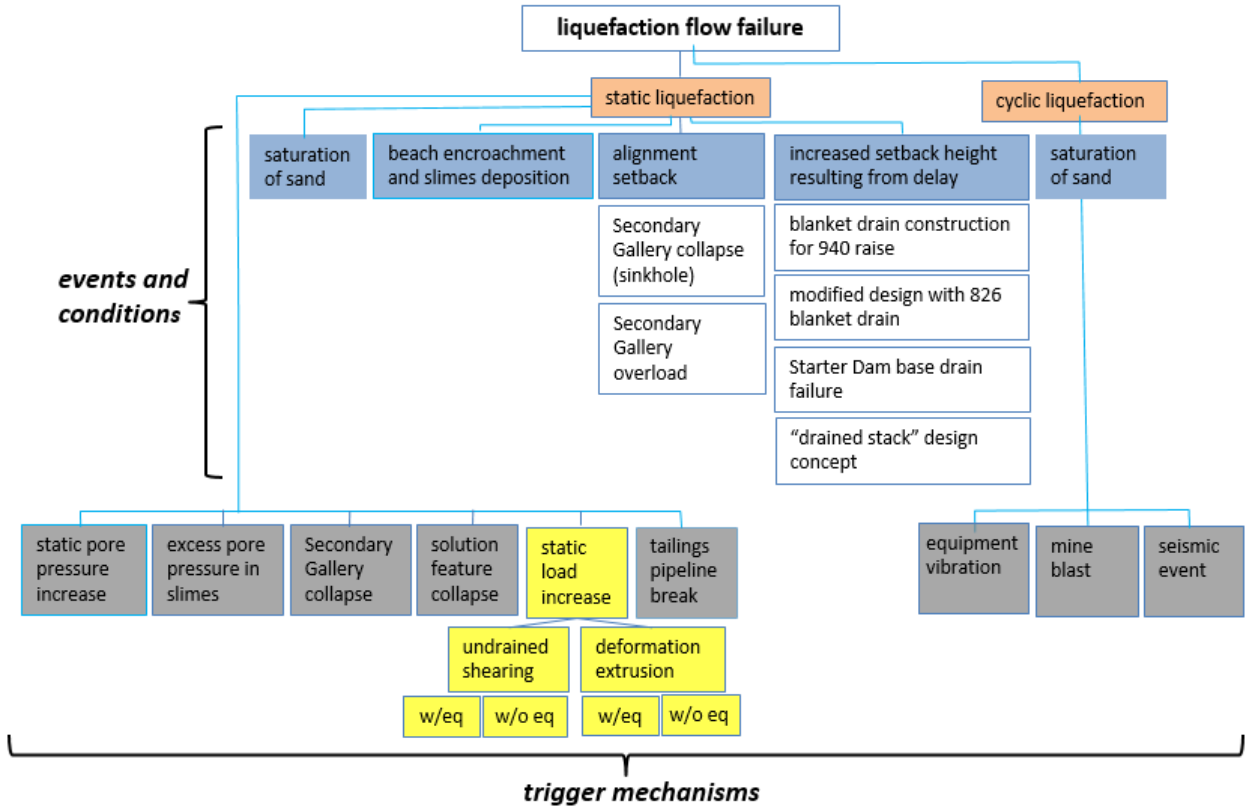

Figure 3-1 Fault tree for liquefaction triggering

The top event on Figure 3-1 is liquefaction flow failure. The next tier of events represents the two fundamental liquefaction processes: static and cyclic, either of which might have been operative. In this representation, cyclic-induced liquefaction flow failure is distinct from cyclic pore pressure contribution to static liquefaction.

The bottom tier of candidate initiating events represent liquefaction trigger mechanisms, and those shaded in grey were ruled out for reasons developed in Appendix K. These are:

- cyclic liquefaction:
  - equipment vibration;
  - mine blasting; and
  - seismic-induced.
- static liquefaction:
  - static pore pressure increase;
  - excess pore pressure in slimes;
  - Secondary Gallery collapse;
  - solution feature collapse; and
  - tailings pipeline break.

The surviving liquefaction trigger mechanism is static load increase, shown in yellow on Figure 3-1 with its two subsidiary processes: undrained shearing and deformation-related extrusion. Both of these might be operative either with or without cyclic pore pressure contribution from the November 5, 2015 earthquake series.

Also important on Figure 3-1 are the antecedent events and conditions shaded in blue that allowed or promoted static liquefaction at the left abutment. These are: (1) saturation of the sand; (2) water encroachment that allowed slimes deposition on the tailings beach; (3) the alignment setback; and (4) the increased height of the setback resulting from continued raising of the dam.

These four factors are central elements of the following sections of this report.

4 WHY DID A FLOWSLIDE OCCUR?

Determining why a flowslide occurred necessarily involves considering the conditions required for liquefaction, the first of which is saturation. In this regard, Section 2 presented the original "drained stack" design concept, that in the view of the Panel was not in principle amenable to liquefaction, and explained design changes that brought about an extent of saturation not anticipated in that concept. The new design allowed saturated conditions within the tailings, as evidenced by the extensive system of piezometers intended to measure it and limiting criteria established to evaluate it.

Another requirement for liquefaction concerns the properties of the materials involved, in this case sand tailings. This section shows how their void ratio—a measure of their propensity to expand or contract during shearing—influenced their susceptibility to liquefaction during the kind of rapid failure that occurred. Along with this is a related requirement for liquefaction: a reduction in strength during rapid shearing that produces flow behavior.

The Panel found no credible pre-failure assessment of liquefaction for the Fundão Dam in any of the documents it reviewed. Nor did it find any boring or cone penetration test (CPT) penetrating the full depth of the tailings that would have made such an assessment possible. For these reasons, the Panel has relied on its own analyses to determine why a flowslide occurred, the first test it has imposed on its explanation of the failure.

4.1 Strength Behavior

When load is applied to soil particles as a shear stress, *shearing* is said to occur. If these particles are in a tightly-packed arrangement—such as dense sands or stiff clays—the soil particles must first move apart to order to move past each other during shearing. This produces an increase in volume of the soil mass, and such soils are said to be *dilatant*. Generally speaking, dilatant soils are strong, which is why mechanical compaction is commonly used to achieve this condition.

By contrast, when shearing a loose particle arrangement—for example, loose sands or soft clays—the opposite occurs. The particles move together and the soil mass compresses. Soils displaying this tendency for volume decrease are called *contractive*. Hydraulically-placed and uncompacted materials such as tailings are often contractive.

When the soil mass is saturated, the spaces between the particles, or *voids*, are filled with water. If the soil is contractive and shearing occurs, the water may inhibit the particles from moving together so that the water itself carries part of the load. This produces pressure in the water, or *pore pressure.* But since water has no strength, the strength of the saturated soil mass can be reduced. Whether or not this occurs depends on whether or not the water escapes from the voids. And this, in turn, depends on yet another necessary condition for flowsliding—the rate of shearing.

Shearing a contractive, saturated soil slowly enough for pore pressure to dissipate as fast as it is generated produces a *drained* condition. Pore pressure does not develop and the soil retains its strength. On the other hand, if shearing occurs too rapidly for pore pressure to dissipate, *undrained* shearing is said to occur. In the case of Fundão, the failure developed within minutes and clearly occurred under undrained conditions. But in addition, the undrained strength of contractive sands

decreases markedly under the large strains imposed during flowsliding. It is this characteristic that gives flowslides their speed and mobility.

4.2 Tailings Volume Change, Undrained Strength, and Liquefaction

Different loading conditions can induce static liquefaction. Figure 4-1 provides stress paths for test data on Fundão sand tailings, where p´ is mean effective confining stress and q is shear stress. Stress paths for two tests are shown, both consolidated to the same stress at the start of shearing.

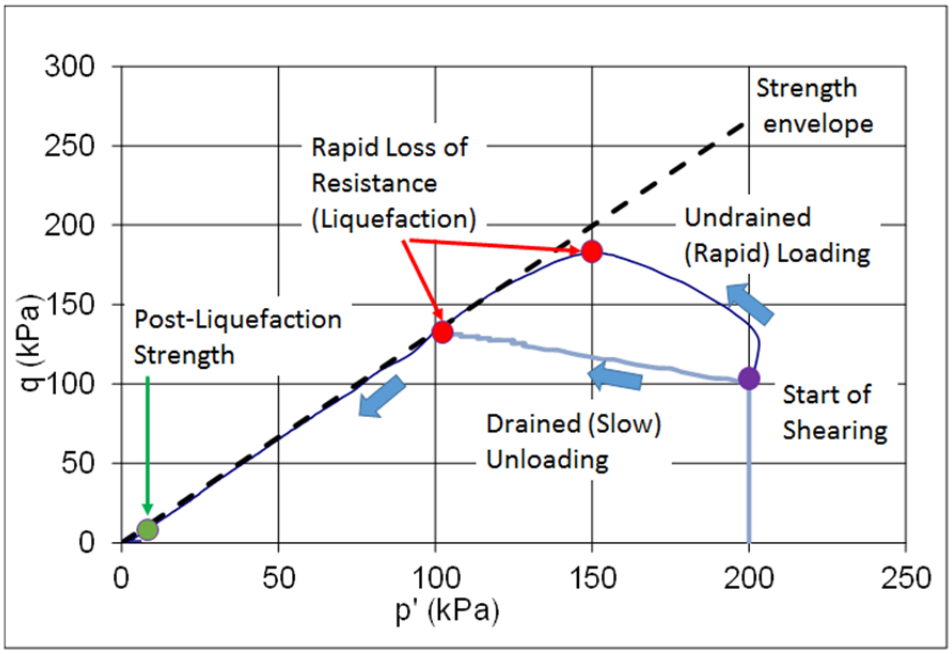

Figure 4-1 Stress paths for undrained loading and drained unloading of sand, Fundão test data

In the first test, conventional undrained loading is applied to simulate rapid shearing. When the stress path reaches the strength envelope it reaches a condition of liquefaction. As shearing resistance reduces due to changes in pore pressure, it progresses downward along the envelope and strength rapidly diminishes until arriving at a very low *post-liquefaction* strength.

The second test represents a different stress path central to understanding the Fundão failure. Instead of being loaded, the sample is laterally unloaded to simulate horizontal spreading. In addition, the unloading process is conducted slowly under drained conditions. As seen on Figure 4-1, the behavior on reaching the strength envelope is the same as before: liquefaction occurs, strength rapidly decreases, and the same post-liquefaction value results. In both tests, the loss of strength accompanying liquefaction is dramatic and nearly instantaneous, so much so that this behavior is sometimes referred to as *collapse*. The parallels between this kind of behavior in the laboratory and that which occurred during the Fundão failure are evident.

Thus, if the necessary conditions are present, liquefaction can occur under either slowly-imposed or rapidly-imposed changes in stress that can be produced by either loading or unloading. The essential

point is that it is the rate of shearing, not necessarily the rate of loading, that controls liquefaction of contractive materials, and the change in shear resistance derives from the intrinsic properties of the soil.

The most important such property is the tendency for volume change during shearing. This depends on two factors: first, how loose or dense the soil is, as characterized by its *void ratio*; and second, the level of stress it experiences. Figure 4-2 plots void ratio e versus effective stress p´. At any given effective stress, there exists some void ratio at which there is no tendency for either increase or decrease in volume during shearing. The *critical state line* (CSL) is the locus of these points and delineates the boundary between dilatant (volume increase) and contractive (volume decrease) conditions.

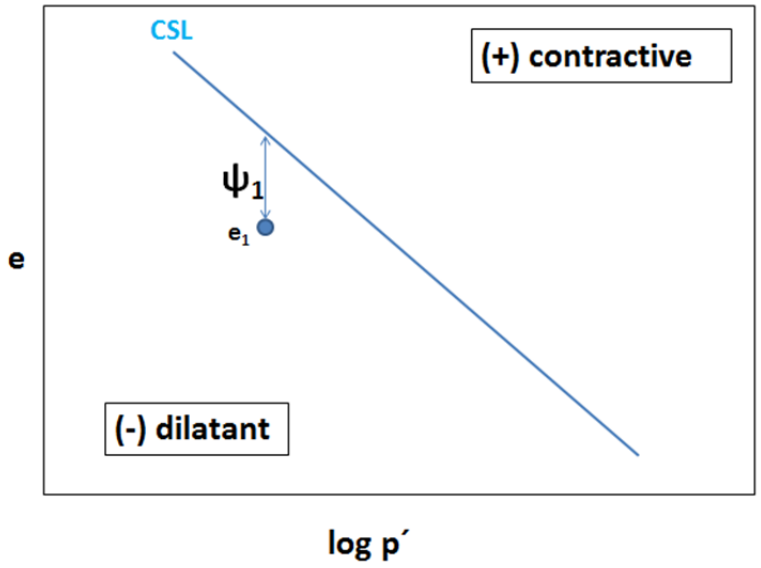

Figure 4-2 Definition of state parameter

The degree of contractiveness or dilatancy can be characterized by the *state parameter* ψ, shown on Figure 4-2 for some existing void ratio e_1. State parameter is defined as the difference in void ratio between e_1 and the void ratio on the CSL at the same mean effective stress. The magnitude of ψ, or the vertical distance of e_1 from the CSL, expresses the degree of contractiveness or dilatancy at that void ratio, with a negative sign convention for dilatancy and positive for contractiveness.

The relationships shown on Figure 4-2 are for constant stress. Figure 4-3 shows what happens when stress increases, for example when loading from embankment raising is imposed.

At the initial void ratio e_1 the tailings are dilatant with negative ψ_1, meaning that they act like a dense sand from an undrained strength standpoint. Under imposed loading and effective stress increase, compression occurs and e_1 reduces to e_2 in Figure 4-3. Now e_2 lies on the other side of the CSL and state parameter ψ_2 has positive sign. Thus, a material that initially had the dilatant behavior of a dense sand takes on the contractive characteristics of a loose sand as a result of the increased stress it now experiences.

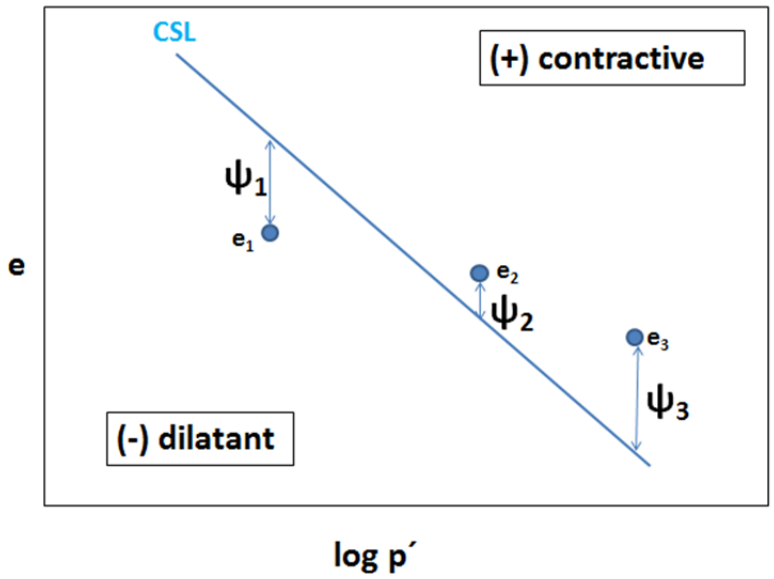

Figure 4-3 Change in state parameter for increasing stress

As loading continues and effective stress increases still more, e_2 reduces to e_3 as the result of further compression, and the magnitude of ψ_2 increases to ψ_3. Thus, not only can continued loading transform a dilatant material into a contractive one, it can also increase its degree of contractiveness.

These principles are applied to the Fundão tailings sand on Figure 4-4 that provides a statistical summary from Appendix C of CPT data on sand tailings obtained by Samarco prior to the failure in early 2015. The five CPTs were located along two transects on the Fundão tailings beach, one behind the left abutment setback and another in the central portion. While in theory contractive materials are those having $\psi > 0$, in practice $\psi > -0.05$ is often adopted as the boundary (Shuttle and Cunning 2007).

Shaded areas on Figure 4-4 indicate relative proportions of contractive material. Upper and lower histograms are for the left abutment and central transects, respectively, at locations given in Appendix C.

On this basis, approximately 70% to 80% of the sand tailings within 75 m of the dam crest are indicated to have been contractive, and 95% or more at greater distance up to 180 m. This demonstrates that the majority of hydraulically-discharged Fundão sand tailings satisfied the contractiveness requirement for liquefaction flowsliding. This is confirmed by CPT-based liquefaction criteria developed by Robertson (2010) on Figure 4-5 that supplements state parameter with liquefaction field case histories. These include flow liquefaction of the Nerlerk offshore berm for the encircled point labeled 19, 20, and 21, a case that figures prominently in the Fundão assessment as subsequently explained in Section 6.

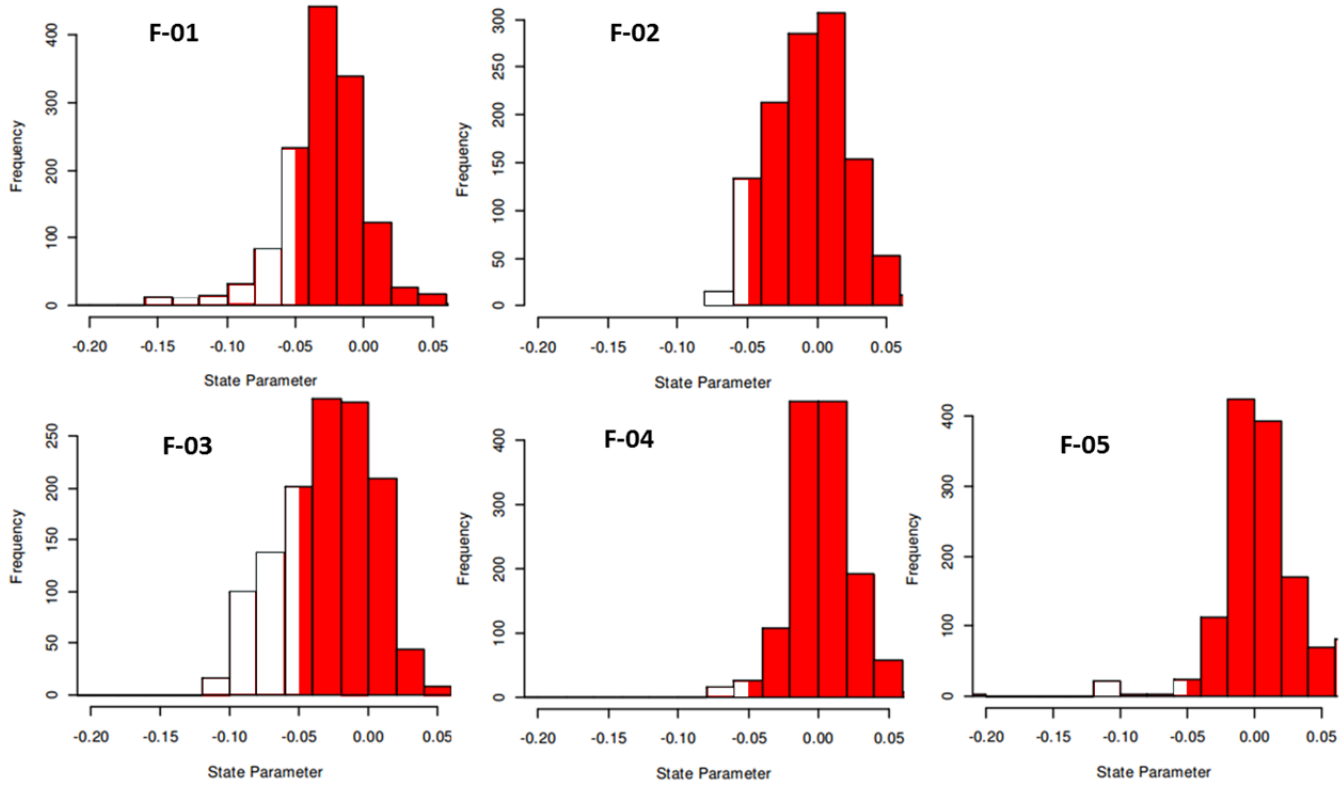

Figure 4-4 Histograms of state parameter for Fundão sand tailings

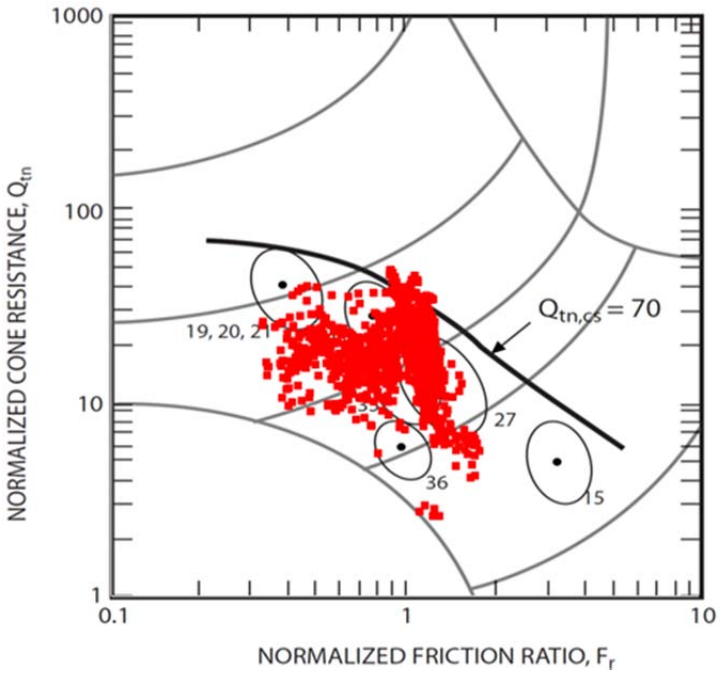

Figure 4-5 Robertson (2010) liquefaction criterion for Fundão CPT F-02 data

The 2015 Fundão CPT data also demonstrate the propensity for reduction in undrained strength of the sand tailings subject to the large deformations that accompany flowsliding. This can be shown by comparing undrained yield (peak) strength to critical (also known as residual or post-liquefaction) undrained strength. Figure 4-6 applies the CPT correlations of Sadrekarimi (2014) for undrained yield strength in simple shear and critical undrained strength.

Figure 4-6 shows that mean undrained strength ratio dropped from 0.21 before the flowslide to 0.07 during it, demonstrating that the Fundão sand tailings were susceptible to significant loss of strength.

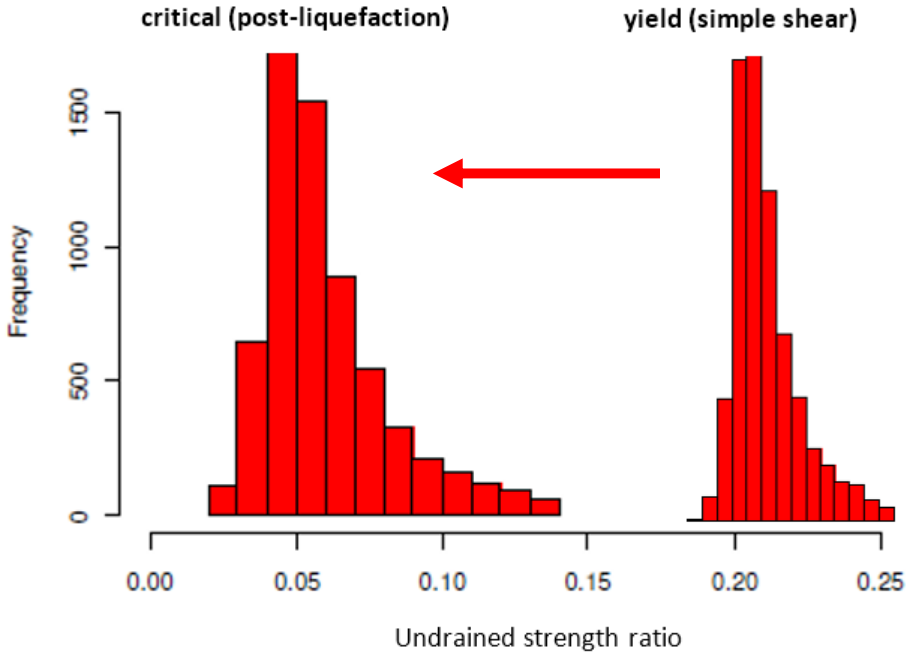

Figure 4-6 Yield (pre-flowslide) and critical (post-flowslide) undrained strengths for aggregated 2015 Fundão CPT data

4.3 Saturation

Saturation is another necessary condition for liquefaction flowsliding. It is useful to chart how saturation conditions of the Fundão Dam changed over time in response to events during the dam's evolution. To begin with, and as explained previously in Section 2.1, the "drained stack" concept of the Germano Buttress provided the model for the original Fundão design. With its high-capacity base drain extending beneath the dam and the sand tailings behind it, the aim was to reduce saturation and the accompanying effects on stability.

The original concept became inoperative after the damage sustained to the Starter Dam in the 2009 piping incident. The revised design that emerged relied instead on a blanket drain at El. 826 m near the top of the sand that had nearly filled the Starter Dam by that time. The El. 826 m blanket drain, which included the Kananet® pipes, was called upon to carry nearly all of the seepage as the dam grew higher and the impoundment larger with time. It became increasingly unable to do so, resulting in expanding volumes of saturated tailings.

The progression of conditions that promoted saturation is best illustrated by the following series of figures that integrates this information. Figure 4-7 shows the blanket drain in July, 2011, shortly after its completion the previous November. At that time the drain spanned the entire width of the Starter Dam. In this early configuration—which most closely resembled the original drained-stack concept—the impoundment size was limited and the drain was beneath the discharged tailings where it could intercept downward drainage to maximum effect.

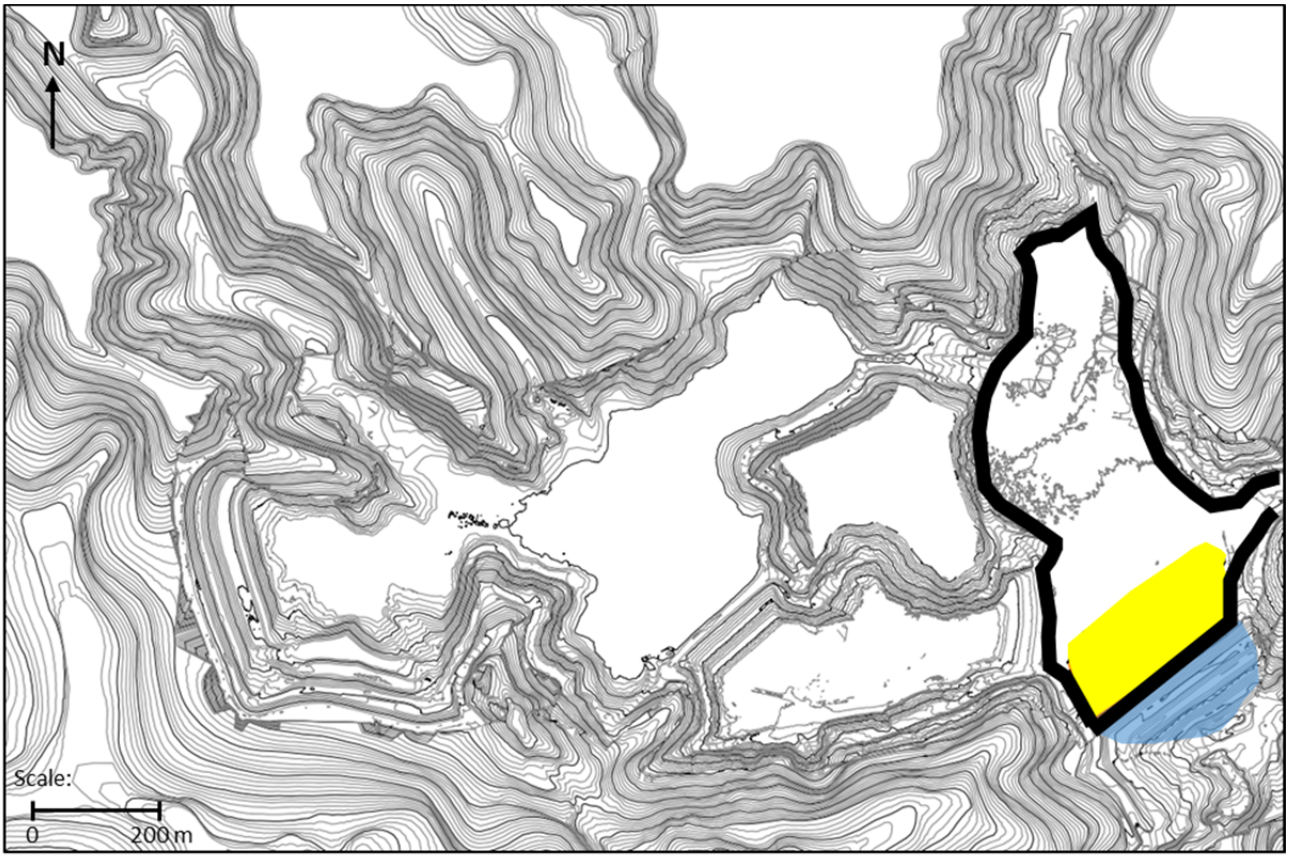

Figure 4-7 July, 2011 configuration showing El. 826 m blanket drain (yellow), Starter Dam embankment (blue) and impoundment outline

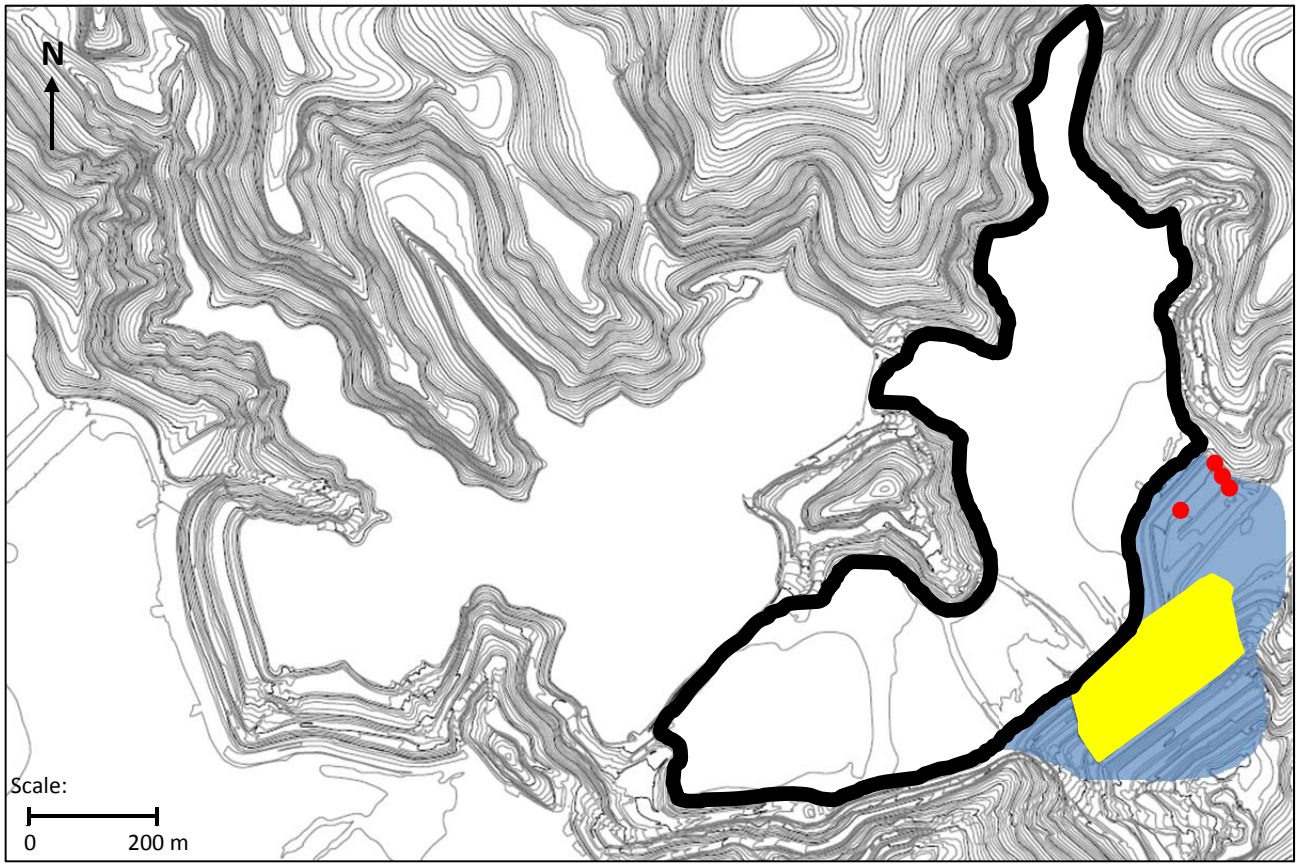

Figure 4-8 August, 2013 configuration showing El. 826 m blanket drain, raised dam, impoundment outline, and left abutment seeps (red dots)

Figure 4-8 shows that by August, 2013 both the embankment and impoundment had widened considerably as the dam grew higher, expanding beyond the limits of the drain on both sides. This had the effect of funneling seepage flow into the much narrower drain, and in the process raising the saturation level in the tailings. At the same time, the impoundment was moving upstream and becoming more distant from the drain as upstream dam raising progressed, also increasing the volume of saturated tailings.

With the left abutment setback by then in place, seeps appeared at El. 855 m in March and June, 2013 as the rising saturation reached the tailings surface, and again in November and December at El. 860 m. This shows that the saturation level at the surface of the left abutment rose some 5 m in elevation during the course of 2013. Localized drains constructed to treat these seeps had mostly near-surface effects, preventing further seepage breakout on the embankment face but not significantly reducing saturation in the tailings mass behind them.

Figure 4-9 shows that by August, 2014 the impoundment had nearly doubled in size, principally on the right side. With this enlargement came a seep on the right abutment at El. 855 m in July, followed by another in January the next year. As upstream raising continued, the impoundment became even further removed from the drain, expanding the volume of saturated tailings behind it still further.

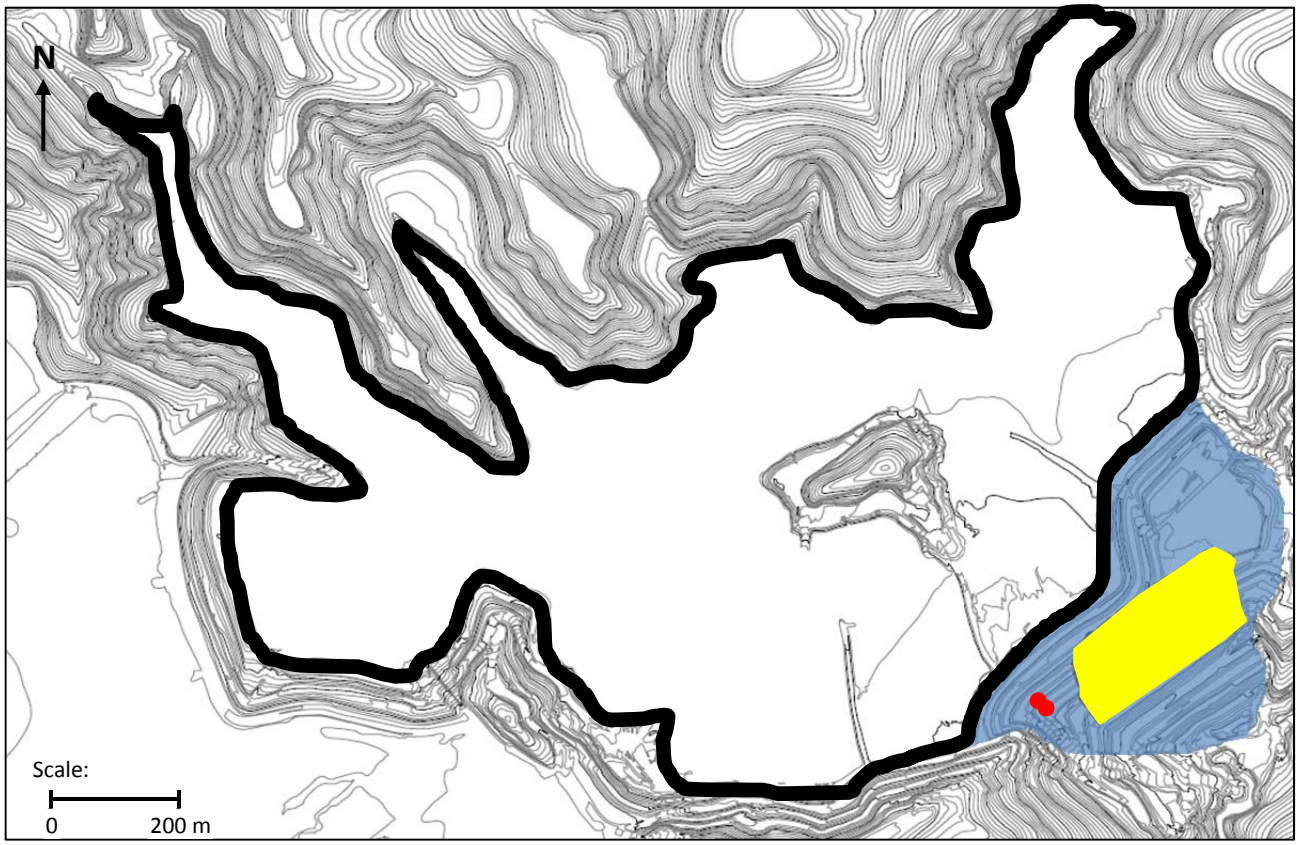

Figure 4-9 August, 2014 configuration showing El. 826 m blanket drain, raised dam, impoundment outline, and right abutment seeps (red dots)

Besides these incremental effects, a more fundamental change occurred on or about August, 2014 when three things happened simultaneously. As shown on Figure 4-10, flow from the El. 826 m blanket drain stopped increasing, then dropped briefly, partially recovered, and remained essentially unchanged thereafter. Also, flows from the Starter Dam base drain (a remnant of the original base drain salvaged after the 2009 piping incident) stopped diminishing and began increasing. In addition, artesian flow appeared at the toe of the Starter Dam.

An explanation consistent with these events is that the El. 826 m blanket drain with its Kananet® outlet pipes reached its maximum capacity. With the drain unable to divert additional seepage, saturation on the right abutment increased, breaking out in July at El. 855 m. At the same time, the diminished effectiveness of the blanket drain caused base drain flow to reverse its previous trend and begin increasing, while related increase in flow into the foundation caused artesian conditions to appear at the Starter Dam toe. And, as discussed subsequently in detail, all of these things were accompanied by the shallow saturation and unprecedented cracking of the left abutment that also occurred in August, 2014.

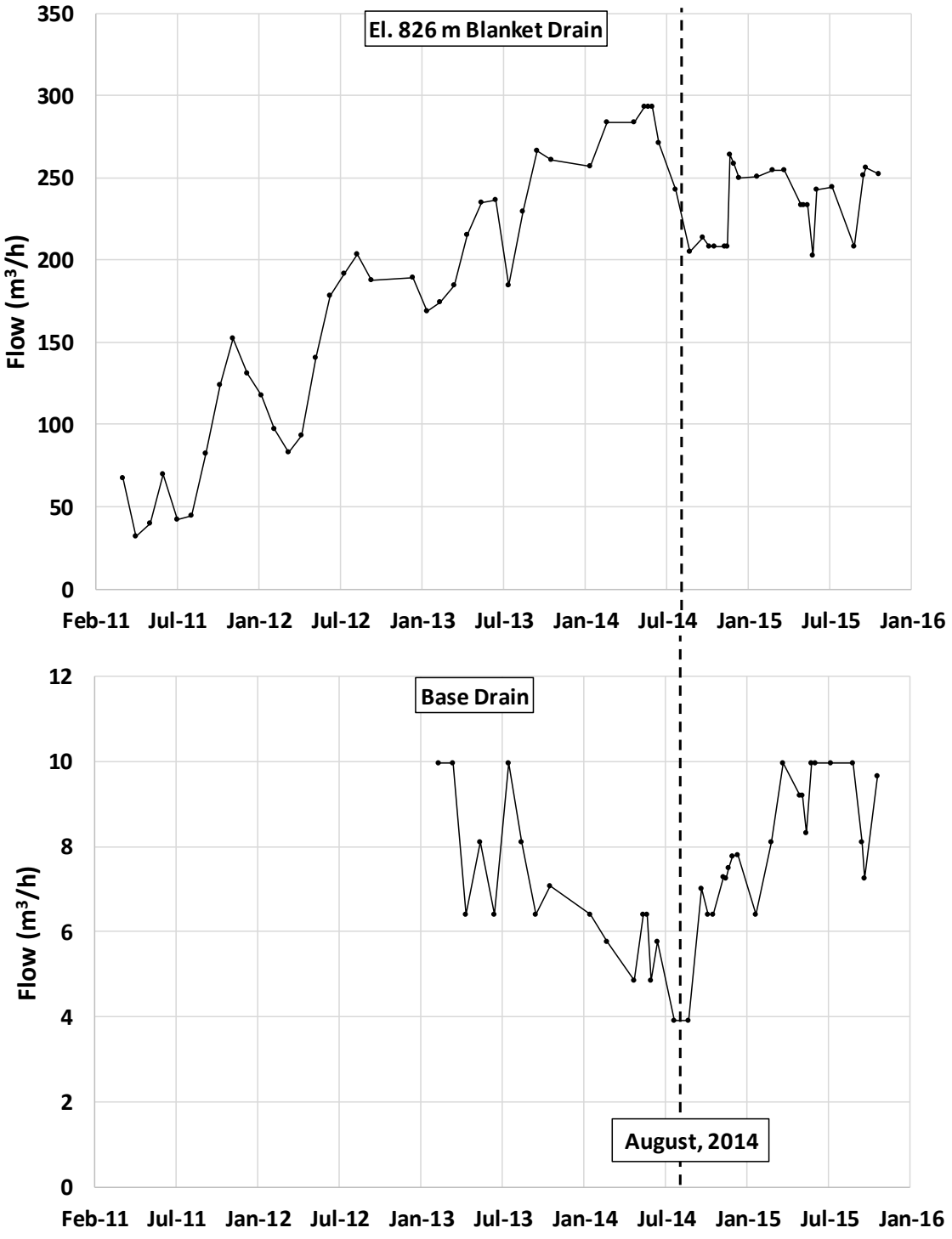

Figure 4-10 Measured flows from El. 826 m blanket drain and Starter Dam base drain

Figure 4-11 shows the drain configuration in November, 2015 with the ever-expanding impoundment. In preparation for the new 940 raise, the new blanket drain at El. 860 m had been completed at the left abutment setback and a companion drain at the right abutment was under construction. Had failure not intervened and had the dam alignment been restored, both of these new drains would have underlain the tailings much as the El. 826 m blanket drain once did. But as it was, neither had any effect on the tailings saturation that had already developed.

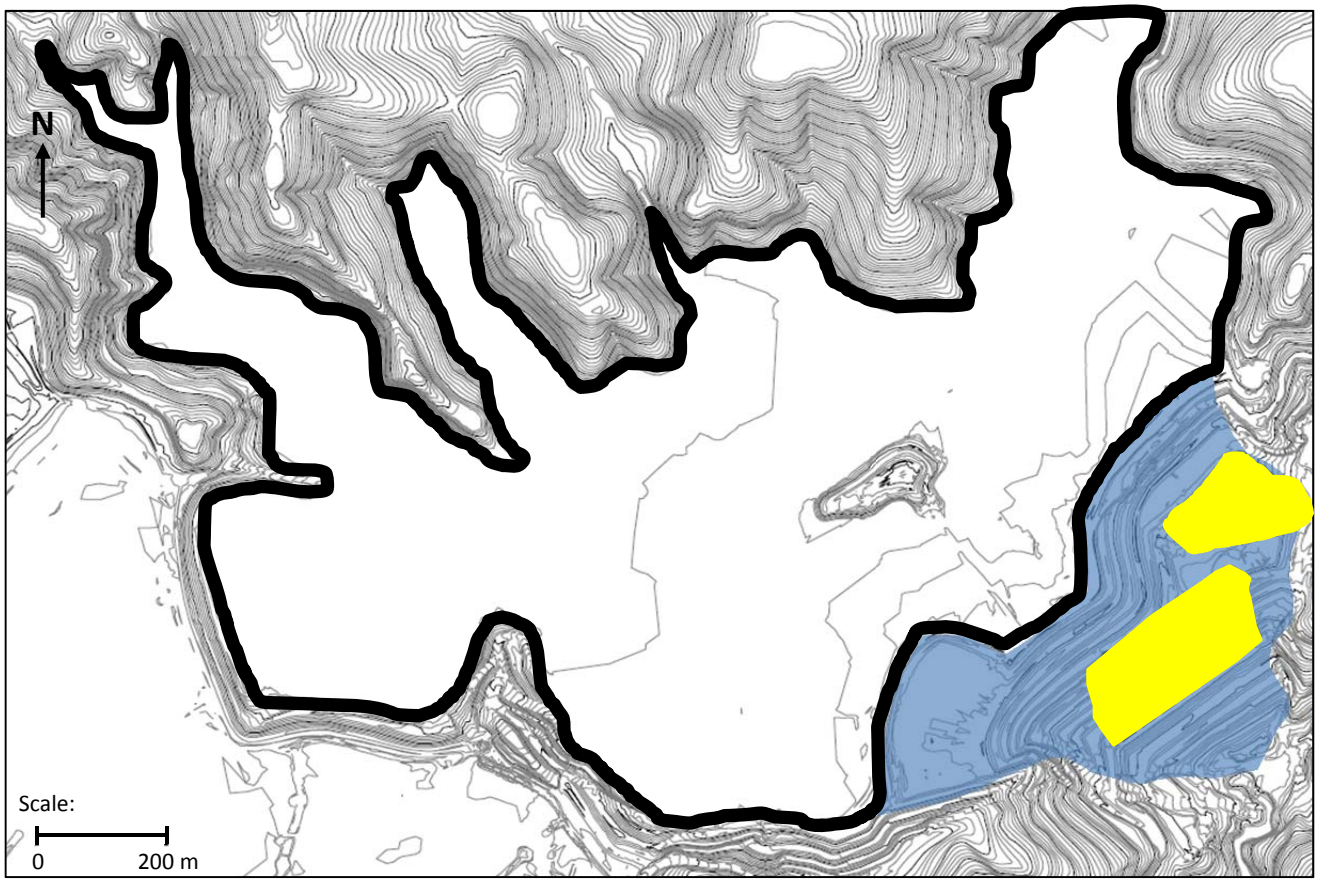

Figure 4-11 November, 2015 configuration showing El. 826 m and El. 860 m blanket drains, raised dam, and impoundment outline

Figure 4-12 summarizes the time-sequence of these impoundment drainage provisions. As upstream raising continued and the impoundment expanded, the El. 826 m blanket drain became increasingly more distant from the tailings it was intended to drain and eventually could no longer keep pace with rising saturation levels. With this, the saturated conditions necessary for liquefaction flowsliding were satisfied.

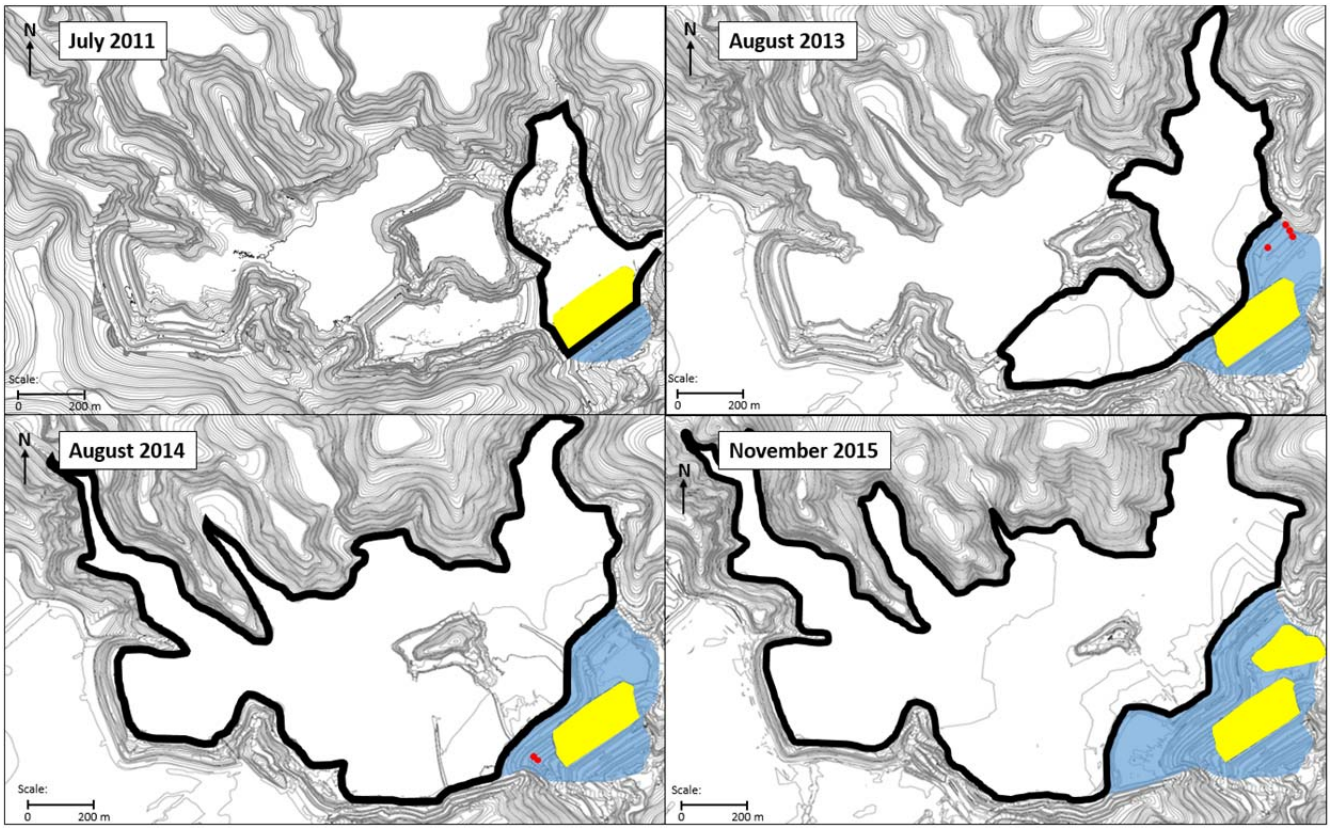

Figure 4-12 Progression of impoundment and drainage provisions with time

The beginning of this section posed the question: Why did a flowslide occur? In response, it has been shown that all of the necessary conditions were present. The sand tailings were contractive, they were saturated, and they were susceptible to severe loss of strength during the rapid failure that developed.

But an important factor has yet to be addressed. And that concerns the slimes.

5 WHY DID THE FLOWSLIDE OCCUR WHERE IT OCCURRED?

The eyewitness accounts summarized in Section 2.7 show that the flowslide of November 5, 2015 initiated on the left abutment where the dam had been set back from its former alignment. Section 4 has established why the flowslide occurred. It remains to explain why the flowslide initiated at the left abutment and not at some other location.

To do so requires identifying features or properties unique to the left abutment. In this respect, the defining feature of the left abutment setback was the presence of slimes beneath the embankment slope. The following discussions explain the characteristics of the slimes, where they were deposited, and how the setback influenced their effect on the embankment. Comparing these factors at the left and right abutments shows why the failure initiated at the former and not the latter.

5.1 The Slimes

5.1.1 Slimes Characteristics

Two types of tailings, *sands* and *slimes* were produced in the plants and conveyed in separate slurry pipelines to the Fundão and Germano impoundments. The sands are cohesionless and the slimes cohesive in character. As indicated on Figure 5-1, the two materials are readily distinguished by their color, the sands being gray and the slimes variously described as red, brown, or chocolate color.

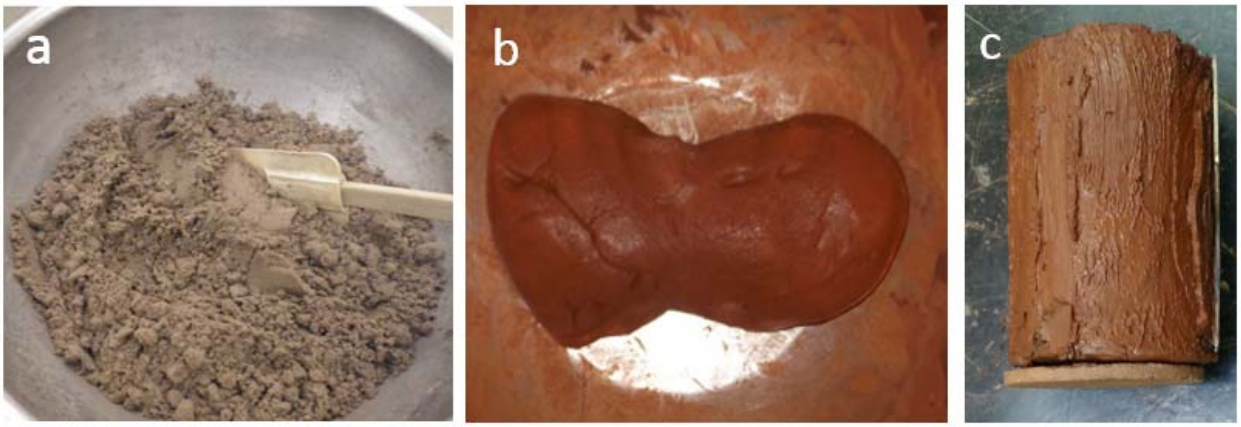

Figure 5-1 Sand and slimes tailings. (a) sand; (b) remolded slimes; (c) intact slimes specimen

The gradations of the two materials are compared on Figure 5-2, which shows that the sands contain approximately 40% silt, while the slimes are comprised entirely of silt and clay-sized particles.

The slimes contain only a small proportion of conventional clay minerals illite and kaolinite, the majority being hematite and goethite with some quartz. X-ray diffraction analysis of mineral composition is shown on Table 5-1.

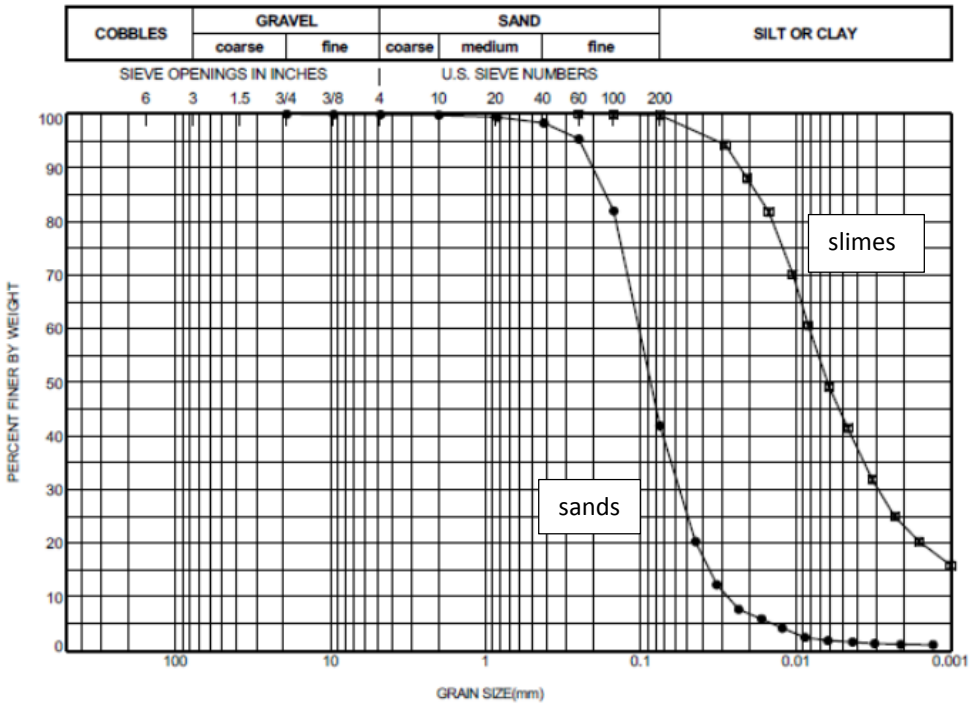

Figure 5-2 Sands and slimes gradation

Table 5-1 Slimes mineralogy

Mineral	Ideal Formula	#1 Slimes
Chalcopyrite ?	$CuFeS_2$	< 0.1
Goethite	α-$Fe^{3+}O(OH)$	30.9
Hematite	α-Fe_2O_3	42.9
Illite-Muscovite	$KAl_2AlSi_3O_{10}(OH)_2$	1.4
Kaolinite	$Al_2Si_2O_5(OH)_4$	4.4
Plagioclase	$NaAlSi_3O_8 – CaAl_2Si_2O_8$	1.1
Quartz	SiO2	19.2
Total		100.0

The concentration of iron-derived minerals in the slimes gives them a high specific gravity of nearly 4.0 that distinguishes them from the lighter sands. Where laboratory testing was available, the Panel was able to use specific gravity as a marker to distinguish the relative proportion of sands and slimes in tested samples. Despite the near-absence of clay minerals, the slimes classify as low-plasticity clay from Atterberg limits, with corresponding low permeability. Index properties of the slimes are given on Table 5-2, along with those for sands for comparison.

Table 5-2 Index properties

Property	Sands	Slimes
percent minus 0.074 mm	40-45	98-100
percent minus 0.002 mm	<2	20-25
specific gravity	2.8-2.9	3.9-4.0
plasticity index	non plastic	7-11
permeability	$3x10^{-4}$ cm/s	$< 10^{-6}$ cm/s

While the two materials in unadulterated form are easily distinguishable based on these measured properties, they are often mixed in various proportions in the field. Without laboratory testing, slimes can be difficult to identify from ordinary soil classification techniques, making their signature color their distinguishing characteristic in the field.

From the standpoint of the behavior of the Fundão Dam, the most important engineering property of the slimes that distinguishes them from sands is deformability. The slimes are softer and more compressible, as indicated by the compression curves on Figure 5-3. It will be shown in the following section that deformability of the slimes was a central factor in triggering liquefaction in the sands.

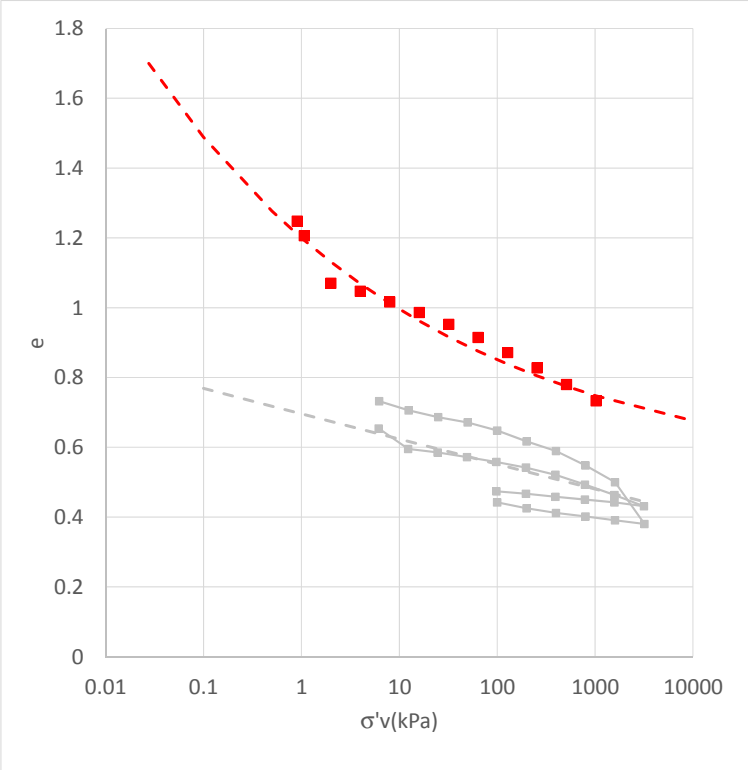

Figure 5-3 e log p curves for sand (grey) and slimes (red) from laboratory and field data; dashed lines used in modeling

5.1.2 Slimes Deposition and Identification

The tailings deposition process governs how sands and slimes are distributed areally and with depth. Figure 5-4 depicts this process in an idealized way when sands are discharged onto an above-water beach and from there into ponded water containing suspended slimes. Spigotting deposits exclusively sand tailings on the beach, while predominantly slimes sediment from the ponded water at greater distance. Between these two areas is an intermediate zone where intermixing of sands and slimes occurs at times when sands are being discharged. When sand discharge is temporarily suspended or relocated elsewhere, slimes layers are deposited that become embedded in and interlayered with the intermixed materials.

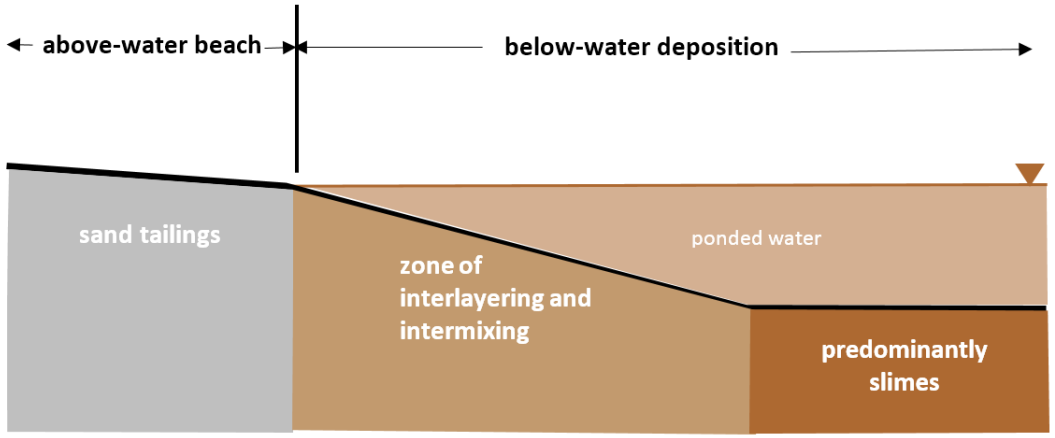

Figure 5-4 Idealized process of sands and slimes deposition

Figure 5-4 represents conditions at a particular moment in time, but the actual process is dynamic and constantly changing. The location of the interface between the beach and ponded water depends on both the depth of water—which varies according to precipitation inflows and water release—and the amount of tailings reaching that location from the sand discharge pipeline—which is regularly relocated. Thus, the dimensions of the three zones are always shifting. For the same reasons, they change with depth as the deposit accretes.

Figure 5-4 constitutes the conceptual basis for reconstructing tailings stratigraphy during the Investigation. The slimes-laden ponded water can be readily identified by its red color. Imagery from a variety of sources and related records provide snapshots of ponded water location and configuration that, when assembled and tracked over time, produce a three-dimensional representation of sands and slimes. The procedures used to create this tailings deposition model are described in Appendix A, and key findings are presented in Appendix B.

The Panel's development of the tailings deposition history involved review and distillation of hundreds of documents and records, most importantly: (1) publically-available satellite photographs; (2) drone photographs and post-2012 topography; (3) monthly Samarco instrumentation reports; (4) weekly construction reports; (5) consultant reports; and (6) interviews with Samarco engineering staff. The consultant reports were the primary source of drill holes, cone penetration tests and

laboratory data on the tailings sands and slimes. The engineering data from these reports are summarized in Appendices C and D.

Topographic information was assembled in Civil 3D using 40 different sets of basin-wide topographic surfaces at successive dam heights from 2009 to November, 2015. The quality of that topographic information increased considerably after Samarco initiated its drone program in early 2013. With the drone aerial photographs and topography, it was possible to input stripped ground topographic surfaces into Civil 3D to model the as-constructed base of Dike 1. This was especially useful because the abutments were stripped as the dam was raised. Some 15 different stripped surfaces were stitched into Civil 3D.

All information was assembled in a geographic information system (GIS) which enabled data to be queried and displayed in multiple views in real time. The Civil 3D model and the GIS system became the common source of the topography, stratigraphy and groundwater data used in the suite of analyses for this work.

5.1.3 Slimes Mapping

It can be recalled from Section 2.1 that the original design concept for Fundão was predicated on free-draining conditions in the sand tailings comprising the embankment. Achieving this required that drainage not be impeded by deposition of lower-permeability slimes. This was to have been assured by physically separating and separately discharging of the sand and slimes tailings behind Dikes 1 and 2, respectively.

Section 2.2 described how this concept was abandoned after the Dike 1 Starter Dam was seriously damaged by piping and internal erosion. In addition, subsequent structural problems with the Main and Secondary Galleries made it necessary to re-route water and slimes from the Dike 2 impoundment into Dike 1. These problems happened during 2011 and 2012 when tailings that would later underlie the left abutment setback were being deposited. The aerial image in Figure 5-5 shows that an Overflow Channel was constructed from the Dike 2 slimes reservoir to the Dike 1 reservoir from January, 2011 to July, 2012. This Overflow Channel introduced slimes into the Dike 1 reservoir.

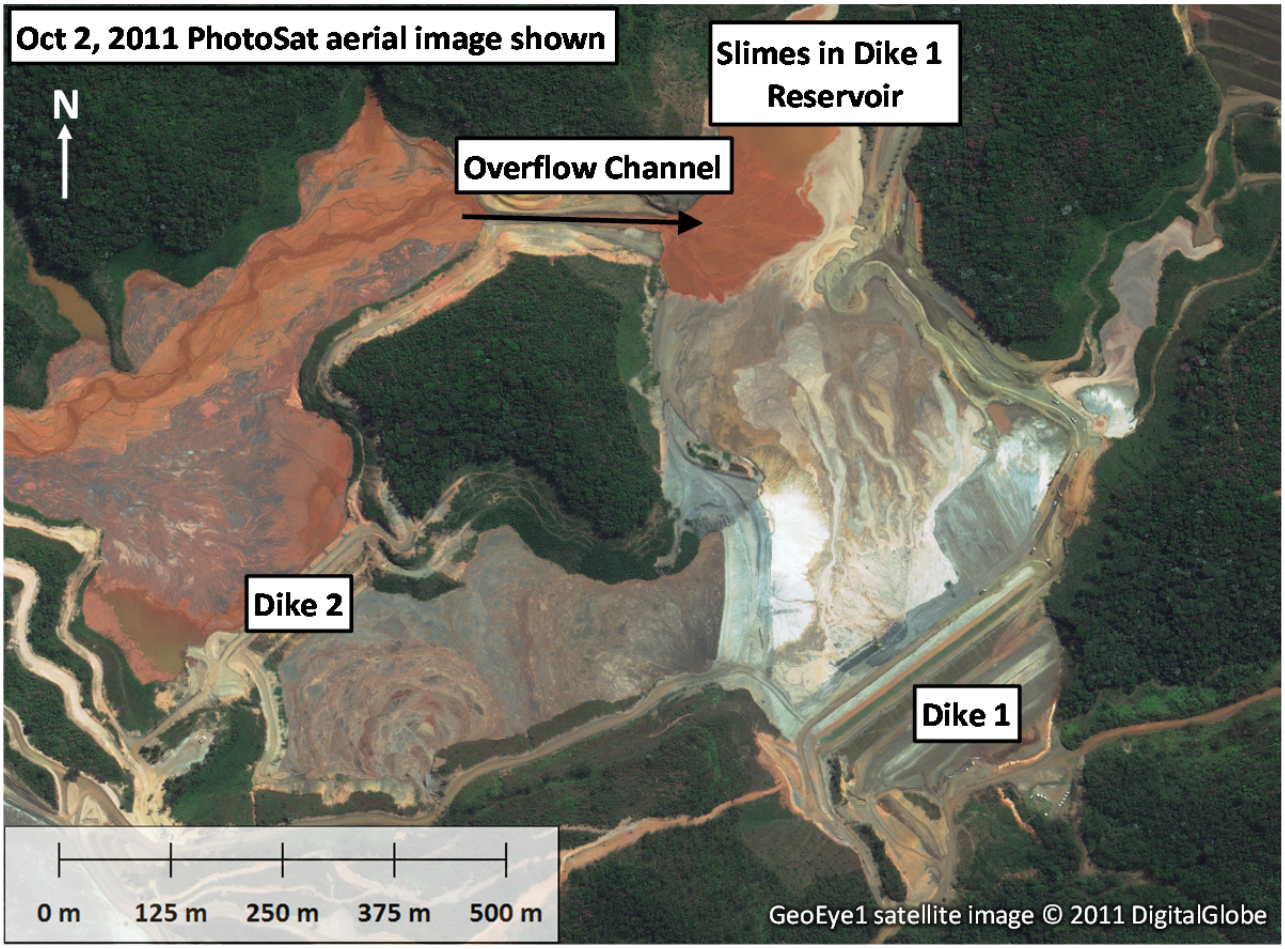

Figure 5-5 Slimes Overflow Channel from Dike 2 reservoir to Dike 1 reservoir

The Overflow Channel was closed in August, 2012 but not before slimes were deposited between El. 824 m and El. 850 m. Operation of the Overflow Channel and resulting slimes deposition is illustrated by imagery at selected dates during late 2011 and early 2012 on Figure 5-6.

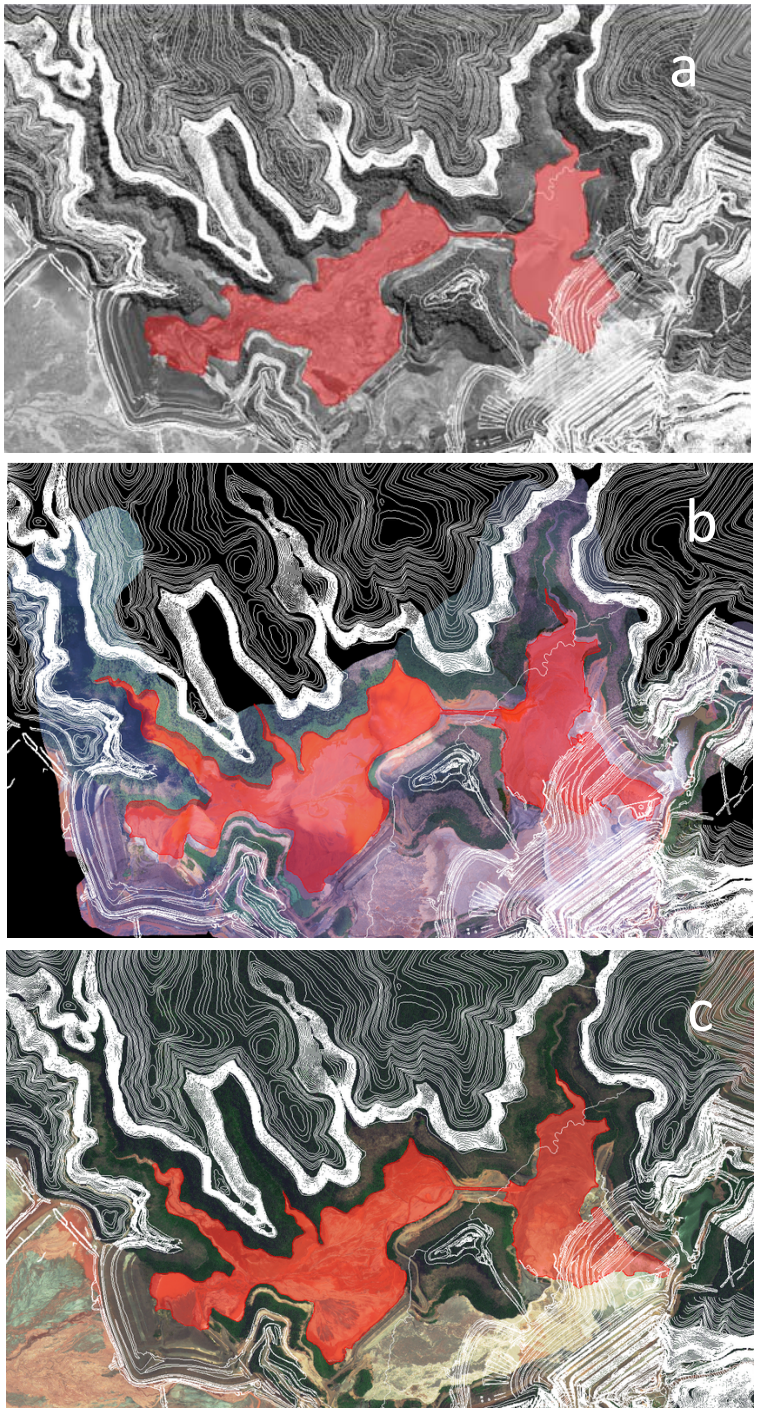

Figure 5-6 Slimes deposition (a) September 20, 2011; (b) January 21, 2012; (c) March 3, 2012. Slimes highlighted in red; final embankment contours in white

5.1.4 Drill Hole Information

The locations of slimes inferred from mapping can be compared to logs of drill holes through the left abutment tailings. Figure 5-7 shows borings and CPTs that penetrated a target interval of El. 830 m to El. 850 m. These holes were drilled at different times and surface elevations, but for reference they are superimposed on imagery from January, 2012. Also on Figure 5-7 for comparison are the outlines of slimes mapped at El. 841 m on that date that also appear on Figure 5-6b.

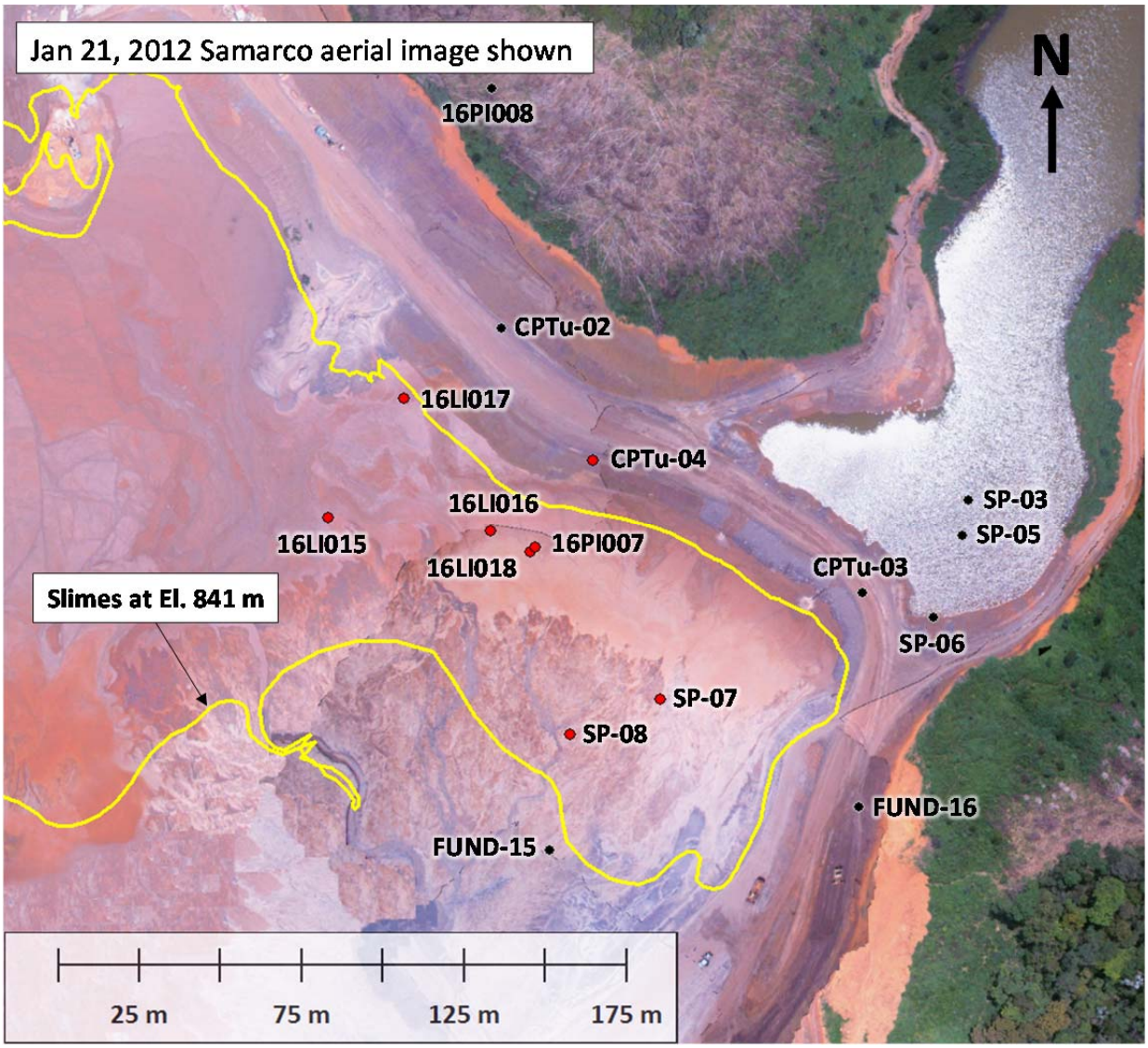

Figure 5-7 Left Abutment Drill Holes. Red circles indicate slimes within target interval of El. 830 m to El. 850 m.

No laboratory testing was conducted on recovered samples from any of the borings, so sample descriptions on the logs rely on visual classification alone with associated uncertainties as discussed in Section 5.1.1. For purposes of this assessment, slimes were taken as material logged as red or

brown in color, as opposed to grey for sands, often noting the presence of clay in varying amounts. Slimes were taken in CPTs as materials having apparent fines content of 100% that are not associated with road fill or other introduced materials. On this basis, Figure 5-7 shows holes indicating the presence of slimes within the target elevation interval in red and holes with no such indications in black. It can be seen that the drill hole information corresponds to the area of mapped slimes. A number of other holes not shown on Figure 5-7 were drilled over the Secondary Gallery for purposes of investigating its foundation conditions. With a surface elevation at or near El. 835 m, they mostly penetrated tailings below the target interval.

Within those holes where slimes were identified, their distribution is more difficult to determine because the tailings were not continuously sampled. However, SP-07 is notable in having distinguished two discrete clay layers corresponding to slimes: a 2 m thick layer at El. 836.36 m and a deeper 2 m layer at El. 828.36 m. Also, CPTu-04 penetrated slimes layers up to several centimeters thick. It is reasonable then from the drill holes to categorize discrete layers of slimes as ranging from a few centimeters to a few meters in thickness, with the remainder of the slimes material intermixed with sand in varying proportions. This characterization is consistent with the zone of interlayering and intermixing portrayed on Figure 5-4.

5.1.5 Slimes Mass Balance

The distribution of slimes estimated from drill hole information can be supplemented on a broader level using a mass balance approach. To this end, slimes production records were compared with the potential slimes volumes between El. 840 m and El. 850 m. A mass balance was derived by assuming a dry unit weight of the slimes taken from measurements of recently-deposited slimes sampled in Germano as part of this Investigation. The mass balance assumptions and calculations are given in Appendix B.

The mass balance provides a measure of the volumetric proportion of constituent slimes and slimes layers within a specified zone. Figure 5-8 portrays the results in cross section. Here, the region designated *predominantly slimes* is nearly 100% slimes, *interbedded slimes* is estimated to contain 20% or more slimes overall, and the zone of *isolated slimes* less than this amount. Although distinct boundaries are shown between these regions, actual conditions are transitional in character.

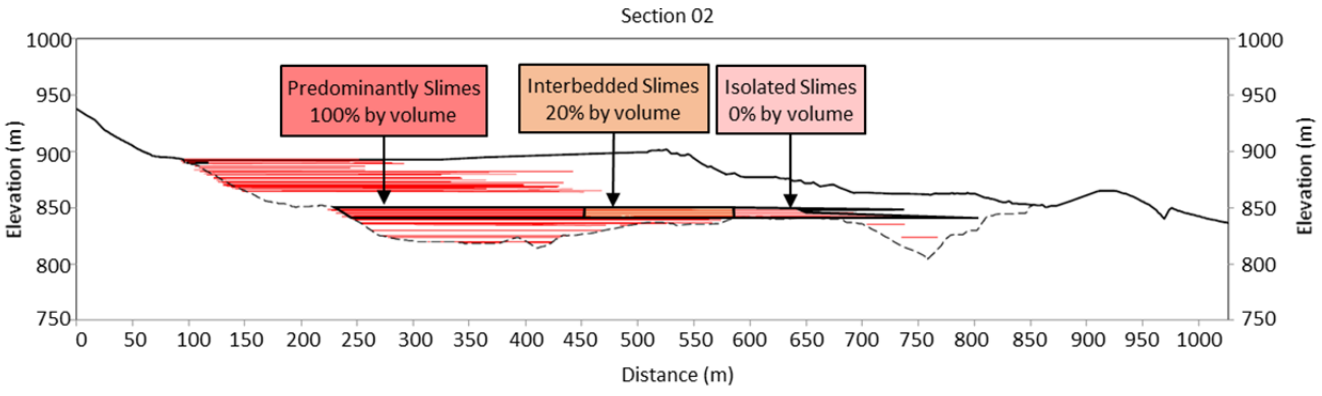

Figure 5-8 Distribution of slimes at left abutment

The preceding discussions have shown that slimes were present at the left abutment, in particular between El. 830 m and El. 850 m, and that their concentration increased with distance behind the dam. How these conditions influenced the embankment requires accounting for the setback.

5.2 The Left Abutment Setback

5.2.1 Events and Circumstances

Circumstances surrounding the modification of the dam alignment that resulted in the setback have been reviewed in Section 2.4. Due to structural problems and construction defects, the dam could not continue to be raised over the Secondary Gallery until repairs had been made. But when these repairs proved unsuccessful, the Secondary Gallery had to be abandoned and filled with concrete. To accommodate tailings storage requirements during these periods, beginning in October, 2012 the dam alignment at the left abutment was shifted back from its former location as shown on Figure 5-9. This created what is called here the *setback*, with the vacant area in front of it the *plateau* or *platform*.

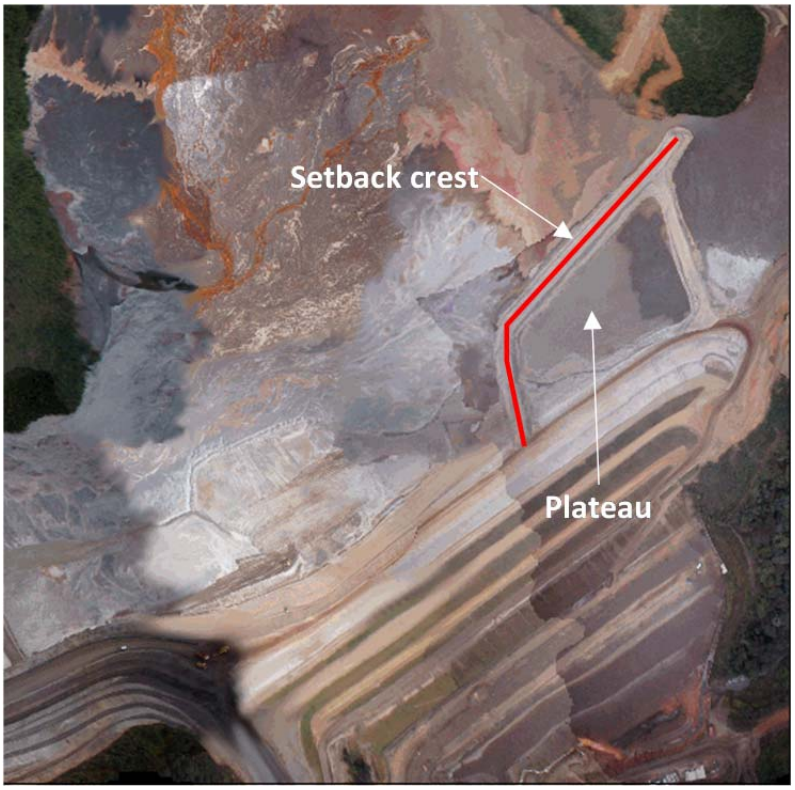

Figure 5-9 Aerial photograph of the setback alignment in October, 2012

The setback was initiated when the plateau was at approximately El. 855 m. By the end of 2013, the crest had risen to El. 877 m, or about 22 m high.

Starting in August, 2013, the first compacted fill was placed to rebuild the setback portion of the embankment and return it to its former alignment while dam raising continued. This occurred until August, 2014 when the slope showed serious signs of distress as reviewed in Section 2.5. The setback was immediately buttressed with a tailings sand berm. By then, the crest had reached El. 885 m, or 30 m high.

Infilling of the setback was further delayed by requirements for the proposed raise of the Fundão Dam to a crest elevation of 940 m. Design analyses concluded that more drainage would be needed to reduce the phreatic surface on both abutments, including a large blanket drain at the left abutment to be constructed in four stages. The first stage was a blanket drain at El. 860 m on the setback plateau. Construction began in November, 2014 and did not conclude until August, 2015 when setback infilling was resumed.

The setback had significant effects. Moving the embankment back toward the impoundment caused it to be raised over the slimes deposited in 2011 and 2012. In addition to influencing foundation conditions, these slimes also changed the seepage regime, elevating the phreatic surface on the left abutment.

5.2.2 Slimes Configuration

The combined effect of the slimes deposition described in Section 5.1 and the setback is best shown by a series of illustrations representing various points in time. The extent of newly-added tailings since the previous time step is indicated on the sections and in plan view on the insets to Figure 5-10. Compacted tailings that were mechanically placed during embankment raise construction are distinguished from the hydraulically-discharged sands by lines separating the two on the cross sections.

Figure 5-10 shows that the alignment setback caused all or most of the embankment to be constructed over slimes. In addition, as the embankment became higher and its crest moved upstream, more of the embankment slope became underlain by the higher proportion of slimes in the interbedded region.

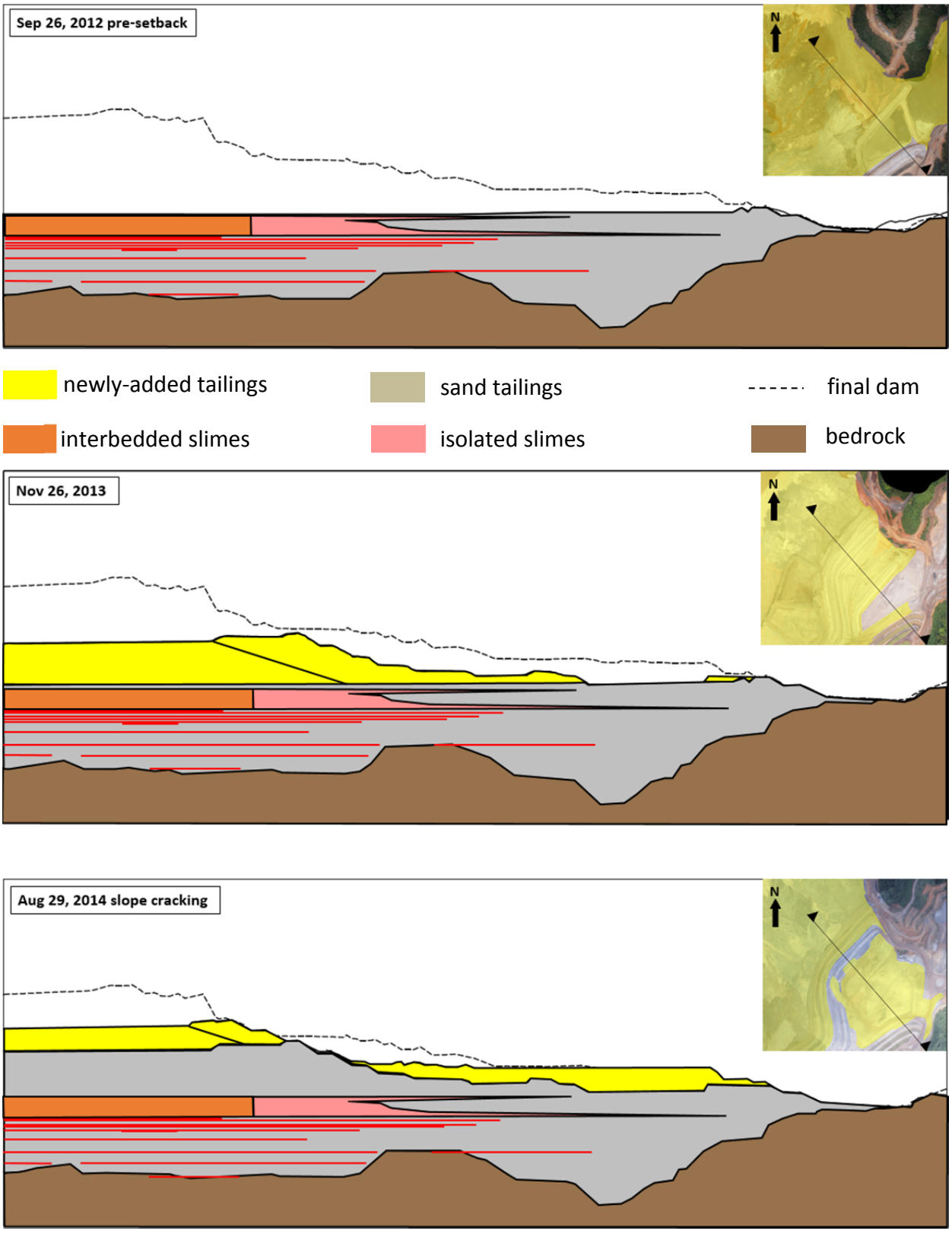
Sep 26, 2012 pre-setback
N
newly-added tailings
sand tailings
final dam
interbedded slimes
isolated slimes
bedrock
Nov 26, 2013
N
Aug 29, 2014 slope cracking
N

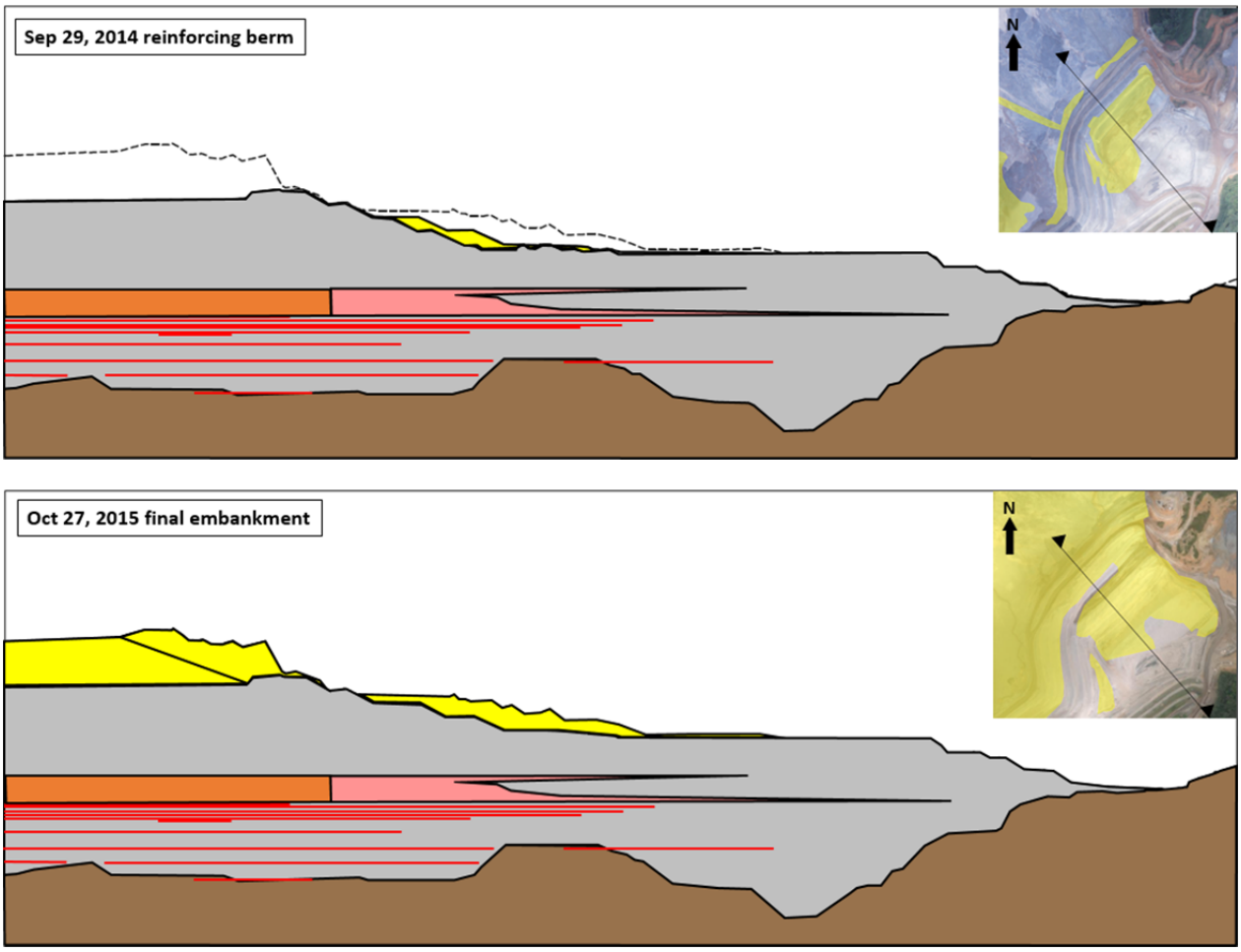

Figure 5-10 Sequential raising of setback embankment over slimes

The areal extent of the slimes depicted on Figure 5-10 deposited in 2011 and 2012 beneath the left abutment setback is shown on Figure 5-11, where again it can be seen that by the time the embankment reached its final height, slimes would be present beneath the entire setback slope and much of the plateau area.

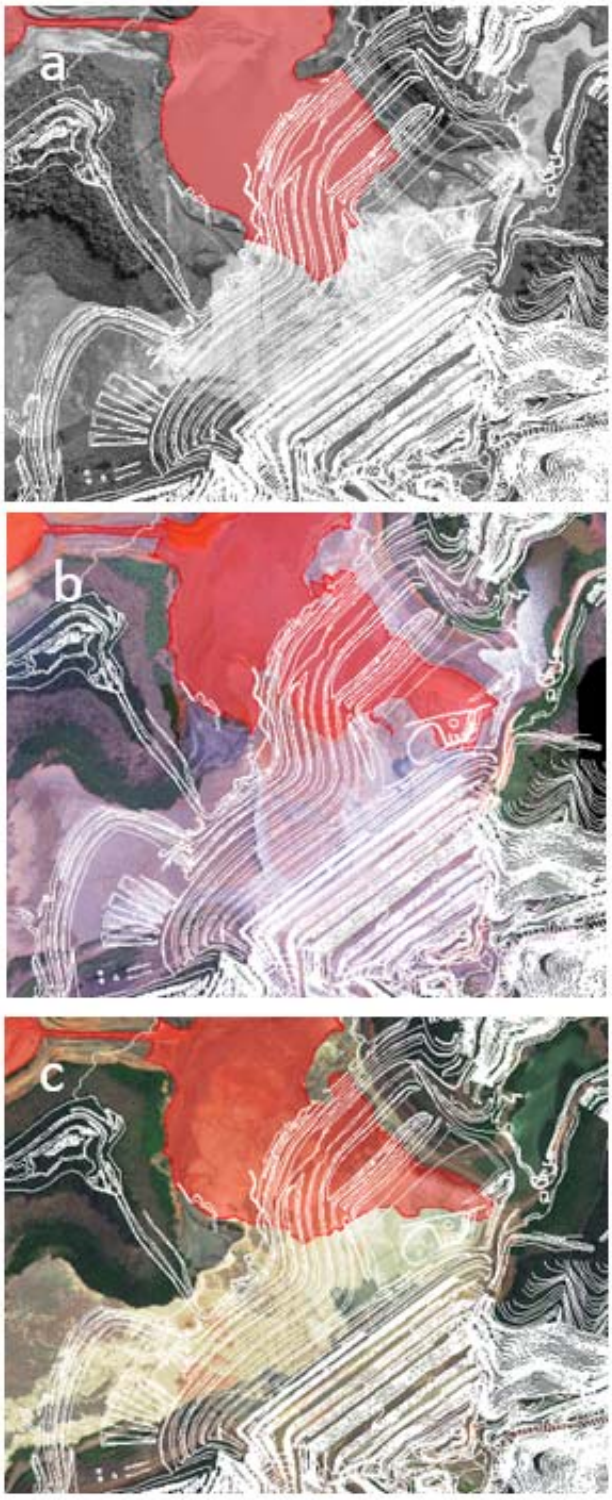

Figure 5-11 Slimes beneath final embankment: (a) September 20, 2011; (b) January 21, 2012; (c) March 3, 2012. Slimes highlighted in red; final embankment contours in white

5.2.3 Rate of Rise

As indicated on Figure 5-12, the rate of rise of the dam crest at the left abutment varied during the life of the setback. The average 1.3 m/mo during 2015, or an annualized rate of 15.7 m/yr, was intermediate between rates experienced during 2013 and 2014. Also during 2015 in the months immediately prior to failure, raising accelerated from as low as 0.4 m to 2.9 m. The small negative rate of rise in September, 2014 was produced by regrading related to construction of the reinforcing berm and is not consequential to the overall trend.

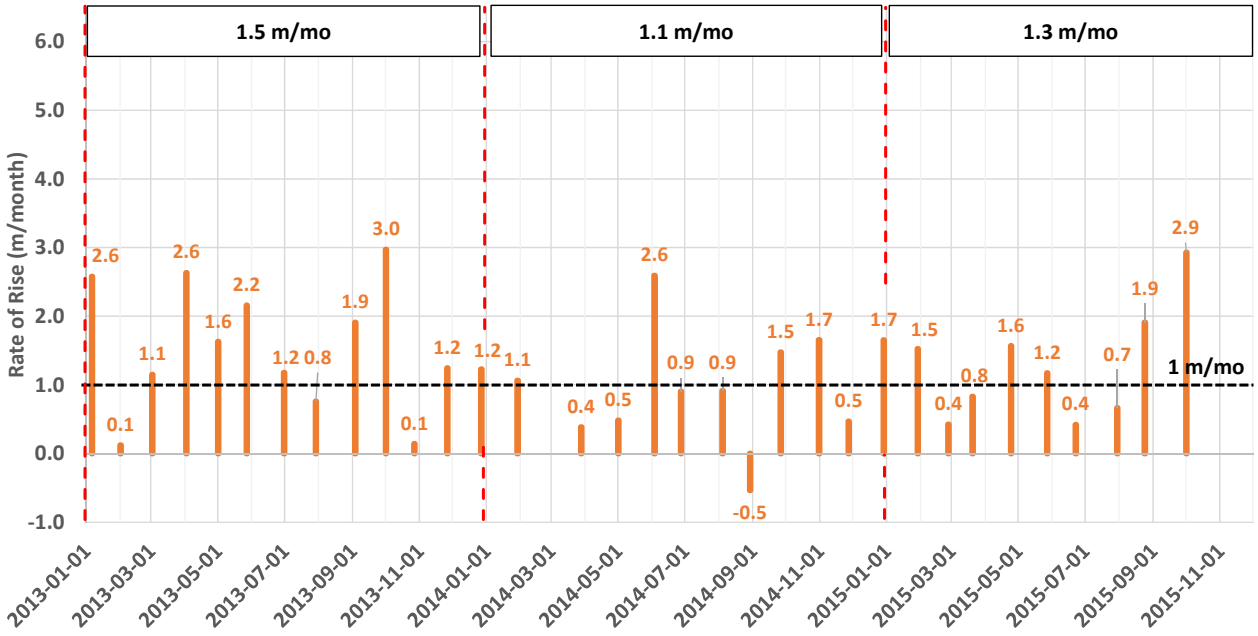

Figure 5-12 Rate of dam crest rise at left abutment setback

5.3 Comparison of Left and Right Abutments

Thus far, it has been established that slimes existed beneath the embankment slope at the left abutment as a consequence of their earlier deposition together with the setback of the dam alignment. To explain why failure initiated here and not elsewhere, it is useful to compare conditions at the left abutment to those at the right, where failure resulted from and was preceded by flowsliding on the left. The question then becomes why failure initiated at the left abutment and not the right. This requires comparing conditions at the two locations.

5.3.1 Right Abutment Conditions

Figure 5-13 shows Section AA at the right abutment and its internal composition based on mapping as described in Section 5.1.3. The distinguishing feature of the right abutment compared to the left is the nearly complete absence of slimes beneath the embankment slope. The only region of slimes lies below El. 825 m where it is confined both upstream and downstream by natural ground. This is in sharp contrast to the left abutment on Figure 5-8 where slimes can be seen to extend beneath virtually the entire length of the slope.

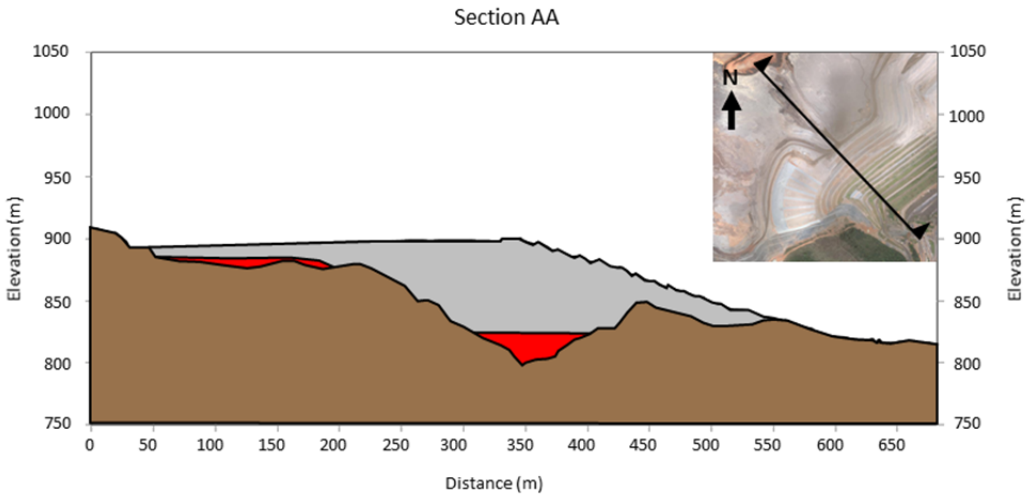

Figure 5-13 Slimes at right abutment Section AA

The left and right abutments can be compared more directly by overlaying the respective sections. Figure 5-14 provides an overlay of Section 01 at the left abutment and right abutment Section AA, coincident at the respective dam crests. Geometrically, the greater overall steepness and extended length of the 3.0H:1.0V right abutment slope stands out.

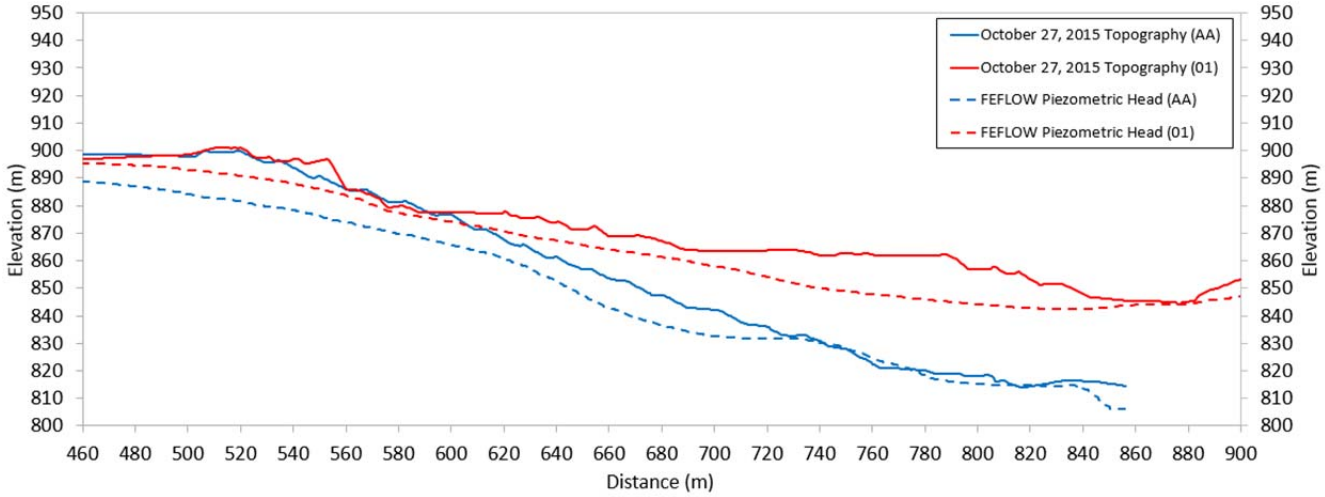

Figure 5-14 Geometry and piezometric comparison of left and right abutments

Also depicted on Figure 5-14 is the difference between the piezometric surface at the two locations, with generally higher conditions on the left that reflect the influence of slimes. This is illustrated in more detail on Figure 5-15.

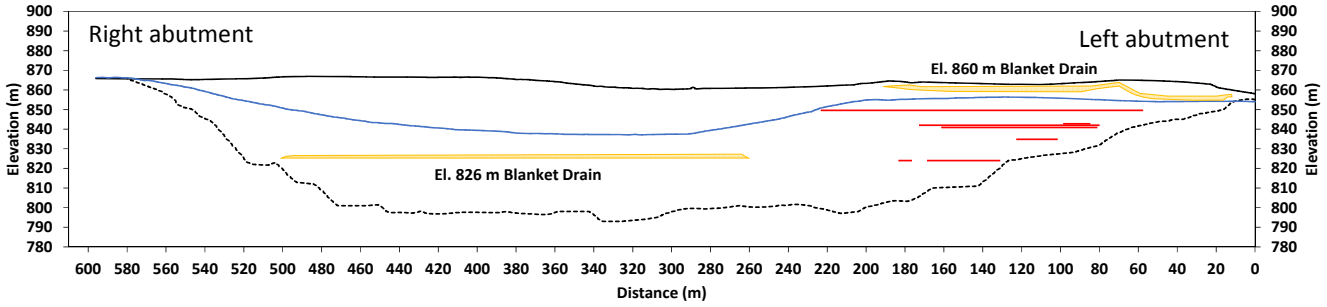

Figure 5-15 Longitudinal section from FEFLOW, view looking upstream. Phreatic surface shown in blue, El. 826 m blanket drain in yellow, slimes in red.

Figure 5-15 is based on results of a 3D steady state and transient seepage analysis of the tailings impoundment performed as part of the Investigation and described in Appendix G. The estimated phreatic surface from this modeling is shown on the longitudinal section. On the left abutment, inflows from Grota da Vale together with the slimes maintain the phreatic surface at a higher elevation. In contrast to the right abutment, the slimes on the left extend outward toward the El. 826 m blanket drain and limit the lateral extent of its influence.

The rate of rise of the embankment crest at the right abutment is shown on Figure 5-16, which can be compared to conditions at the left from Figure 5-12. Average annual rates are generally similar except during 2015 when the right abutment was raised at a higher rate of 1.6 m/mo compared to 1.3 m/mo on the left. The right abutment experienced an unusually high rate of rise of 5.4 m/mo in August, 2015 on a newly-initiated realignment of the crest that was set back from the former location to allow for drain construction depicted on Figure 2-12.

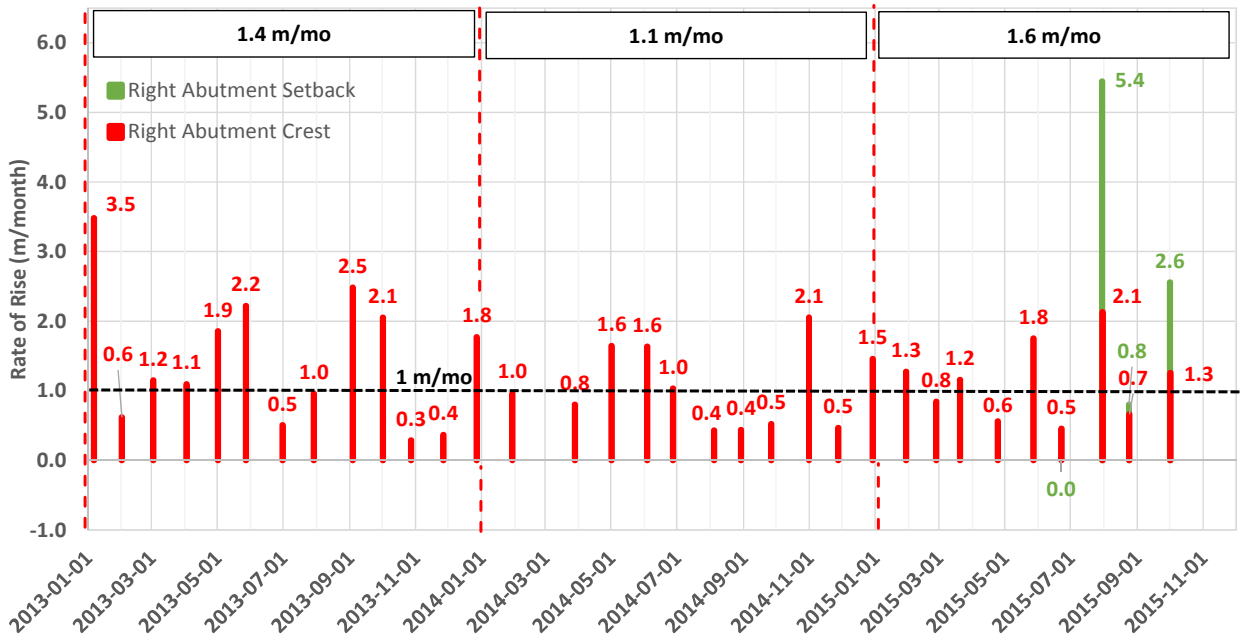

Figure 5-16 Rate of rise at right abutment

Conditions conducive to failure at the right abutment therefore include greater slope steepness and higher rate of rise than the left abutment, although these are mitigated somewhat by the lower piezometric conditions. The net effect can be evaluated by means of stability analysis.

5.3.2 Right Abutment Stability

Section 4.1 reviewed the aspects of soil behavior that give rise to flowsliding in saturated, contractive materials. Shearing that occurs slowly enough to allow pore pressures to dissipate is said to occur under *drained* conditions, while *undrained* conditions pertain to rapid shearing associated with flowsliding.

Stability analyses for these two conditions adopt corresponding strength parameters. *Effective-stress analysis*, or ESA, uses friction angle and cohesion to represent drained shearing, while *undrained strength analysis*, or USA, for undrained shearing uses undrained strength typically expressed as a ratio to the effective vertical overburden stress.

Stability analyses for the right abutment Section AA on November 5, 2015 are shown on Figure 5-17 for both ESA and USA, where a calculated factor of safety (FS) less than 1.0 indicates failure. The ESA adopts a friction angle of 35 degrees and 5 kPa for compacted tailings fill and 33 degrees and zero kPa for hydraulically-discharged tailings, while the USA uses an undrained strength ratio in compression of 0.25 for tailings below the piezometric surface.

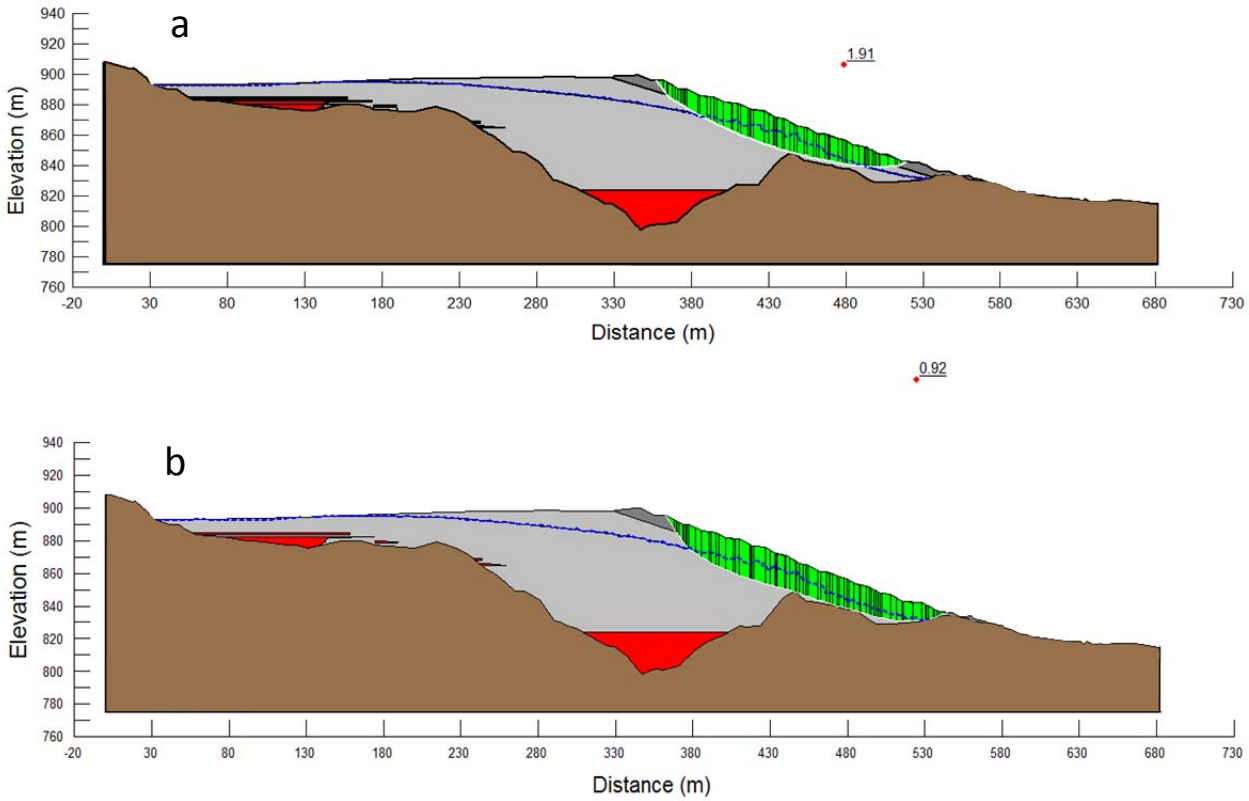

Figure 5-17 Stability analyses at right abutment Section AA; (a) effective stress (ESA); (b) undrained strength (USA)

Figure 5-17 shows FS = 1.91 for ESA conditions and FS = 0.92 for USA. Hence, with a USA factor of safety less than 1.0, rapid failure and associated flowsliding should have initiated at the right abutment if undrained conditions had been operative. The fact that failure did not initiate there means that undrained strength was not fully mobilized and that drained conditions represented by the ESA prevailed at the right abutment. It is equally apparent that the rate of embankment rise at the right abutment was not itself sufficient to mobilize undrained strength in the sand tailings.

5.4 Flowslide Occurrence at the Left Abutment

The conditions discussed in this section make it possible to answer the question of why failure initiated at the left abutment rather than at the right. Two main factors were operative. First, compared to the right abutment, the left abutment had higher and more adverse piezometric conditions. But most importantly, the embankment slope was underlain by slimes at the left abutment causing undrained strength to be mobilized, conditions that did not exist at the right abutment. Undrained shearing and subsequent reduction in undrained strength—the phenomenon of static liquefaction—resulted in the left abutment flowslide. The triggering mechanism for static liquefaction, and the role of the slimes in producing this mechanism, are explained in the following section.

6 WHY DID THE FLOWSLIDE OCCUR WHEN IT OCCURRED?

6.1 Triggering Mechanisms

Section 4 of this report outlined the conditions required for liquefaction flowsliding. These are: the presence of loose, contractant tailings; the existence of saturated conditions; and rapid failure producing undrained conditions with accompanying reduction in undrained strength. The Fundão flowslide occurred because all of these necessary conditions were present.

Section 5 considered why the flowslide occurred at the left abutment. It was shown that softer, more compressible slimes were deposited in areas intended to be exclusively sand beach, and that the setback of the dam alignment resulted in these materials being present beneath the embankment slope as it was further raised upstream. By contrast to the left abutment, undrained strength was not mobilized at the right abutment, which was not underlain by slimes, and neither were high rates of construction sufficient to induce liquefaction there. The reason that the flowslide occurred at the left abutment is that the presence of slimes-enriched tailings inhibited drainage, enhanced saturation, and promoted undrained shearing.

This section considers what caused liquefaction flowsliding to occur as it did on November 5, 2015. As part of its assessment, the Panel noted that the failure did not occur earlier in the left abutment construction sequence when conditions such as those in the August, 2014 cracking incident were manifested, but that it did occur shortly after the earthquake sequence earlier that day. The timing of the failure event, and the operative conditions at this and other times, goes to the question of liquefaction triggering. Clearly, the softer slimes at the left abutment—and in particular how they responded to increased stress during dam raising—must play a prominent role in any theory of causation.

Drawing on their own experiences and those of others, Martin and McRoberts (1999) have emphasized the need for a physical trigger to initiate rapid shearing, and they catalog numerous potential triggers:

1. Oversteepening at the toe due to erosion, localized initially-drained slumps and construction activities such as excavation.
2. Loading due to rapid rate of impoundment raising, steepening at the crest, and construction activities at the crest.
3. Changes in pore pressure due to increased pond levels, accelerated rates of construction, movements, and other processes.
4. Overtopping due to severe storms, failure of diversion facilities, seismic deformation resulting in loss of freeboard.
5. Vibrational loading due to earthquakes, construction traffic, blasting.

These and other physical trigger mechanisms unique to the Fundão Dam have been considered in Appendix K. It is evident from the above that when contractant tailings are present in the structural portion of a tailings dam, the evaluation of liquefaction triggering is a formidable task.

Of particular interest was static liquefaction initiated by a rise in phreatic surface alone. In the early deliberations of the Panel, this ranked highly as a potential cause. As discussed in Appendix K, the levelling-off of piezometric pressures in the months prior to the failure provides evidence against it. Cyclic liquefaction also received attention, but had it been the sole triggering mechanism, the right abutment would have failed before the left, as discussed in Appendix K.

As summarized on Figure 3-1, the surviving candidate liquefaction triggering mechanisms are static load increases generated directly by either undrained shearing of the slimes or by deformations at the base of the sand leading to collapse. Either trigger mechanism might be augmented by earthquake effects if shown to be consequential. While their end result is similar, their stress paths differ. In the case of undrained shearing, the question arises whether the load due to embankment construction, coupled with the deformation of the underlying slimes-enriched material, can directly induce pore pressures in the loose sand sequence that would lead to undrained failure.

The shearing mechanism is based on undrained shear in the underlying slimes material together with mobilized frictional resistance in the overlying sands. Liquefaction in the overlying sands would be induced by uncontrolled deformation of a sliding mechanism with a factor of safety of unity. An example of a tailings dam that exhibited this failure mechanism is the Los Frailes dam in Spain. In a later portion of this section and in Appendix I, the relationship between undrained strength in the underlying slimes and factor of safety will be presented, as will the sliding developed in the slimes associated with the factors of safety. It will be shown that sliding in the slimes would induce failure associated with a deformation mechanism prior to the initiation of shear failure. In addition, the shear failure mechanism as presently analyzed does not take into account additional three dimensional resistance, which will be substantial. Moreover, shear failure mechanisms are often accompanied by the development of a down-drop block, or graben, at the initiation of the movement, and eyewitness reports do not provide any evidence of such a feature. For both the analytical results to be discussed and the additional items mentioned above, the Panel favors the deformation mechanism as the basis for initiating the failure when it occurred.

The alternative deformation-related trigger mechanism is termed here *lateral extrusion*, with reference to horizontal spreading of the softer slimes due to loading that induces a corollary elongation effect in the overlying sands. The mechanism of lateral extrusion is somewhat more indirect. It asks whether stress changes in the sand above the slimes-enriched layer, as it is undergoing deformation, result in a stress path that leads to collapse and static liquefaction.

Although not included on the list of Martin and McRoberts (1999), lateral extrusion as a static liquefaction trigger mechanism is not new or without precedent. It has been identified by Jefferies and Been (2016) in their discussion of the static liquefaction of the Nerlerk berm, where they state that:

> "The dangerous nature of declining mean-stress paths in terms of liquefaction behavior, caused by basal extrusion, was not understood in 1983."

Much of the subsequent content of this section is devoted to the lateral (basal) extrusion mechanism, incorporating developments much more recent than those referred to above.

The case of static liquefaction of sands associated with the 1938 failure of the Fort Peck Dam has some similarity to the Nerlerk case in that it has been interpreted to have been caused by shear failure of a weak shale foundation. The difference resides in the basal straining mechanism but the net result in creating stress changes in the saturated sand above is similar.

An important case of static liquefaction occurred at the Germano Complex itself in 2005. As shown in Figure 6-1, a low dike being raised over interlayered and intermixed slimes in the Baia 4 area experienced a sudden, high-mobility failure that moved rapidly over a distance of 80 m. The Baia 4 failure was attributed to liquefaction.

Figure 6-1 2005 Baia 4 static liquefaction failure

The Baia 4 failure provided the basis for determining parameters for slimes-rich layers used in modeling of the Fundão failure. Specifically, parameters relating to the peak undrained shear strength of these layers and the reduction in strength at large deformations were derived by back calculation from pre-failure and post-failure conditions. In these respects, the Baia 4 failure provided an important link between the theoretical studies conducted by the Panel and actual experience at the Germano Complex itself (see Appendix C for details).

Numerical simulations were also grounded in other field experience from the Germano Complex. As explained in Appendix I, field loading trials in 2008 and 2013 provided deformation response and consolidation properties for the slimes-rich layers.

6.2 Loading Conditions

As discussed in Section 4, the ability for rapid loading to result in rapid failure, and hence liquefaction of loose saturated sands, is well understood. However, this is not the case with slower loading.

Sasitharan et al. (1993) demonstrated that a loose granular deposit can collapse as a result of slow loading, as well as during rapid loading, mobilizing a resistance that is much less than the ultimate frictional resistance.

Skopek et al. (1994) demonstrated the mechanics of collapse by following the loading paths utilized above with dry sand and found a sudden volume decrease at essentially the same stress condition, consistent with the data noted above. These two sets of experiments demonstrate the value of the collapse testing to find a yield surface separating collapsing from non-collapsing states in loose, contractive soils like tailings.

Testing is also of value in understanding the role of cyclic loading from earthquakes leading to liquefaction. This is illustrated on Figure 6-2.

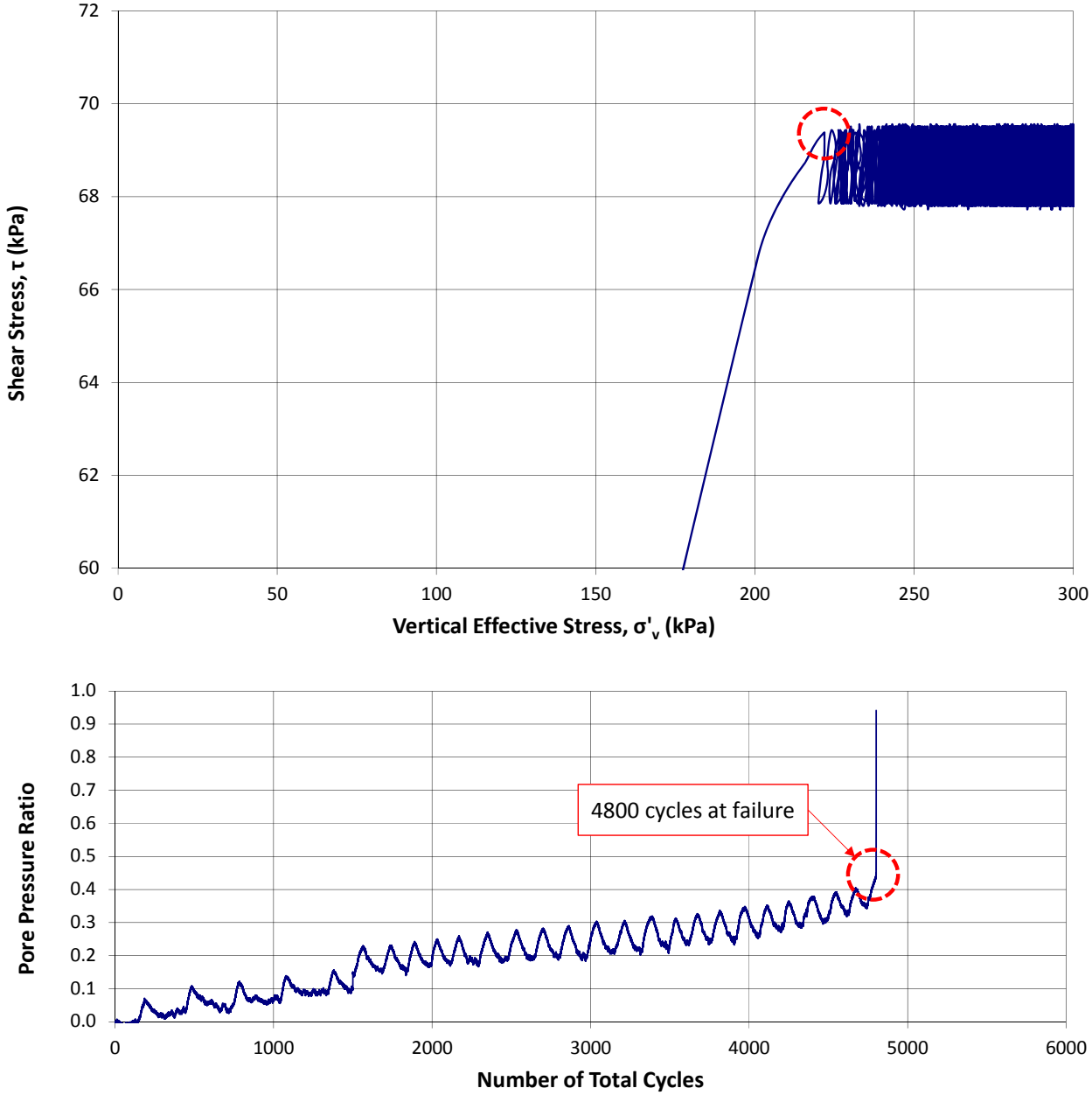

Figure 6-2 Stress path during cyclic loading

During cyclic loading shear stresses vary with time, and this can induce an increase in pore pressure resulting in a reduction of p'. As shown, the stress path migrates to the yield surface and, upon intersection, liquefaction under the applied static stresses results. The sensitivity to cyclic loading depends upon the magnitude of the cyclic shear stress, the duration of dynamic loading, the existing static stresses, and the state of the tailing sands. This topic is discussed in more detail in Section 6.5,

where cyclic tests representing the specific earthquake loading for the Fundão Dam will be presented.

In addition to the stresses applied, the loading due to embankment raising must also be considered. This was based on actual survey data, as illustrated in Appendix B. As previously shown on Figure 5-12, the rate of rise at the left abutment reached a value of 2.9 m/month. There is no evidence that this rate had a material effect on the sands, but it could certainly induce an increment of undrained loading on the underlying slimes.

6.3 Ground Conditions

The assessment of ground conditions that influence the formulation of the trigger mechanisms relies on piezometric data prior to the failure and CPT profiles to determine the contractive/dilative behavior of the deposit in the vicinity of the left abutment.

With respect to the piezometric data, Appendix E contains the plots of piezometers in the vicinity of the left abutment up to the time of the failure. Seepage simulation, summarized in Appendix G, extrapolates this data and its trends. The significance of this data in assessing potential trigger mechanisms is also discussed in Appendix K of this report.

With respect to the CPT profiles, the Panel has utilized the Robertson (2010) procedure previously shown on Figure 4-5 for evaluating the contractant/dilatant behavior of the deposits, primarily because it incorporates liquefaction failures of tailings dams and other deposits for immediate comparison. All CPT interpretations are available in Appendix C.

There have been three campaigns of CPT testing in the vicinity of the left abutment where failure was initiated. They also have a bearing on the slumps that developed in 2014; see Section 2 of the Report:

1. April, 2014;
2. September, 2014 – March, 2015; and
3. June, 2015.

The first campaign was limited in scope and reliability but does provide some information in the vicinity of the large-scale cracking that developed in August, 2014. This CPT data does not indicate contractive behavior, but rather dilatant or close to the contractant/dilatant boundary. This is consistent with the absence of any significant mobility of the affected material and the observation that none of the small slumps that preceded it in 2013 propagated by undrained retrogression. There is some indication of densified layering within the profiles, suggesting that the mass of tailings adjacent to the slope may have benefitted from densification associated with construction traffic on the beach.

The second campaign from September, 2014 to March, 2015 has the most data in the region of interest. CPTs F-01 to F-05, which explore from El. 854 m to El. 889 m, all reveal contractant characteristics of beach material, consistent with the existence of potential collapse behavior. Relevant data has previously been summarized on Figure 4-4.

The third campaign, conducted in June, 2015, provided less insight into conditions at the left abutment because it covered a substantial area, even outside of Fundão. Sounding FUND-06 encountered dilatant sand over an isolated loose layer between El. 862 m and El. 864 m. Sounding FUND-07 encountered dilatant sand from El. 895 m to El. 886 m, followed by soft phyllite to a depth of El. 865 m.

6.4 The Lateral Extrusion Mechanism

6.4.1 Detailed Description

The lateral extrusion mechanism is predicated on the presence of saturated, loose sands overlying soft slimes, with confinement of the slimes that varies according to the constructed profile.

As the structure increases in height, the slimes are loaded vertically but tend to extrude or spread laterally, rather like squeezing toothpaste from a tube. In doing so, the overlying sands tend to move with the slimes but lack ductility. As a result, stress changes arise that tend to reduce lateral confinement of the sands. This induces collapse of saturated sand or development of cracks in unsaturated material.

This mechanism, without liquefaction, is well known to designers of embankments on soft clays. Under these conditions the lateral deformation of the foundation often results in vertical tensile cracking of the overlying embankment fill. At failure, the shear strength of the fill cannot be relied upon because of the absence of shear resistance along the open cracks that it sustains.

6.4.2 Extrusion and Collapse of Saturated Loose Sand

The Panel has experimentally demonstrated the lateral extrusion mechanism leading to collapse by conducting drained triaxial compression tests that adopt a specially-designed stress path. Designated *extrusion collapse* tests, they simulate the reduction in horizontal stress in the sand due to slimes extrusion while keeping the vertical stresses constant. Details of the test procedures and data obtained are provided in Appendix D, which includes the results from the tests that were performed. The results of two tests are shown on Figure 6-3, one on a contractive specimen with an initial state parameter $\Psi = +0.01$ and another with $\Psi = +0.04$. These values are on the contractive side of CPT data previously shown on Figure 4-4 and as such tend to bracket the characteristic state in the field. In both cases, as the shear stress along this loading path approaches the ultimate friction line, collapse occurs in an abrupt and sudden manner after only small deformations in the sand. This testing provides both a qualitative demonstration and a quantitative reference for collapse of Fundão sand associated with the extrusion mechanism.

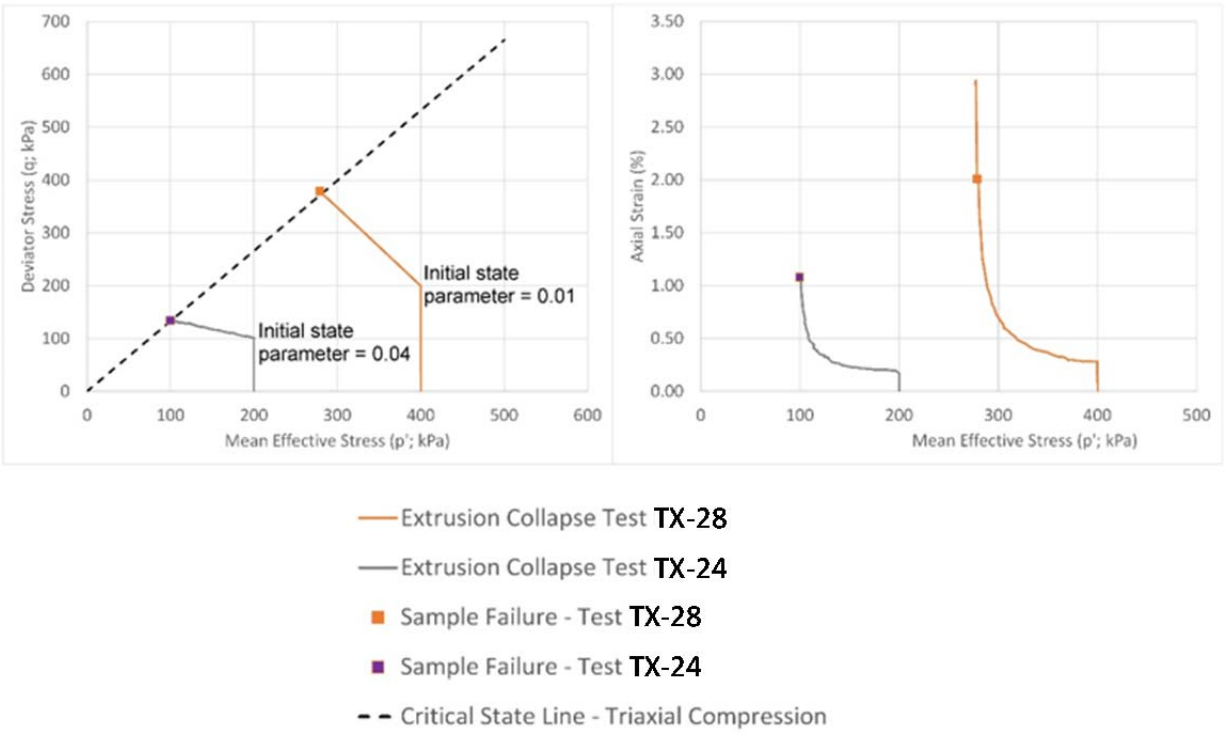

Figure 6-3 Extrusion collapse tests on Fundão sand

6.4.3 Numerical Simulation - Formulation

In order to analyze the lateral extrusion mechanism and resulting collapse, the Panel has undertaken numerical simulation of the construction of the Fundão Dam left abutment section. This analysis follows the history of construction, the evolution of piezometric pressures, the deformation within the slimes and sands, and the spatial variation of the state parameter. An important output from the analysis will be the demonstration of stress paths to failure comparable to those utilized in Section 6.4.2 for quantifying collapse behavior.

The cross-section adopted for the analysis is based on Section 01, at the left abutment provided in Appendix B. Materials within the cross-section have been grouped into the following material types:

1. Bedrock: All materials below the “stripped ground” survey were assigned to this material type;
2. Uncompacted tailings sand not intermixed or interbedded with slimes;
3. Slimes/sand deposits in varying proportions, designated as:
   - predominantly slimes;
   - mixed sand and slimes;
   - interbedded slimes; or
   - isolated slimes; and
4. Compacted sand.

The embankment configuration was modeled at four-month time intervals throughout the majority of the construction history, starting at the end of 2011. For the final six months (June to November, 2015), this time interval was reduced to monthly in order to gain additional resolution of model response close to the time of failure. Details of the modeling process and its formulation are presented in Appendix I.

The geotechnical properties for each of the materials listed above constitute a fundamental input to the modeling. Formulations of increasing complexity were adopted in an iterative manner to provide a check on model performance. This gave confidence in the results from analyses based on the most complex formulation for loose sand behavior, the critical state model NorSand presented by Jefferies and Been (2016). Parameter sensitivity analyses were completed for the critical state model to assess variations of the influence of the strength and continuity of the slimes layer.

Elastic properties for the sand were based on shear wave velocity measurement in Appendix C converted to an approximate large strain modulus. The elastic properties for the slimes were based on one-dimensional consolidation test data calibrated to a 2008 field loading trial by Samarco described in Appendix F.

The shear strength for beached sand was set at a frictional angle of $\phi' = 33°$, based on tests conducted by the Panel in Appendix D. The compacted tailings sand was modelled with a friction angle of $\phi' = 35°$ and 5 kPa cohesion, in accordance with the values used by others during designs.

The slimes were given a peak shear strength of $\phi_p = 12.4°$, equivalent to an undrained strength ratio of 0.22. This reduced linearly to one-third of the initial value at a plastic strain of 20%, reflecting a modest sensitivity. Support for this formulation is provided in Appendix C from back-calculation of the Baia 4 failure described in Section 6.1.

Critical state parameters assigned to the uncompacted tailings sand were derived from triaxial compression laboratory tests provided in Appendix D. One parameter needed for the critical state formulation was derived from modeling single-element response (equivalent to a laboratory test) as discussed in detail in Appendix I. In addition, it was necessary to declare an initial state parameter to seed the analysis. Following recommendations of Jefferies and Been (2016) and utilizing CPT data from the 2015 field campaign, this seed value was set at $\Psi = -0.02$.

It is also necessary to characterize the various sand-slimes mixtures listed above. Here, no direct experimental information is available, hence judgment is needed to establish both elastic and strength properties. Both elastic and strength properties of the slimes described above were blended with those of the sand in accordance with estimated proportions of those materials within the cross-sections. “Predominantly Slimes” were treated as pure slimes and “Isolated Slimes” were considered as pure sands. “Mixed Sand and Slimes” were a 50:50 mixture and “Interbedded Slimes” were taken to be 80% sand. The resulting properties are summarized in Appendix I.

The formulation of the behavior of the sand/slimes mixtures and their relative proportions is the greatest source of uncertainty in the analysis. As a result, sensitivity analyses have been conducted to explore how variations in assumed sand/slimes behavior influence the model results.

One final element in the formulation of the analysis is the treatment of the pore-water pressures. The pore-water pressures were assigned by setting the phreatic surface based on the integration of piezometric response provided by the hydrogeologic model summarized in Appendix G. As such, no stress-induced pore pressures are considered.

As shown in Appendix F, the slimes appear to fully consolidate on average over the loading history from 2011 to failure. However, in the model it is assumed that increments of loading generate an undrained response. The pore pressures developed are assumed to dissipate prior to the next load increment and do not accumulate over time.

6.4.4 Numerical Simulation - Results

An important check on any complex numerical model is to replicate the experimental information that constitutes the building blocks of the comprehensive constitutive relationship needed to undertake more complex analysis. Figure 6-4 and Figure 6-5 show the results of a simulation of a drained triaxial compression test and an undrained stress-controlled triaxial compression test. The latter follows a stress path simulating the effect of the extrusion mechanism in the slimes on the overlying sand developed in Section 6.4.2 above. The correspondence between numerical simulation and experiment is encouraging. The model strength result is about 3% less than the experimental value and it will be used as a reference to assess proximity of the simulation to collapse.

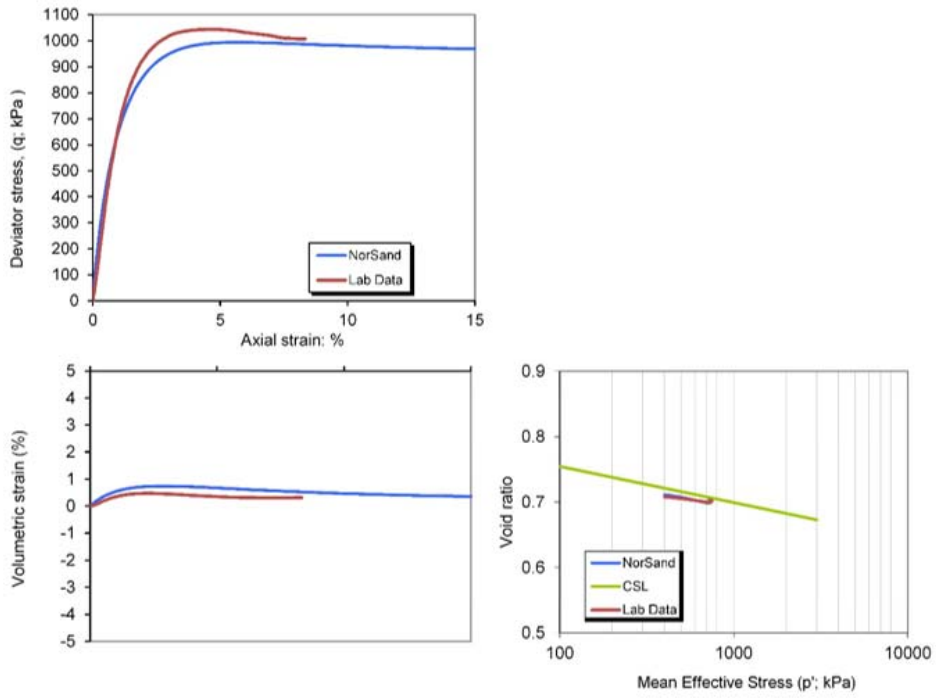

Figure 6-4 Simulated drained triaxial compression test (Test ID TX-12)

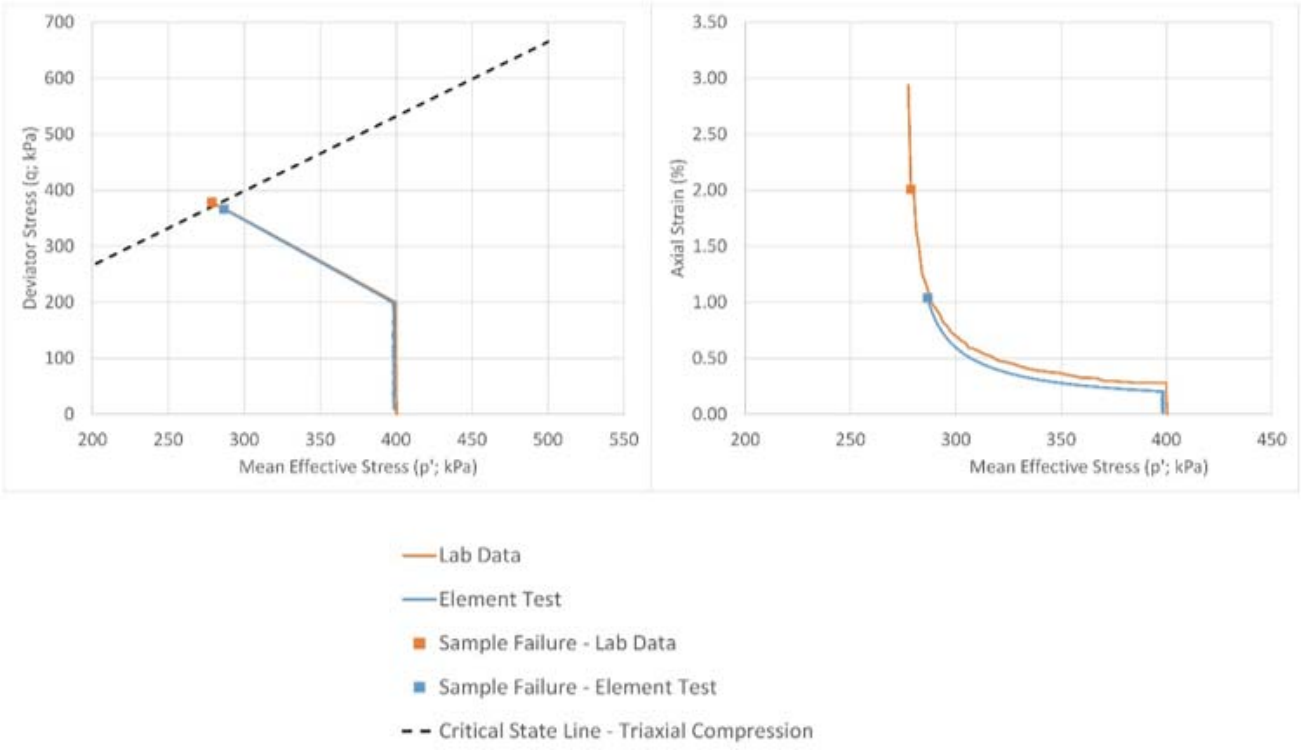

Figure 6-5 Simulated extrusion collapse test (Test ID TX-28)

Appendix I presents the results and general conclusions from a variety of simulations intended to explore the sensitivity to assumptions with respect to the distribution of slimes-enriched deposits and to their assumed geotechnical properties. In the view of the Panel, the case that best represents the evolution of collapse in the saturated loose sands overlying the slimes rich deposits is presented on Figure 6-6.

The Mobilized Instability Ratio (MIR) is a criterion for the triggering of collapse. It is defined as the ratio of the deviator stress and mean effective stress to the ratio at the onset of collapse. The color zonation represents the MIR related to the collapse strength determined from laboratory tests. The maximum value computed is 80%. Numerical convergence limitations inhibit the modeling from progressing further. However, the information available from the simulation provides compelling support for the hypothesis that collapse was triggered by lateral extrusion of the slimes-rich deposits.

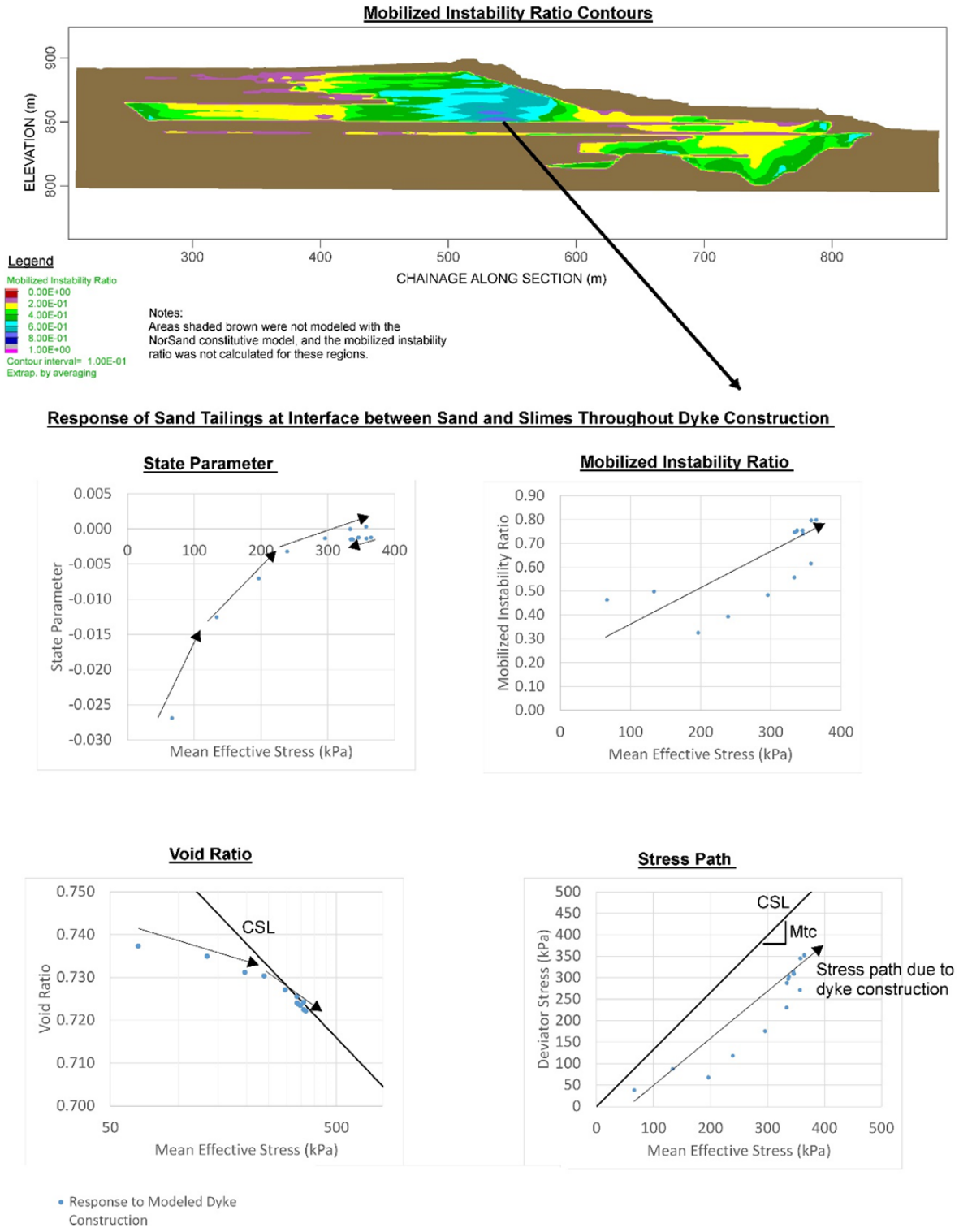

Figure 6-6 Mobilized Instability Ratio

Figure 6-6 also plots the stress path calculated throughout construction of the Fundão Dam. Operation of the lateral extrusion mechanism is cumulative during construction as reflected by the results plotted. The stress path has been calculated at the base of the sand which is the location where collapse would be initiated. The calculation indicates that 80% of the available collapse resistance has been mobilized with the strength as prescribed in the analysis and determined by laboratory tests. Numerical instability, from a computational perspective, precluded advancing the calculations further.

Figure 6-7 provides a comparison of laboratory data from Figure 6-5 with the simulated field stress path on Figure 6-6. It shows that the field stress path displays similarity to the controlled laboratory stress path and is migrating towards the ultimate strength line. As noted above, numerical convergence limitations preclude completing the analysis.

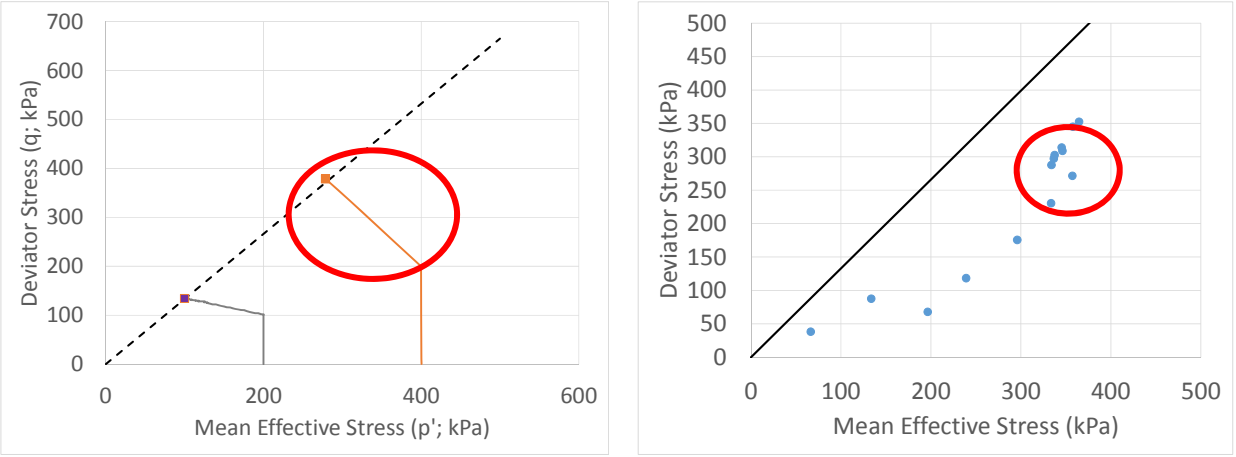

Figure 6-7 Comparison of laboratory and simulated field stress path

Figure 6-8 plots horizontal deformations along the slimes/sand interface at various stages of construction of the Fundão Dam. It illustrates that the largest lateral movements occur beneath the slope and downstream of the crest. This implies compressive straining in the downstream direction and extension straining in the upstream direction. Extension strains result in a reduction of horizontal confinement consistent with the lateral extrusion hypothesis.

It is also of interest to note that the maximum horizontal displacements beneath the lower part of the slope coincide with eyewitness reports of slope movement having initiated on the lower benches, as described in Section 2.7.

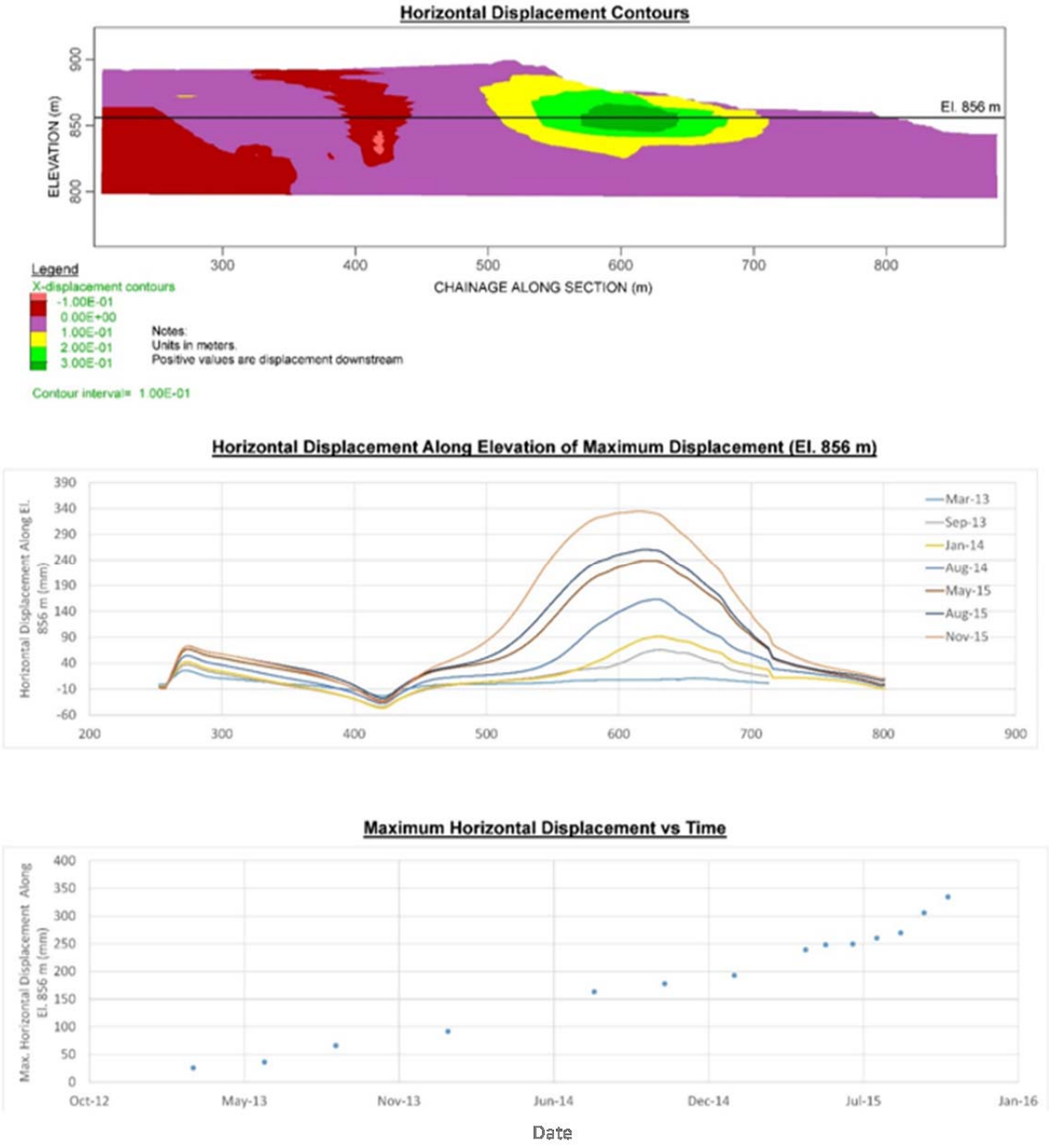

Figure 6-8 Horizontal displacements at sand/slimes interface

6.5 Displacements to Trigger Liquefaction by Lateral Extrusion

In order to determine the sliding deformation that would overcome the limitations of numerical convergence issues and meet a MIR of unity, the numerical analysis has departed from following the loading history and now imposes a specified slip to calculate the MIR response. As shown in Appendix I, a sliding displacement of 600 mm is required for an MIR of unity. By extrapolation, from

past values relating MIR and mobilized shear strength it is found that the sliding displacement of 600 mm would be calculated if the undrained strength ratio were equal to 0.14. This value is consistent with the sensitivity of the slimes.

6.6 Comparison Between Shearing Mechanism and Lateral Extrusion

In order to use this critical sliding displacement to evaluate the relative likelihood of the lateral extrusion mechanism triggering liquefaction versus other mechanisms, it is necessary to compare the 600 mm value with slip associated with a shearing mechanism that could develop due to the mobilization of low strengths in the slimes-rich layers. The shearing mechanism is a sequence involving undrained yielding of the slimes-rich layer leading to a general shear failure throughout the dam slope, which in turn results in an acceleration of displacements that triggers liquefaction. In order to evaluate which of these mechanisms was the more probable liquefaction trigger, the Mohr-Coulomb model discussed in Section 6.4.3 was used to estimate the magnitude of deformations that would develop at the onset of general shear failure due to yielding in the slimes-rich layer. Details are presented in Appendix I.

The pattern of displacements resulting in November, 2015 if a factor of safety of unity was approached is shown on Figure 6-9. The pattern of displacements is similar to that shown previously for the NorSand model analyses.

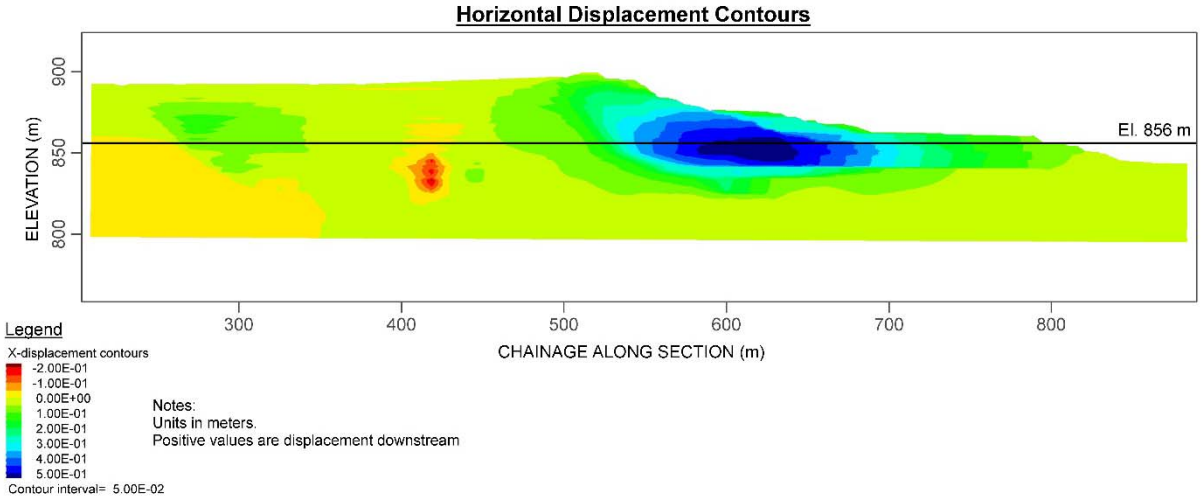

Figure 6-9 Horizontal displacements resulting from Mohr-Coulomb analysis approaching a factor of safety of unity

The deformation model used for failure analysis is equivalent to limit equilibrium analysis and hence provides a linkage between sliding displacement at failure and factor of safety. As discussed earlier in this section, a factor of safety of unity represents a trigger for the onset of liquefaction. The deformations associated with the onset of liquefaction with the shearing mechanism are much greater than those associated with the lateral extrusion mechanism. Therefore, liquefaction would be initiated by lateral extrusion prior to the development of shear failure.

The Panel regards the results from the numerical simulation as providing compelling support for the lateral extrusion mechanism accounting for the occurrence of the flowslide on November 5, 2015.

6.7 The Role of Earthquakes

6.7.1 Earthquake Loads

The Panel has relied on the Atkinson Report (2016) for evaluating the seismic history at the damsite and for recommending ground motions to be considered in response analyses (Atkinson 2016). The seismology report summarizes the regional seismicity and the instrumental records that were obtained from the earthquakes that occurred just prior to the collapse of the dam. It concludes that the site experienced natural earthquakes, as summarized in Table 2-1, with a Moment Magnitude, M_w, of up to 2.5 and epicenters close to the dam. As reviewed in Appendix K, earthquake loading from such small shocks would not usually be considered consequential to structures with robust design and operation. However, as discussed in detail above, the dam was in a very fragile state at the time of the earthquakes and the question arises whether the earthquakes hastened its collapse. Hence, a more detailed evaluation was warranted.

Understandably, there is considerable uncertainty in the determination of ground motions, and the Panel requested that the seismologists provide a range of ground motions and associated estimates of likelihood. These records form the basis of the dynamic response analysis needed to calculate the magnitude of stresses in the dam induced by the earthquake and the duration of earthquake loading. Both the median and 84th percentile (mean plus one standard deviation) ground motions were used for the dynamic response analyses.

6.7.2 Dynamic Response Analysis

Details of the dynamic response analyses are presented in Appendix J, and the soil properties used in these analyses are summarized in Appendices C and D.

Prior to calculating the dynamic response of the dam to the prescribed earthquake loading, the dynamic response was calculated at the site where the earthquake was experienced and where the subjective intensity characterization was first assembled. The intent of the calibration was to confirm that, within the bounds of the uncertainty associated with these analyses, the calculated ground motions were reasonable. Calculations were conducted by means of an industry standard method called SHAKE. The seismological advisors concurred that the calculated response was acceptable.

The recommended median and 84th percentile ground motions were then used to calculate the cyclic stresses and number of significant cycles to be considered in assessing the dynamic response of the dam. These ground motions are used to calculate both potential pore pressure development in saturated sand above the slimes as well as potential displacements in the slimes-rich deposits.

Cyclic Loading and Pore Pressure Response

It was the intent to apply the cyclic loading discussed above to a test specimen of sand on the brink of collapse, having been brought to that state by reducing horizontal stresses following the path associated with the lateral extrusion mechanism. However, it was not practical to apply the small

stresses calculated, and significantly larger stresses were applied during testing. Figure 6-2 illustrates the type of response that would indicate that the imposed earthquakes could have a significant effect on failure of the dam. In specific tests undertaken on the fragile test specimen, many more cycles (>1000) were applied than the 4-5 indicated by the calculations. Details of the testing are summarized in Appendix D. Collapse occurred only after more than 1200 cycles at stresses significantly larger than indicated by the analysis to have been produced by the earthquakes and no specific excess pore pressures were generated.

The Panel concludes that no cyclic induced pore pressures resulted from the assumed earthquake loading.

Cyclic Loading and Sliding in Slimes

Another potential result of the imposed earthquake loading is to induce deformations in the slimes-rich deposits as a result of the cyclic stresses discussed above. These deformations are calculated by adopting the earthquake motions computed at the top of the slimes and imposing them directly into analysis to calculate the seismic induced slip using a classical method entitled Newmark-type analysis and using a well-accepted computer program called SLAMMER. Details of these calculations are presented in Appendix J.

Reflecting the uncertainty in the prescribed ground motions, six time histories were selected from those recommended by Atkinson (2016). Those selected reflected the upper-bound of the range evaluated in the seismic study. The average calculated displacement was 5 mm. This can be compared with the rate of displacement calculated by the deformation analyses prior to failure. Estimates of rate of displacement from both NorSand and Mohr-Coulomb analyses indicate rates of approximately 1 mm per day. Hence, the displacements calculated from the SLAMMER analyses are of limited significance when compared with the rates of displacements associated with static loading alone. Nevertheless, given the proximity of the dam to collapse due to prior construction loading, this likely accelerated the failure process that was already well-advanced

6.8 Timing of the Failure

The introductory portions of this section posed the following three questions, which are answered below.

Why did flowsliding not occur on August, 2014 cracking incident?

The August, 2014 cracking incident did not display the mobility associated with flowsliding indicating that liquefaction did not occur. Figure 4-3 previously explained in principle how increased loading can cause a formerly dilatant material to become contractant. This effect is displayed in the NorSand model of conditions prevailing on or about August of 2014. As shown on Figure 6-10 on August, 2014 the sand is on or close to the CSL, which is a boundary between contractant and dilatant behavior. At this point the sand became loose enough to exhibit volume change and associated cracking but was not sufficiently loose to exhibit liquefaction. Also, Section 4.3 explained that a fundamental change in seepage patterns happened on or about the same time. Together these two changes, one in sand behavior and the other in saturation, produced the observed effects.

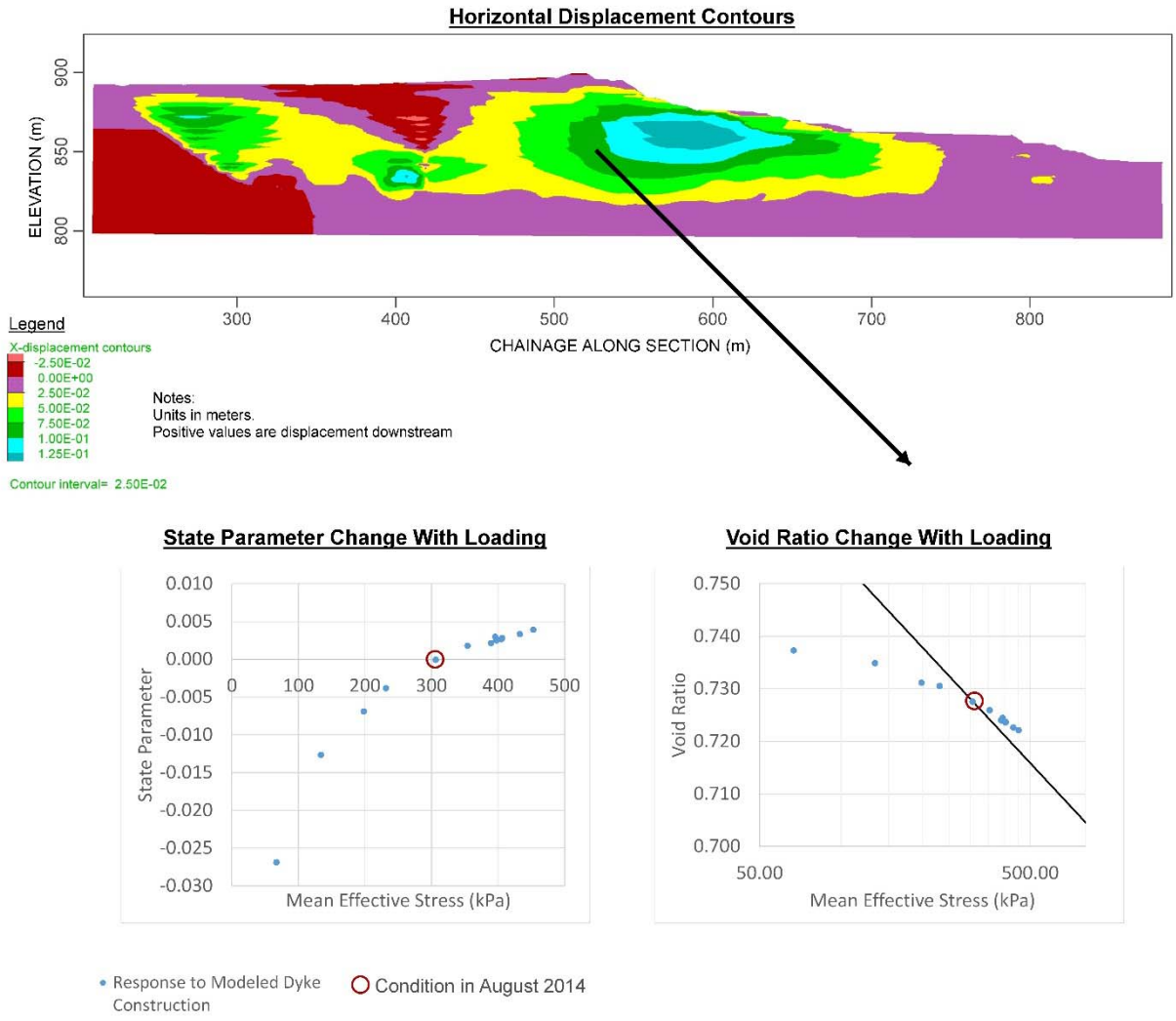

Figure 6-10 Example NorSand model output

Why did flowsliding occur under the conditions that prevailed on November 5, 2015?

The Panel concludes that the flowslide that occurred on November 5, 2015 was instigated by a lateral extrusion mechanism seated in the slimes-rich deposit at depth in the embankment that resulted in a reduction of lateral confinement of the overlying contractant and saturated sand. The extrusion mechanism created sufficient sliding displacement to generate a MIR of unity which is the criterion for triggering collapse.

Why did flowsliding occur following the earthquakes?

The earthquakes were small and would normally not be regarded as consequential for an ordinary dam. The Fundão Dam was subjected to lateral extrusion in the slimes-rich deposits beneath the left abutment and stress readjustment associated with this mechanism was leading it to collapse and liquefaction.

The prescribed earthquake motions have two potential effects on the dam. One is cyclic stresses that induce pore pressures in the sand and the other is cyclic stresses that induce deformations in the slimes-rich deposits. Experiments conducted on samples of sand representative of the stresses prior to collapse did not develop any pore pressure response due to the applied earthquake motions. However, the same earthquake motions applied to the behavior of the slimes-rich deposits indicated sliding displacements in the range of several millimeters. These displacements are of limited significance when compared with the displacements associated with static loading alone. Given the proximity of the dam to collapse due to prior construction loading, these earthquake induced displacements likely accelerated the failure process that was already well-advanced.

7 CONCLUSIONS

The mandate to the Panel was to conduct an investigation into the cause(s) of the breach of the Fundão Tailings Dam on November 5, 2015. To fulfill this mandate, the Panel was expected to provide its independent and unbiased professional judgement and expertise in determining the immediate cause(s) of the Incident and that this report would identify these immediate cause(s).

The Panel has responded to its mandate by framing three questions with accompanying answers. These questions and a summary of the responses, presented below, identify the immediate causes.

Question 1: Why Did a Flowslide Occur?

The original design concept for the Fundão Dam employed an unsaturated sand zone to support the weak slimes zone. Unsaturated sand is not amenable to liquefaction and hence the original design was robust in this regard. However, difficulties were encountered in executing the design and a modified design was put forward and adopted. As part of this modification, a change in the design concept was also adopted and saturated conditions were permitted to develop in the sand.

The flowslide required three conditions to develop: (1) saturation of the sand; (2) loose uncompacted sand; and (3) a trigger mechanism. Depositing sand tailings by hydraulic means resulted in loose conditions. The growth in the saturated conditions is well-documented. Hence, all the conditions prevailed for liquefaction to develop resulting in a flowslide, provided it was triggered. Triggering is discussed in the response to Question 3.

Question 2: Why Did the Flowslide Occur Where It Occurred?

Eyewitness accounts revealed that the flowslide initiated on the left abutment, where the dam had been set back from its former alignment. Studies of the depositional history associated with the growth of the Fundão Dam revealed that slimes encroached into the area preserved for sand deposition alone. The design incorporated a 200 m zone separating the two deposits but historical information reveals that slimes had encroached into the area on a number of occasions. The presence of slimes introduces a barrier to downward drainage and a zone of potential weakness that might affect stability. Deposition in the area of the right abutment was almost slimes free.

The setback was implemented to accommodate repairs to a deficient conduit at the base of the impoundment as well as the construction of additional horizontal blanket drains to facilitate subsequent dike-raising. This change in geometry resulted in substantial embankment loading over slimes-rich deposits. This distinguishes the left abutment area from the right and accounts for the location of flowslide initiation.

Question 3: Why Did the Flowslide Occur When It Occurred?

The initiation of a flowslide requires not only the presence of saturated contractant tailings but also a trigger mechanism to initiate the process that mobilizes undrained shearing and hence flowsliding. Following an evaluation of potential trigger mechanisms, the Panel concluded that lateral extrusion initiated the failure.

The lateral extrusion mechanism develops as the dam increases in height, loading the slimes-rich zone vertically which tends to extrude or spread laterally, rather like squeezing toothpaste from a tube. This results in stress changes in the overlying sands which reduce their confinement, leading to collapse.

This mechanism for collapse was modelled by tests in the laboratory and by computational modeling that predicted to an acceptable degree that collapse should have occurred about the time that the dam was raised to the height that was attained on November 5, 2015.

The role of the earthquakes that occurred just prior to collapse was also investigated quantitatively. Calculations with recommended design motions reveal that about 5 mm of displacement may have been induced in the slimes. Given the proximity of the dam to collapse due to prior construction loading, this likely accelerated the failure process that was already well-advanced.

ACKNOWLEDGEMENTS

We would like to express our appreciation to Klohn Crippen Berger, which provided indispensable engineering and organizational assistance. We especially wish to recognize the efforts of Cindy Wang, without whose creative skill and determination in synthesizing reams of information and data our efforts could never have proceeded far. In addition, we wish to recognize the contribution of Joe Quinn not only for his leadership and analytical modeling but also his role in the field and laboratory studies. The contribution of Chris Dickinson and his colleagues resulted in an important synthesis of all seepage related issues.

Most of all, the Panel wishes to acknowledge the sacrifices of the victims, their loved ones, and those left homeless. We can only hope that our work may in some small measure help to prevent such occurrences from ever happening again.

REFERENCES

Atkinson, G. 2016. *Analysis of Ground Motions from Nov. 5, 2015 Earthquake Sequence near Fundão Dam, Brazil.* Report to CGSH on July 20, 2016.

Jefferies, M. and K. Been. 2016. *Soil Liquefaction: A Critical State Approach.* 2nd ed. London: Taylor & Francis.

Martin, T.E. and E.C. McRoberts. 1999. "Some Considerations in the Stability Analysis of Upstream Tailings Dams," in *Tailings and Mine Waste '99: Proceedings of the 6th International Conference on Tailings and Mine Waste, January 24 to 27, 1999.* Rotterdam, Netherlands: A.A. Balkema.

Pimenta de Ávila, J. 2011. "The Drained Stacking of Granular Tailings: A Disposal Method for a Low Degree of Saturation of the Tailings Mass," in *Proceedings of the Tailings and Mine Waste Conference, Vancouver, BC, November 6 to 9 2011.* Vancouver: University of British Columbia.

Robertson, P.K. 2010. "Evaluation of Flow Liquefaction and Liquefied Strength Using the Cone Penetration Test." *Journal of Geotechnical and Geoenvironmental Engineering.* 136(6): 842-853.

Sadrekarimi, A. 2014. "Effect of the Mode of Shear on Static Liquefaction Analysis." *Journal of Geotechnical and Geoenvironmental Engineering.* 140(12): 04014069-1-04014069-12.

Sasitharan, S., P.K. Robertson, D.D. Sego and N.R. Morgenstern. 1993. "Collapse Behaviour of Sand." *Canadian Geotechnical Journal.* 30(4): 569-577.

Shuttle, D.A. and J. Cunning. 2007. "Liquefaction Potential of Silts from CPTu." *Canadian Geotechnical Journal.* 44(1): 1-19.

Skopek, P., N.R. Morgenstern, P.K. Robertson and D.C. Sego. 1994. "Collapse of Dry Sand." *Canadian Geotechnical Journal.* 31(6): 1008-1014.